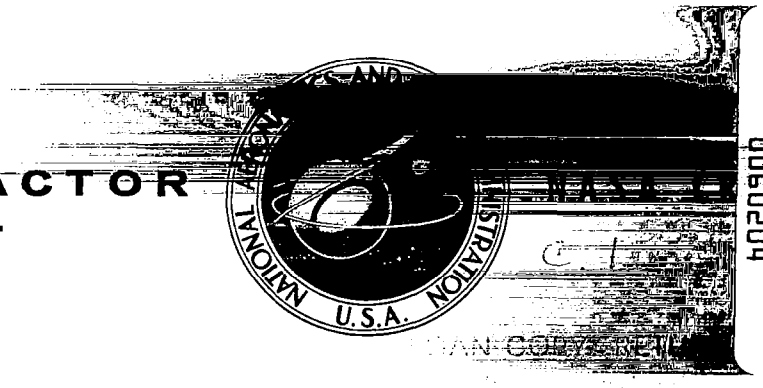

NASA CONTRACTOR REPORT

NASA CR-659

A STATISTICAL TECHNIQUE FOR THE DYNAMIC ANALYSIS OF VEHICLES TRAVERSING ROUGH YIELDING AND NON-YIELDING SURFACES

by B. D. Van Deusen

Prepared by
CHRYSLER CORPORATION
Detroit, Mich.
for

NATIONAL AERONAUTICS AND SPACE ADMINISTRATION • WASHINGTON, D. C. • MARCH 1967

NASA CR-659

A STATISTICAL TECHNIQUE FOR THE DYNAMIC ANALYSIS OF VEHICLES TRAVERSING ROUGH YIELDING AND NON-YIELDING SURFACES

By B. D. Van Deusen

Prepared under Contract No. NASw-1287 by
CHRYSLER CORPORATION
Detroit, Mich.

for

NATIONAL AERONAUTICS AND SPACE ADMINISTRATION

For sale by the Clearinghouse for Federal Scientific and Technical Information
Springfield, Virginia 22151 – CFSTI price $3.00

ABSTRACT

A technique has been developed which allows prediction and analysis of the dynamic response of vehicles traversing yielding and non-yielding rough surfaces. Virgin terrestrial and extraterrestrial surfaces are classified according to their frequency and amplitude distribution. A single parameter has been defined which, when properly interpreted, is sufficient to completely specify their surface roughness. This classification determines the nature of a random input to an analog computer simulation of the vehicle and surface dynamic models. Parametric model analysis can then be performed with the output criteria specified statistically.

In addition, deterministic inputs can be used, and a simplified linear model technique is presented using transfer function concepts.

ACKNOWLEDGEMENT

The author is grateful to the Jet Propulsion Laboratory and Mr. Gerald M. Smith for supplying digital evaluation data from the last two P-3 camera frames of Ranger VIII, and to the U.S. Geological Survey and Mr. Lawrence C. Rowan for supplying digital slope data from the last partial P-3 camera frame of Ranger VII. I am also grateful to Mr. Douglas Michel, NASA-OART, and Dr. John P. Raney, NASA-Langley Research Center, for their guidance and suggestions in monitoring this research program.

This work was performed under the guidance and direction of Mr. Franklin A. Ayer, the Chrysler Program Manager. Other members of the Chrysler research team were: V. J. Borowski, R. G. Gergle, C. H. Hoppe, R. F. Hughes, G. E. McCarron and J. M. Sneyd, all of whom authored portions of the appendices. Special acknowledgement is due Dr. C. R. Lewis and Mr. J. Lunan, Chrysler Research Office, and D. F. Callahan and L. R. Biasell, Chrysler Planning Office, Defense-Space Group, for their support of the study. The figures in the report were drafted by Miss G. Ross and the report was typed by Miss Y. Parkinson.

TABLE OF CONTENTS

TABLE OF CONTENTS Continued

TABLE OF CONTENTS Continued

ILLUSTRATIONS

ILLUSTRATIONS Continued

ILLUSTRATIONS Continued

ILLUSTRATIONS Continued

TABLES

I. INTRODUCTION

The effects of surface roughness on the design and operation of vehicles has been investigated for a number of years. An analytical approach to the study of these effects requires a mathematical model of the vehicle which is excited by the surface profile. Initial attempts [1] [2] to study this problem in the automotive industry consisted of subjecting mathematical automobile models to well defined mathematical inputs such as sine waves, step functions, triangular waves, etc. Verification of the analysis was accomplished by constructing specific obstacles and driving instrumented automobiles over them. While this technique served to verify the analysis it was difficult to optimize design, or study behavior since the validity of the input was questionable.

As better methods of measuring and recording actual surface profiles were developed, the aircraft industry became involved in analyzing the effects of runway roughness on aircraft. A statistical method (power spectral density)[3] for classification of runway profile was adopted and a number of measurements were made[4] [5]. Attempts were made to statistically analyze simple linear aircraft models. The problem associated with this analysis was the interpretation of the output. Methods have recently been developed[6] which use a deterministic runway profile as an input to a dynamic model. Where a specific section of profile is of interest, as in aircraft runway analysis, it is more meaningful to look at a deterministic input for analysis. This allows, not only the evaluation of the response of a particular airplane to a particular runway, but also the prediction of those runway sections where repair work might contribute to smoother dynamic performance.

At the same time that the aircraft industry was developing the statistical approach for aircraft analysis, the Army became interested in this approach for studying dynamic problems

of military vehicle cross-country operations[7][8]. In this case, where no specific path of travel is defined, statistical classification of surface roughness appeared to be a promising method of attack.

When the problem of operating surface vehicles in extraterrestrial environments is considered, the analytical approach becomes a practical necessity. The cost and complexity associated with experimental testing in extraterrestrial environments precludes this approach to vehicular design. It thus becomes necessary to develop accurate analytical techniques which permit investigation of design parameters. There is, seemingly, a paradox between the two analytical approaches to vehicle dynamics, i.e., deterministic versus random input functions. This paradox stems from the fact that for a vehicle operating in an extraterrestrial environment, the concern is with the encounter of a singular obstacle which may result in a catastrophic failure, such as vehicle roll-over. It is argued that with the statistical approach, these obstacles are smoothed, in some sense, over the surface such that an obstacle (be it a lunar crater or a terrestrial rock) is "lost" in the statistical definition of the surface. Conversely, the statistical approach appears very promising since no discrete traverse of a surface segment can be chosen for analytical evaluation or optimization of vehicle design. The basic premise behind the approach to vehicle dynamics outlined in this report is that the statistical determination of surface roughness is a necessity for characterizing virgin terrestrial or extraterrestrial surfaces. This approach not only allows meaningful investigation of the probability of encountering a singular obstacle, but it is the only rational and accurate way of determining this probability.

This report is based on an application of existing statistical techniques. An approach is outlined which, when expanded, should provide a means for optimization of vehicle design and study of the behavior of vehicles traversing rough surfaces. To this end four objectives were established at the onset of this research study.

These objectives are:

1. To define surface roughness in a concise and meaningful fashion with a minimum number of parameters and in a form usable for vehicle analysis.

2. To include the dynamics of yielding surfaces in vehicle model analysis.

3. To analyze non-linear systems for both vehicle and surface dynamic models.

4. To develop output criteria for vehicle optimization determined by the probability of exceeding design limits.

One method of meeting all of these objectives is to specify the surface roughness statistically, such that a representative time trace can be generated for input to an analog computer simulation of the vehicle. Figure 1 shows a block diagram of the conceptual approach.

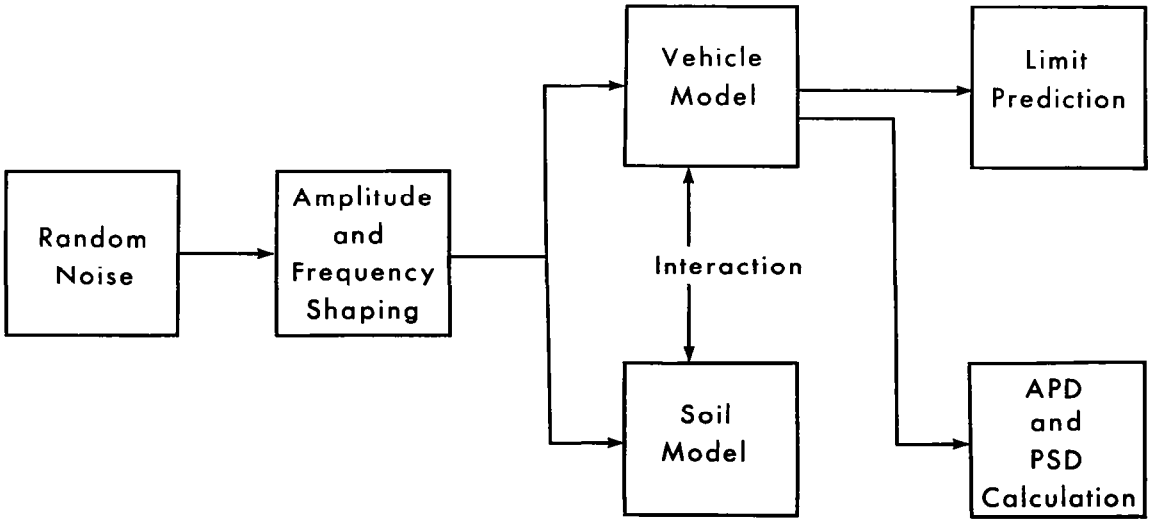

Figure 1 BLOCK DIAGRAM FOR NON-LINEAR SYSTEM ANALYSIS

II. SURFACE ROUGHNESS

After reviewing the existing methods of classifying surface roughness, it was concluded that the power spectral density (variance density spectrum) offered the most promise for the present application. A number of investigators have observed that the P.S.D. of natural surfaces and most man-made surfaces (aircraft runways and highways) can be expressed by Equation 1.

$$P_d(\Omega) = C' \Omega^{-N} \tag{1}$$

Where $P_d(\Omega)$ is the P.S.D. of the surface displacement (profile height) with units of meters^2/cycle/meter, Ω is a spacial frequency in cycles/meter and C' and N are constants for any given spectral estimate. Figure 2 shows a number of published P.S.D.'s. Table 1 lists a description of these profiles and computed values of C' and N. N is a dimensionless constant and C' is an empirical constant whose dimensions vary with the value of N.

Table 1 shows that N is approximately 2.0 for both natural and man-made surfaces. Man-made surfaces can be artificially constructed to give any value of N. Man's influence may accentuate some frequency component making Equation 1 invalid for some surfaces (washboard roads, plowed fields, expansion joints in concrete pavements, etc.). The P.S.D.'s from surfaces 12 and 13 in Figure 2 and the results of lunar surface analysis in Appendix A indicate that natural surfaces have no favored or predominant frequency and that the value of N in Equation 1 is approximately 2 for these surfaces. This gives Equation 2 for the P.S.D. of virgin terrestrial or extraterrestrial surfaces.

$$P_d(\Omega) = C\Omega^{-2} \tag{2}$$

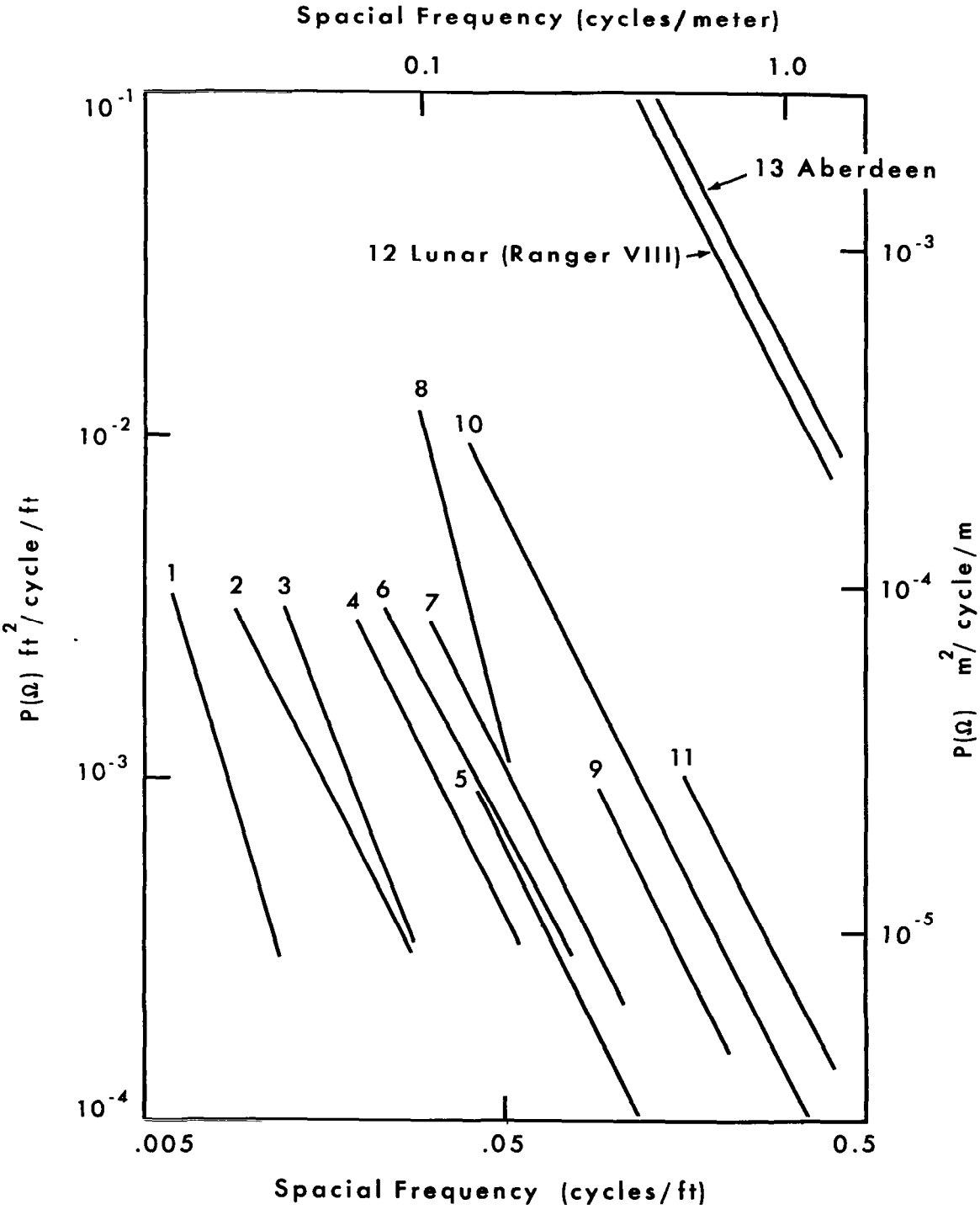

Figure 2 P.S.D. ESTIMATES FROM RUNWAYS, HIGHWAYS, TERRAIN & LUNAR SURFACE

Table 1 VALUES OF C' AND N FOR P.S.D.'s OF FIGURE 2

P.S.D. Number	Description	Reference	N	C'	C''	C'''
1	Runway (σ = .016)	NASA-TND-510	3.8	4.3×10^{-11}	1.0×10^{-12}	1.6×10^{-11}
2	Runway 3	NACA-TN-4303	2.0	7.0×10^{-8}	6.1×10^{-6}	2.2×10^{-7}
3	Runway 1	NACA-TN-4303	2.6	1.9×10^{-8}	9.6×10^{-8}	2.9×10^{-8}
4	Runway 35	NACA-TN-3305	2.1	2.7×10^{-7}	1.6×10^{-5}	7.7×10^{-7}
5	Smooth Highway	REF. 7	2.1	4.8×10^{-7}	2.6×10^{-5}	1.2×10^{-6}
6	Runway (σ = .250)	NASA-TND-510	1.9	6.4×10^{-7}	8.7×10^{-5}	2.3×10^{-6}
7	Runway 12	NACA-TN-3305	2.0	8.2×10^{-7}	6.0×10^{-5}	2.5×10^{-6}
8	Runway 4(200'/sec)	AGARD-REP 119	4.1	2.1×10^{-8}	9.1×10^{-11}	5.3×10^{-9}
9	Smooth Runway	NACA-TN-3484	2.1	2.4×10^{-6}	1.3×10^{-4}	6.6×10^{-6}
10	Highway with Gravel	REF. 7	2.1	4.4×10^{-6}	2.4×10^{-4}	1.1×10^{-5}
11	Rough Runway	NACA-TN-3484	2.1	8.1×10^{-6}	4.3×10^{-4}	2.3×10^{-5}
12	Lunar Profile	Appendix A	2.0	3.6×10^{-4}	3.6×10^{-2}	1.2×10^{-3}
13	Aberdeen	REF. 8	2.0	4.8×10^{-4}	4.8×10^{-2}	1.6×10^{-3}

NOTE; C' = Value Computed for $P_d(\Omega)$ in m^2/cycle/m

C'' = Value Computed for $P_d(\Omega)$ in cm^2/cycle/cm

C''' = Value Computed for $P_d(\Omega)$ in ft^2/cycle/ft

The constant C indicates that no predominant frequency is expected. This constant has the dimension of length and is a measure of surface roughness. The exponent of -2 predicts that the amplitude of a surface undulation is directly proportional to its wave length.

2.1 Slope Distribution.

It is of interest to compare Equation 2 with other published methods of surface classification. The U. S. Geological Survey has been processing various lunar photographs in an attempt to map and classify sections of the lunar surface. These photographs range all the way from low resolution earth based photographs to the highest resolution Ranger photographs. The surface slope at numerous points has been measured by optically scanning each photograph and accounting for changes in surface reflectivity. Since resolution varies considerably between photographs the base length over which the slope is measured covers several orders of magnitude.

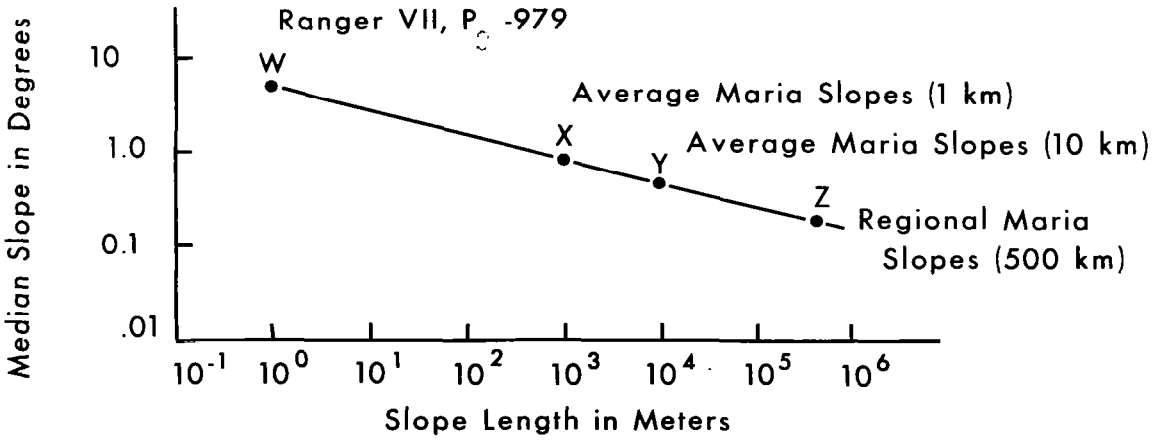

Figure 3 MEDIAN SLOPE vs SLOPE LENGTH

Figure 3 is a U.S.G.S. plot of the median slopes versus base length. The four data points, each measured from a different photograph, fall on a straight line in this log-log plot. This relationship is expressed by Equation 3. S is the median slope in degrees, K is a constant and $\triangle L$ is

$$S = K(\triangle L)^{-1/2} \tag{3}$$

the base length. Since S is less than 10° in every case the height of rise Y over the segment $\triangle L$ is approximately:

$$Y \propto S\triangle L \propto (\triangle L)^{1/2} \tag{4}$$

The wave length is proportional to $\triangle L$ and inversely proportional to Ω, the spacial frequency. Noting this fact and also noting that $P_d(\Omega) \propto Y^2/\Omega$ yields:

$$P_d(\Omega) \propto Y^2/\Omega \propto \Omega^{-2} \tag{5}$$

which agrees with the form of Equation 2. Thus, Equation 2 appears to be applicable over a wide range of spacial frequency covering several orders of magnitude.

2.2 Curvature

The Bendix Systems Division has proposed a method of lunar surface classification using "curvature".[9] This is essentially an adaptation of a method used by the metal-working industry for assessing the smoothness of contoured surfaces. For three elevation points, or heights, the perpendicular height $\triangle H$ of the center point above the line joining the two outermost points is computed for various base lengths. The base length $\triangle L$ is the horizontal distance between the two outside points. To demonstrate this method the authors of Reference (9) used a 65 x 65 matrix of elevation points (points spaced 1.25 feet apart) from an 80 x 80 foot area of the Bonito Lava Flow. A $\triangle L$ of 2.5 feet (3 data points) was used to compute a $\triangle H$ for every possible combination. A standard deviation for $\frac{\triangle H}{(\triangle L)^2}$ was then computed. The process was repeated with $\triangle L$ = 5 ft. (5 data points ignoring the 2nd and 4th points) to arrive at a new value of the standard deviation. This process was continued until $\triangle L$ of 80 ft (65 data points) was reached. A log-log

plot of the standard deviation σ of $\frac{\triangle H}{(\triangle L)^2}$ versus $\triangle L$ is shown in Figure 4. The authors

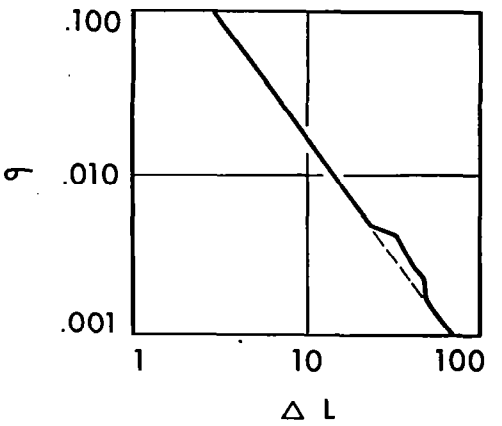

Figure 4 Plot of σ versus $\triangle L$ from ref. 9

arrived at the formula

$$\sigma = K(\triangle L)^n \tag{6}$$

where the two numerical factors K and n were said to "uniquely describe a particular surface." The values obtained for these constants were K = 0.412 and n = - 1.449. Equation 6 can be re-written in the form of Equation 7 by assuming n to be - 1.5 and noting that σ is a measure of $\frac{\triangle H}{(\triangle L)^2}$.

$$\frac{\triangle H}{(\triangle L)^2} \propto (\triangle L)^{-1.5} \tag{7}$$

Noting that $\triangle H$ is, in some fashion, proportional to profile height and $\triangle L$ is proportional to the wave length and inversely proportional to spacial frequency Ω, Equation 7 becomes:

$$Y\Omega^2 \propto \Omega^{1.5} \tag{8}$$

Squaring both sides of Equation 8 and dividing by Ω^5 yields:

$$P_d(\Omega) \propto Y^2/\Omega \propto \Omega^{-2} \tag{9}$$

Equation 9 is identical with Equation 5 and again agrees with the form of Equation 2.

2.3 Power Spectral Density

The power spectral density is a second moment or variance density spectrum. The concept of variance is important since variance is additive and provides the only meaningful method of dividing a random function into its frequency components. In order to classify surface profiles using P.S.D. techniques it is essential that the profile record be a sample function from a stationary random process. Stationarity implies that the statistical properties of the profile height do not change with position. While this is not strictly true for the surface in question, it is customary to assume quasi-stationarity and estimate the P.S.D. from finite samples of the surface profile. This estimated P.S.D. allows a reasonably accurate measurement of the frequency content of a particular surface and thus is useful for surface classification.

If the surface profile is measured as digitally sampled data points over a finite traverse, then numerical methods can be used to arrive at an estimate of the P.S.D. Appendix A gives a complete development of the concepts necessary for P.S.D. estimates from finite samples together with processing of lunar data and a computer program for P.S.D. estimates from Fourier series coefficients.

A discussion of the interpretation of P.S.D. and its relationship to the Fourier series coefficients is offered by the author in reference (10).

2.4 Space Domain Smoothing

Since Equation 2 predicts that the amplitude of the surface profile varies proportionately with the wave length, it is difficult to separate the concept of non-stationarity from the probability of encountering a wave length of the order of, or longer than, the data sample. In order to cope with this problem several investigators have developed methods of removing "non-stationary" trends from the data. This problem resolves to one of separating an observed elevation profile into two

sub-series, one containing only long wave lengths (the trend), and the other containing only components of shorter wave length (detrended data). It has been argued by two investigators[8][11], that the most realistic filter appears to be based on a linear moving average. The author of Reference (11) noted: "While the method has previously been used to filter out non-stationary trends from other types of data, the theoretical implications of the distortions resulting in the filtered profile are not clearly understood." It can be shown that, while this linear detrending attenuates the lower frequencies with a period of the order of the average, it does this at the expense of altering or contaminating the data in the range of interest.

In order to cope with this problem, an exponentially weighted average has been developed for detrending the data. This exponentially weighted average appears similar to the effect derived from an electrical high pass filter[12]. When the signal is available in analog fashion, it is necessary to weight only the past history of the signal and compute a one-sided exponential average. This results in the characteristic phase shift associated with analog filters. When the data is available in digital form it is possible to calculate the exponentially weighted average in both the past and the future. This two sided exponentially weighted average is a 6 db per octave filter with zero phase shift. Equation 10 expresses the mathematical process of computing this exponential detrending of the data.

$$F_d(x) = F(x) - \frac{1}{2\lambda} \int_{a=0}^{a=\infty} \left[F(x+a) + F(x-a)\right] e^{-a/\lambda} da \qquad (10)$$

Where $F_d(x)$ is the detrended filtered) function, $F(x)$ is the original function and λ is the exponential weighting constant (time constant in the time domain). Appendix A develops the numerical method for computing this detrending which was used to process Ranger data and gives the computer program. In this case the numerical integration was performed out to 3λ.

The necessity for smoothing the data in the time domain depends, to a large extent, on the nature of the data. No detrending is necessary if the function is stationary and the range of sample data is much larger than any expected wave length. In the case of profile measurements it has been predicted here that the amplitude varies directly with the wave length, hence detrending is a necessity to achieve an accurate estimate of the P.S.D. While it might appear, at first glance, that the "trend" would only alter the components of long wave length, it actually will alter all components. If the trend is significant it might easily obscure the real data of interest. Figure 5 shows both the undetrended and the detrended P.S.D. calculated for the Lunar surface from Data Set 4 (See Figure A-7) in Appendix A. This data has a substantial linear trend and the effect of this trend is to raise the estimate of the surface roughness at each frequency. An estimate of the P.S.D. for the finite sample of the trend alone is of the form predicted by Equation 2. A further discussion of the contamination of data trends is offered in Appendix A.

2.5 Frequency Domain Smoothing

In general, it is also necessary to smooth the estimate of the P.S.D. in the frequency domain. This necessity is due to the fact that an uncertainty exists between the estimate of the magnitude and the frequency resolution based on the length of the data sample. Two types of spectral windows are employed in Appendix A; one based on a linear average and the other on an exponentially weighted average. The concept of spectral windows is well developed in the literature[13] and no further discussion will be undertaken here except to make two observations.

(1) The concept of an exponentially weighted average for smoothing in the frequency domain appears promising and arguments as to the time domain effect of this spectral window can be made which are essentially reciprocals of the arguments made in Section 2.4.

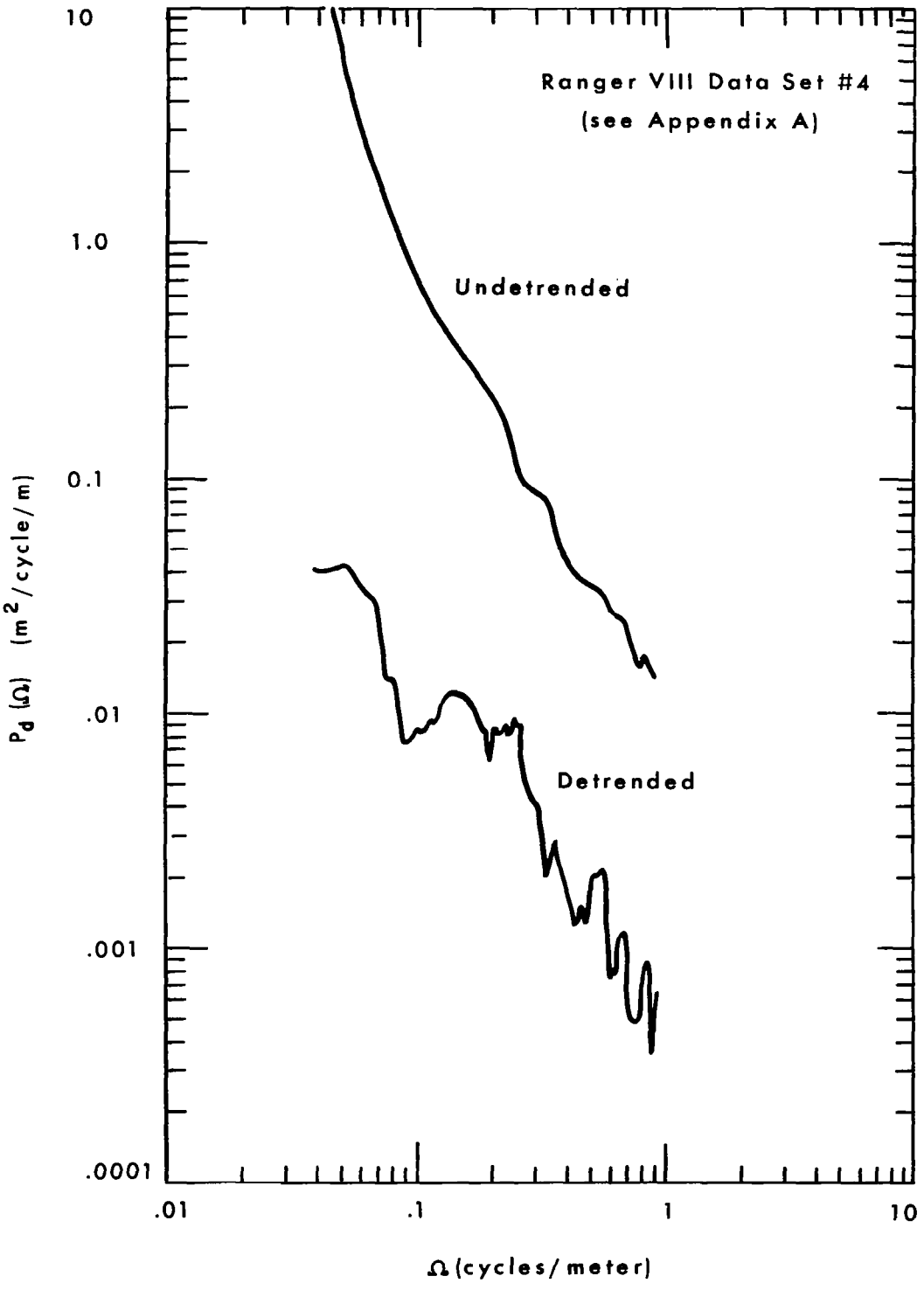

Figure 5 COMPARISON OF DETRENDED AND UNDETRENDED P.S.D.

(2) Assuming a spectral shape, as in Equation 2, and forcing the data to fit this shape, results in the ultimate in frequency domain smoothing. Thus, for the P.S.D., if the frequency content is fixed, an accurate estimate of the magnitude can be obtained from rather crude data.

2.6 Variance

In order to expand on the second observation above, it is of interest to explore the concept of variance. Variance is a measure of the deviation from the mean and, in the case of a surface profile, is a measure of roughness. The variance is also the integral on frequency of the P.S.D. Thus, it would appear from Equation 2, that the variance of the surface profile would be:

$$\text{Var} = \sigma^2 = \int_0^\infty C\,\Omega^{-2}\, d\Omega \tag{11}$$

The integral of Equation 11 does not exist however, due to the singularity at zero frequency. This is another way of looking at the need for space domain smoothing. It was noted in Section 2.4 that the exponentially weighted average detrending is a 6 db per octave filter with zero phase shift. The significance of this technique is that the exponential character allows a rigorous frequency domain interpretation of the space domain filtering. Substituting the square of the filter transfer function (the power ratio) into Equation 11 gives Equation 12, which can be integrated (See Appendix A).

$$\text{Var} = \sigma^2 = \int_0^\infty \frac{C\,\Omega^{-2}\, d\Omega}{\left[1 + \left(\frac{1}{2\pi\Omega\lambda}\right)^2\right]^2} = \frac{C\pi^2\lambda}{2} \tag{12}$$

Equation 12 shows the relationship between the variance of the data, detrended with filter constant λ, and the value of C. This relationship is important for two reasons.

(1) It allows a verification of the surface profile frequency content predicted by Equation 2. That is, it is possible to detrend data with different values of λ and compute variance. If the computed value of C is invariant with changes in λ then Equation 2 is valid. Table 2 gives such a comparison for two different λ's using the Lunar data of Figure 5. This method can also be used to establish the maximum usable value of λ since the value of C will be substantially increased by effective trends.

(2) If Equation 2 is a valid description of the surface, it is possible to compute C and thus the P.S.D. of a surface profile from only the variance of the detrended data. In the case where crude data is available this estimate is expected to be more rigorous than the actual P.S.D. calculation.

Table 2 COMPUTATION OF C FOR LUNAR DATA

λ (meters)	Variance (meters^2)	C (meters)
5	6.15×10^{-3}	2.5×10^{-4}
1	1.29×10^{-3}	2.6×10^{-4}

2.7 Variance of Slope Calculation

To show the relationship between the slope calculation of Section 2.1 and the value of C, consider the following argument. The height of a sinusoid is given by:

$$Y = \sin (2\pi \Omega x) \tag{13}$$

The height difference $\triangle Y$ over an increment $\triangle L$ is:

$$\triangle Y = \sin\left[2\pi\Omega(\triangle L + x)\right] - \sin(2\pi\Omega x) \tag{14}$$

The variance of $\triangle Y$ over the entire range of the sine wave is:

$$\begin{aligned} \text{Var}(\triangle Y) &= \underset{X\to\infty}{\text{Limit}} \frac{1}{2X}\int_{-X}^{X}(\triangle Y)^2\,dx \\ &= \frac{1}{2\pi}\int_{0}^{2\pi}\left[\sin(2\pi\Omega(\triangle L + x)) - \sin(2\pi\Omega x)\right]^2 d(2\pi\Omega x) \\ &= 2\sin^2(\pi\Omega\triangle L) \end{aligned} \tag{15}$$

Equation 15 is the variance of the height change for a fixed base length $\triangle L$ and a unit amplitude sine wave. Slope variance is:

$$\text{Slope Var} = \frac{\text{Var}(\triangle Y)}{(\triangle L)^2} = \frac{2\sin^2(\pi\Omega\triangle L)}{(\triangle L)^2} \tag{16}$$

In order to convert Equation 16 to the P.S.D. form for a surface profile, Equation 2 is utilized to give the "amplitude" of the sine wave. This yields:

$$P_s(\Omega, \triangle L) = \left[C\Omega^{-2}\right]\frac{4\sin^2(\pi\Omega\triangle L)}{(\triangle L)^2} = 4\pi^2 C\left[\frac{\sin(\pi\Omega\triangle L)}{\pi\Omega\triangle L}\right]^2 \tag{17}$$

A factor of two has been included in Equation 17 to account for the convention that the variance is the integral of the P.S.D. on frequency from 0 to ∞. Equation 17 gives the formula for the variance of the slope due to the contribution of the surface roughness in a unit frequency range about Ω for a fixed $\triangle L$.

For a true differentiation of the profile $\triangle L \to 0$ and Equation 17 becomes:

(18)

Noting that the P.S.D. of the derivative of a function is equal to $(2\pi \Omega)^2$ times the P.S.D. of the function, Equation 18 is consistent with Equation 2 and predicts that the slope P.S.D. is "white" or independent of frequency.

The effect of the "artificial" differentiation by using a fixed $\triangle L$ can be seen by comparing Equation 17 with Equation 18. At zero frequency the two are identical but at any frequency above zero the artificial differentiation gives an attenuation as shown in Figure 6. The variance of the fixed $\triangle L$ slope calculation can be computed by integrating Equation 17 over frequency.

$$\sigma_s^2 = \int_0^\infty 4\pi^2 C \left[\frac{\sin(\pi \Omega \triangle L)}{\pi \Omega \triangle L}\right]^2 d\Omega = \frac{2\pi^2 C}{\triangle L} \tag{19}$$

The standard deviation of the slope is then:

$$\sigma_s = \pi \left(\frac{2C}{\triangle L}\right)^{1/2} \tag{20}$$

Many times slope is measured in degrees (see Section 2.1). For practical values of $\triangle L$ the angle is less than 10°, and the tangent of the angle is approximately equal to the angle. Thus:

$$\sigma_s \text{ (in degrees)} = \frac{180\ \sigma_s}{\pi} = 180 \left(\frac{2C}{\triangle L}\right)^{1/2} \tag{21}$$

Equation 21 allows a calculation of the value of C from slope distribution data. While detrending is important in this case it is not as crucial as in the profile determination since the singularity at $\Omega = 0$ no longer exists. Detrending should be accomplished in the original data before conversion to slope information, but this is difficult if the data is originally in slope form. Direct substitution of a slope variance (from USGS data or similar data) will yield only an approximate value of C and this approximation is dependent on the trend of the data sample.

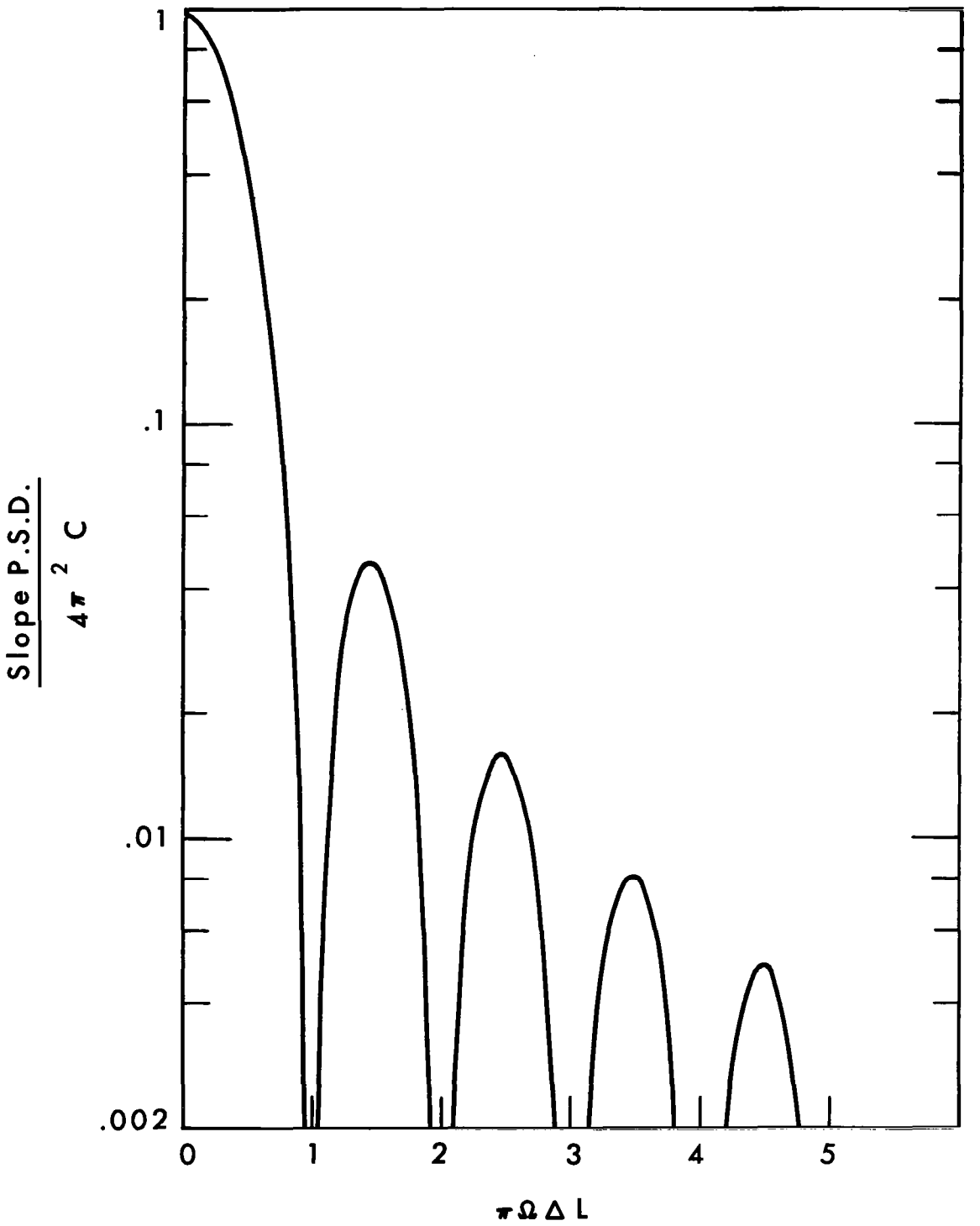

Figure 6 FREQUENCY CONTAMINATION OF FIXED ΔL SLOPE CALCULATION

2.8 Spacial and Temporal Frequencies

For vehicle model analysis, temporal frequencies are usually of interest since vehicle resonances are functions of time. The transformation between spacial frequency (cycles/meter) and temporal frequency (hertz or cps) is that of the speed of a vehicle over the surface as given by expressions 22.

$$f(\text{cycles/sec}) = \Omega\,(\text{cycles/meter})\ V\ (\text{meters/sec})$$

$$P(f)\ (\text{meters}^2/\text{cycles/sec}) = P(\Omega)\ (\text{meters}^2/\text{cycles/meter})\ \frac{1}{V}\ (\text{sec/meter}) \qquad (22)$$

Substituting these relationships in Equation 2 yields:

$$P_d(f) = VCf^{-2} \qquad (23)$$

Similarly substituting expressions 22 into Equation 18 yields:

$$P_v(f) = 4\pi^2\ VC \qquad (24)$$

Equation 24 is an important concept since it states that the vertical velocity input P.S.D. to a vehicle traversing the surface is white.

Equations 23 and 24 show an interesting relationship with vehicle speed. The level of the input to the vehicle is directly proportional to vehicle speed. If the vehicle system is linear it is predicted that the vibrational activity of the vehicle will increase in direct proportion to the speed.

2.9 Amplitude Probability Distribution

The P.S.D. defines the frequency content of a random stationary variable F(x). In addition to the frequency content the amplitude distribution must be defined to completely specify the variable in a statistical fashion. The amplitude probability distribution (A.P.D.)

is the probability that the function F(x) will exceed the level Y. If a finite sample of a continuous random stationary function F(x) is available, an estimate of the A.P.D. is the percent of the horizontal distance that the function is above the level Y as given by Equation 25.

$$\text{A.P.D. } (Y) = \frac{1}{X} \int_0^X \delta(F(x) > Y)\, dx \tag{25}$$

Where $\delta(F(x) > Y)$ is defined by the relation:

$$\delta(F(x) > Y) = 1 \text{ if } F(x) \geq Y$$

and

$$\delta(F(x) > Y) = 0 \text{ if } F(x) < Y \tag{26}$$

If the data is available as digital points, an estimate of the A.P.D. can be determined by counting the number of points above the given level and determining the ratio of this number to the total number of available points as a function of the level Y. A digital computer program written to perform this estimation is presented in Appendix A. The A.P.D. function has the form shown in Figure 7. The derivative of this function is the amplitude probability density function, also shown in Figure 7, which is the familiar bell-shaped or normal curve for a Gaussian distribution. The amplitude probability density function is a measure of the probability that the level of the function is in the increment $\triangle Y$ about Y.

Figure 8 shows three examples of amplitude probability density plots of the slope distribution for the lunar surface from the United States Geological Survey. Appendix A includes a number of A.P.D. plots calculated from digital traces from Ranger VIII photographs. It is noted that in every case the Gaussian distribution is predicted within the statistical reliability of the data available.

Probability Distribution Function

Probability Density Function

Figure 7 PROBABILITY DISTRIBUTION & DENSITY FUNCTION

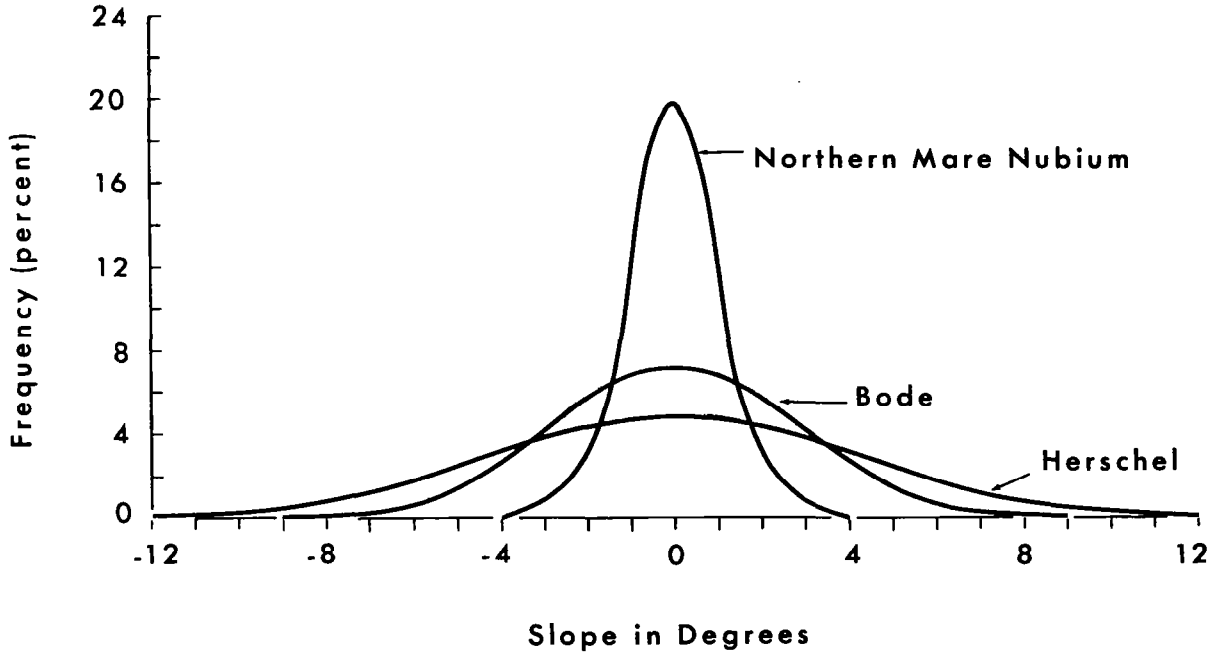

Figure 8 TYPICAL SLOPE FREQUENCY DIAGRAMS

If a process is Gaussian with zero mean, the standard deviation is sufficient to completely define the A.P.D. and thus the probability of exceeding any given level. As was noted previously the variance (and thus its square root, the standard deviation) is undefined for an undetrended surface profile as predicted by Equation 2. If the profile is detrended, the variance is directly proportional to the exponential parameter λ as given by Equation 12, and the standard deviation is given by the relationship.

$$\sigma = \left(\frac{C\pi^2\lambda}{2}\right)^{1/2} \tag{27}$$

Thus, the parameter C completely specifies the P.S.D. of the surface profile and also specifies the A.P.D. of the detrended profile as a function of the exponential parameter λ. This detrending will, of course, lower the estimate of the probability at each level; but if the data sample is long enough the significant portion determined by vehicle dynamics characteristics can be maintained.

2.10 Summary of Surface Roughness

It has been shown that the power spectral densities of virgin terrestrial and extraterrestrial surfaces have a constant shape (as depicted by Equation 2). This shape predicts that no predominant frequency component exists and that the amplitude of the various frequency components is proportional to their wave length. Available information also shows that the amplitude probability distribution of surface roughness is Gaussian. It is concluded that discrepancies, from either of these well behaved functions, which are estimated from finite data samples are due to either the trend effects of the available sample or artifacts in the particular surface which are non-representative and therefore should be ignored in a statistical surface description. It is, therefore, suggested that a single parameter (C from Equation 2) completely specifies the roughness of representative profile traces in a statistical sense. While available information does not

allow accurate measures of either the amplitude probability distribution or the power spectral density, it does allow rather accurate measures of the properly detrended variance (and thus C via Equation 12). Using the above arguments, both the P.S.D. and the A.P.D. can be estimated from a knowledge of the variance. This surface model is used to characterize random inputs for prediction and analysis of vehicle motions.

III. YIELDING SURFACE DYNAMIC MODEL

A considerable amount of work has been done in soft-soil mechanics, but most of this activity has been directed toward the prediction of vehicles under equilibrium conditions. Methods exist to predict drawbar pull, power requirements, sinkage, etc., but there is no comprehensive theory for dynamic wheel-soil interaction. In order to explore this area, a simple dynamic soil model has been developed. The details of the soil model and its relationship with existing soft-soil mechanics is discussed in Appendix B. The purpose of this section is to briefly define the soft-soil model, to show a method of incorporating the influence of vehicle speed over the surface, and to give an analog computer network capable of simulating wheel-soil interaction.

3.1 Soil Model

It is shown in Appendix B that a mass-spring-damper system with a highly non-linear spring rate is a reasonable model for vertical soil reaction to loading of a fixed area flat plate. This model is represented by the schematic of Figure 9 and has the form of Equation 28.

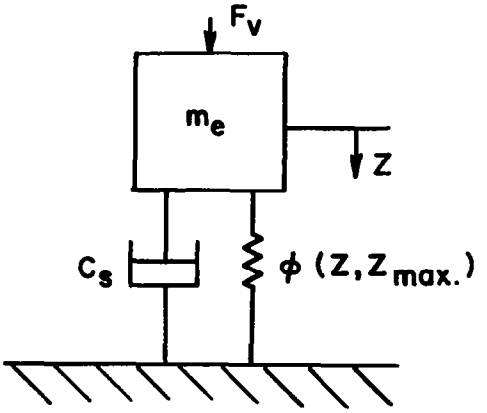

Figure 9 SOIL MODEL

$$m_e \ddot{Z} + C_s \dot{Z} + \phi (Z, Z_{max}) Z = F_v \tag{28}$$

The effective mass (m_e) represents the inertia effect of the soil in proximity of the loading area. From elastic theory this effective mass is:

$$m_e = c_1 \rho \left(\frac{A}{\pi}\right)^{3/2} \tag{29}$$

C_s has the form of a linear viscous damping coefficient and represents the energy dissipation due to radiation damping (pressure wave propagation in a semi-infinite medium) from elastic theory.

$$C_s = \frac{A b_o}{\pi} \left(\frac{E \rho}{2 + 2\nu}\right)^{1/2} \tag{30}$$

$\phi (Z, Z_{max})$ is the spring rate which is a function of the sinkage Z and the maximum penetration Z_{max}. If $Z < Z_{max}$ then $\phi (Z, Z_{max})$ is the elastic recovery rate k_s given by

$$\phi (Z, Z_{max}) \text{ for } Z < Z_{max} = \frac{C E \sqrt{A}}{1 - \nu^2} = k_s \tag{31}$$

In Equations 29, 30 and 31:

A = area of wheel footprint

ρ = Soil mass density (See Table B-5)

ν = Poisons Ratio for Soil (See Table B-4)

E = Young's Modulus for Soil (See Table B-3)

c_1 and b_o are constants depending on ν (See Table B-2)

C is a constant depending on A (See Table B-1)

If $Z = Z_{max}$ (consolidation), $\phi (Z, Z_{max})$ is a non-linear rate derived from standard plate penetrometer measurements of sinkage versus pressure. Bekker Equations[19], Assur Equations[22] or similar equilibrium relationships can be used for definition of this functional relationship (See Appendix B).

3.2 Analog Computer Circuit

An analog computer network which simulates soil behavior as characterized by Equation 28, is shown in Figure 10.

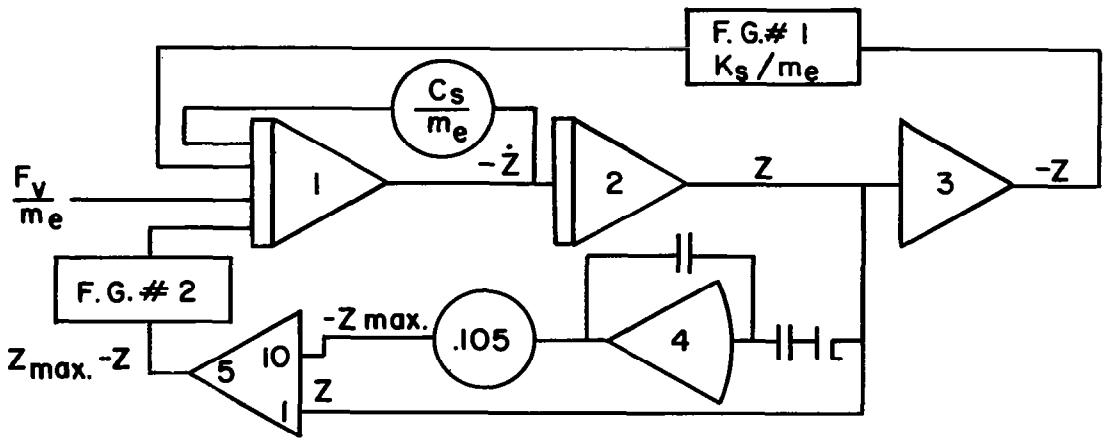

Figure 10 ANALOG COMPUTER NETWORK FOR SOIL MODEL

Amplifiers 1, 2 and 3 and function generator No. 1 form a feedback loop which represents the effect of initial soil loading (consolidation). Function generator No. 1 is programmed to provide the non-linear pressure sinkage curve divided by the effective soil mass. The damping coefficient around amplifier 1 is the linear damping constant C_s/m_e. Amplifiers 4 and 5 and function generator No. 2 form a compensation circuit which becomes active only when the soil penetration is less than the maximum penetration. Amplifier 4 has one microfared capacitive input and feedback. It acts as a summing amplifier since the input and feedback impedances are equal, but it has the additional capacity of storing. The diode in front of this amplifier cuts off the signal at any time the stored value of maximum penetration is less than the actual value of penetration at that time. The maximum penetration is then subtracted from the actual penetration in amplifier 5. If this difference is zero (initial loading) there is no input to the

circuit through function generator 2. If this difference is less than zero, function generator 2 is programmed to add the proper spring rate such that the sum of the outputs of the two function generators gives the linear spring constant k_s divided by m_e. The potentiometer between amplifiers 4 and 5 is used only to compensate for the non-zero cut-off point of the diode and is not necessary if the computer used has a hard limiter. Using function generators for the non-linear functions, it is possible to duplicate any realistic curve both for initial loading of the soil and for the recovery phase.

In order to simulate the effect of traversing the surface at a constant velocity V_x, it is necessary to change the characteristics of amplifier 4 in Figure 10. This amplifier is essentially the memory circuit for maximum penetration. One method of simulating the effect of a wheel traversing the surface is to give amplifier 4 a "poor memory". The memory deterioration is a function of the time it takes to replace the wheel contact area. If the wheel loading were constant there would be no need to compensate for speed effects on the vertical motion since a constant sinkage, i.e., maximum penetration, would be maintained independent of horizontal position for a homogeneous soil. A dynamic loading due to surface profile effects on the soil and vehicle, however, requires a recovery of the maximum penetration as new soil is encountered. In order to investigate this phenomenon consider the two idealized wheel models (a) and (b) in Figure 11. Model (a) is a rigid circular wheel of radius R which encounters a bump of height H. In this representation the path of the wheel center is an arc of a circle of radius R. The duration of the bump encounter is: (See Reference 14).

$$t = \left(\frac{2RH - H^2}{V_x^2}\right)^{1/2} \tag{32}$$

Thus the duration of the bump encounter is a function of the height of the bump H which is not very practical for a random input. It does suggest however that the radius R is a reasonable estimate of

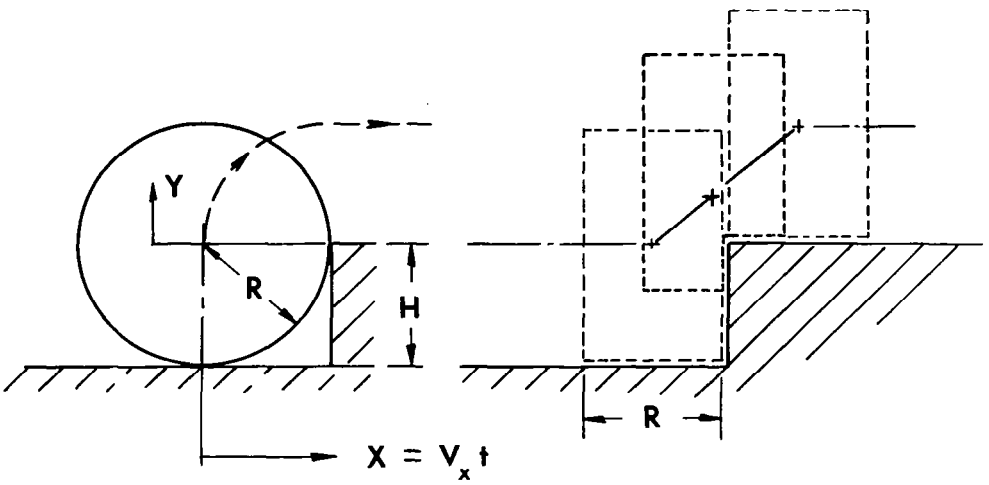

(a) Rigid Wheel (b) Enveloping Wheel

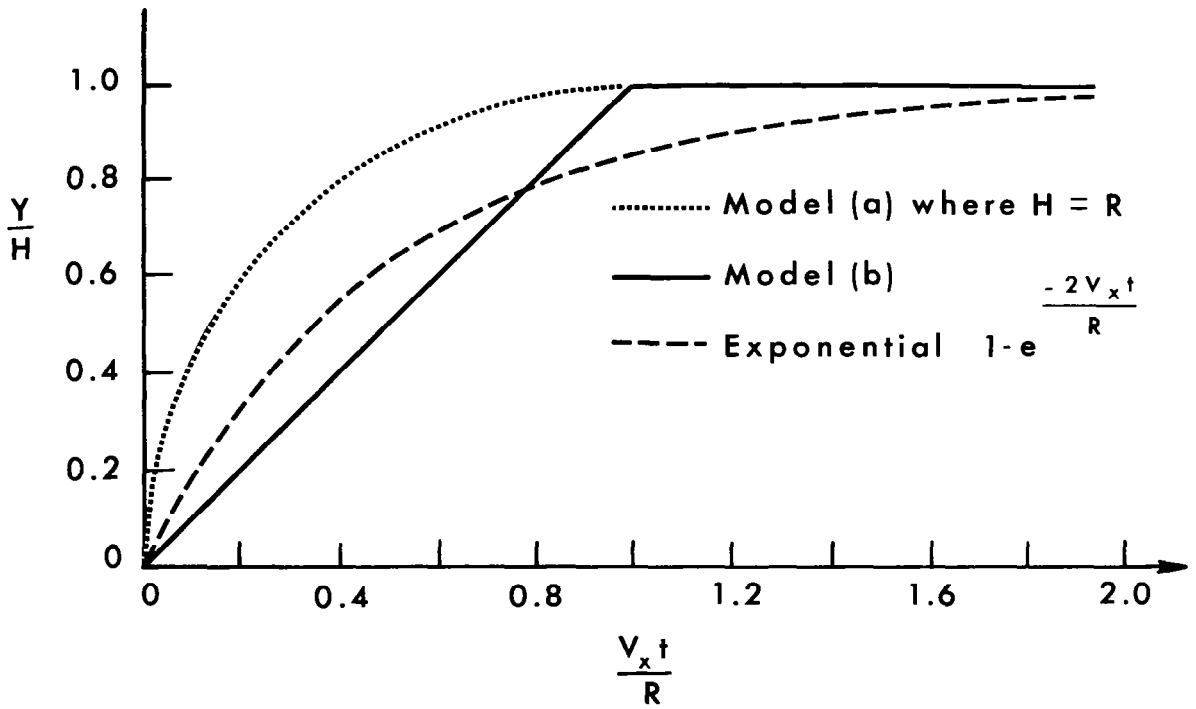

Figure 11 SURFACE RESTORATION vs VEHICLE SPEED

the contact length. The other extreme, model (b) is an idealized enveloping wheel where the height of the hub is directly proportional to the percent of the contact length that has encountered the bump. Assuming that the contact length is equal to the radius this gives the bump duration, independent of bump height, as:

$$t = \frac{R}{V_x} \tag{33}$$

A more realistic compromise [15] between these two idealized extremes is the exponential function shown in the graph of Figure 11. Using this exponential function as the memory deterioration gives the convolution integral of Equation 34. This is the instantaneous maximum penetration under a moving wheel, which is a function of time, vehicle speed and wheel radius as well as the past history of penetration.

$$Z_{max}(t, V_x, R) = \frac{2V_x}{R} \int_{-\infty}^{t} Z(\tau)\, e^{\frac{2V_x}{R}(\tau - t)}\, d\tau \tag{34}$$

In order to simulate this effect in the analog computer circuit, the capacitors on both the input and feedback of amplifier 4 in Figure 10 have been replaced by an R-C network having a time constant equal to $2V_x/R$. This maintains the inversion characteristic of amplifier 4 when $Z = Z_{max}$, since the input and feedback impedances are still equal, but has the effect of giving the memory circuit for maximum soil penetration an exponential decay such that new soil is always being encountered.

3.3 Surface Vehicle Interaction

It will be assumed, for the purpose of argument, that the lower element representing a vehicle wheel is a mass which might be considered the rim mass of a flexible steel wheel. Figure 12

shows a representation of this mass above the soil model of Figure 9.

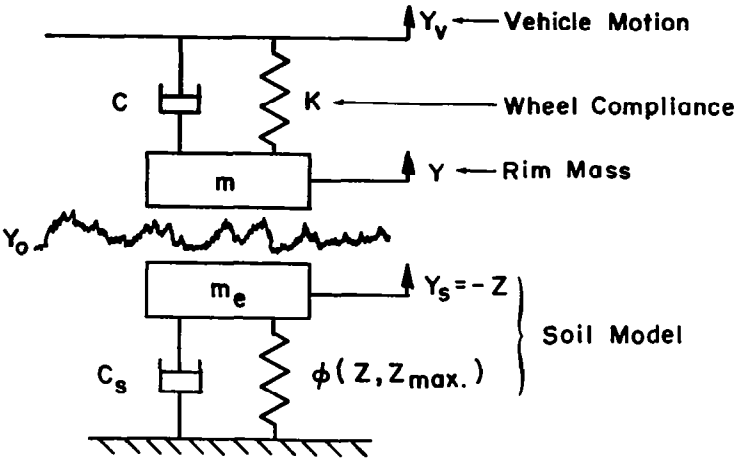

Figure 12 WHEEL-SOIL INTERACTION MODEL

The equations of motion describing this system are givey by:

$$\text{Rim Mass} \quad m\ddot{Y} = -C(\dot{Y} - \dot{Y}_v) - K(Y - Y_v) + F_v \tag{35}$$

$$\text{Surface} \quad m_e\ddot{Y}_s = -C_s\dot{Y}_s - \phi(Z, Z_{max})Y_s - F_v \tag{36}$$

where

$$F_v = \infty \text{ if } Y < Y_s + Y_o$$

$$F_v = 0 \text{ if } Y \geq Y_s + Y_o$$

The random surface profile Y_o determined by the statistical classification of Section II, is interposed between the rim mass and the effective soil mass in such a fashion that the wheel rim cannot penetrate the deformed surface profile. The wheel however, can leave the surface resulting in surface-vehicle separation. This effect is simulated by a high gain amplifier with a diode in the feedback as shown in Figure 13. The output of the high gain amplifier is proportional to the force F_v acting on the vehicle model in the upward direction and the surface model in the downward direction.

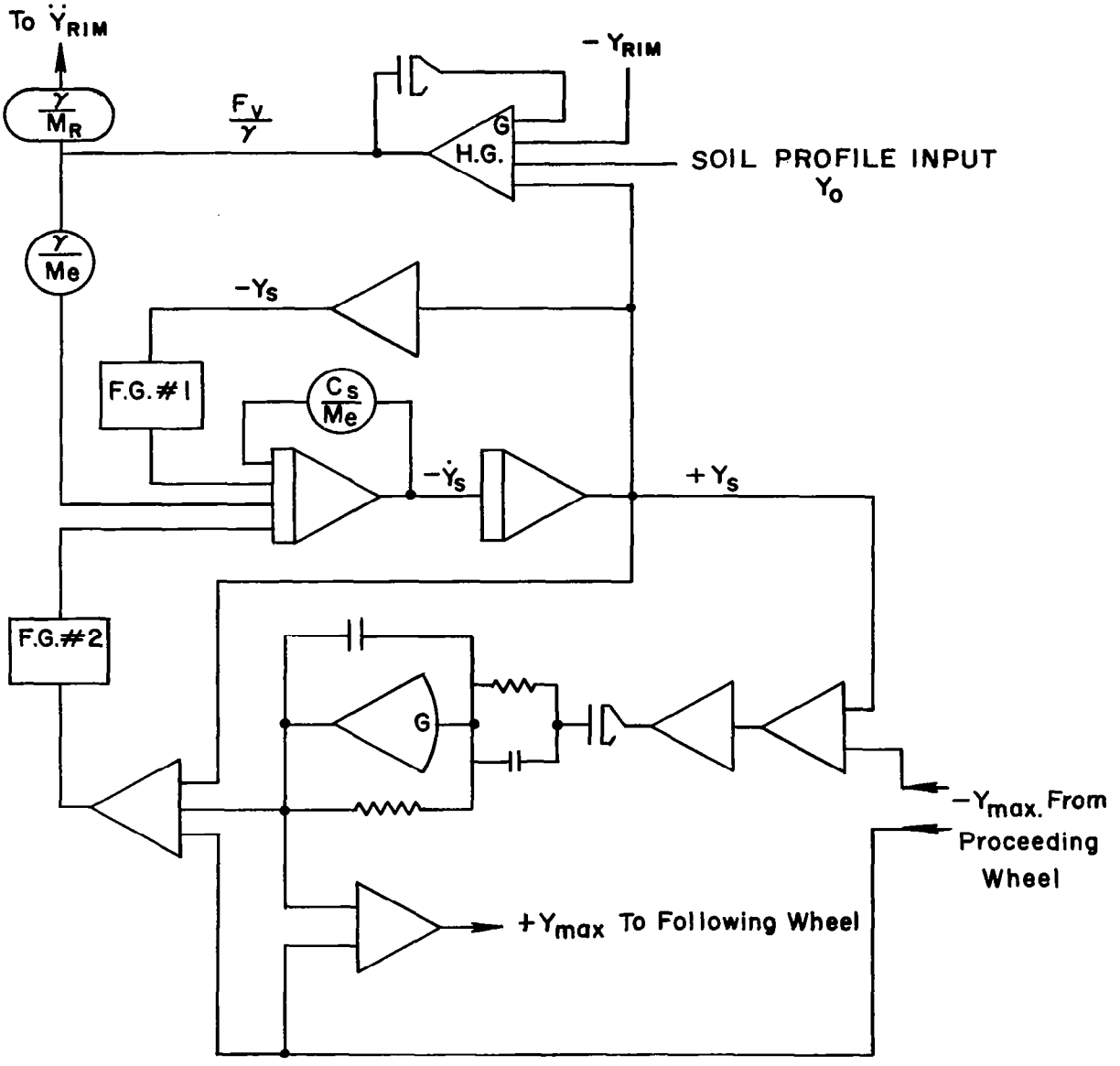

Figure 13 Analog Network for Yielding Soil Under Moving Vehicle

3.4 Effect on Following In-Line Wheels

In order to account for the effect of a preceding wheel on a following in-line wheel, it is necessary to record two functions and time delay these for input to the following wheel. The first function is the surface profile which must be delayed and fed into the following in-line wheel-soil model. The second is the effect of the maximum surface penetration of the preceding wheel as an instantaneous value. This will be used to set the memory circuit of the following wheel to a present maximum penetration. The following wheel then will encounter the stiff spring constant k_s until such time that it penetrates below the maximum penetration of the preceding wheel. In this case the circuit will act as before and the non-linear initial loading function will come into effect. Actually the profile that the rear wheel sees is not the same profile that the front wheel has seen, but it is this profile altered by the dynamic effects of the preceding wheel. In order to account for this phenomenon the maximum instantaneous penetration of the front wheel is added to the surface profile as shown in Figure 13. In this way the following wheel sees a new profile dictated by the difference between the initial profile to the preceding wheel and the maximum penetration at that point. This allows for smoothing effects on the profile roughness due to the traverse of the preceding wheel. This circuit may be duplicated n times to simulate n in-line following wheels where the input to each wheel is taken from the wheel immediately preceding the one in question.

IV. VEHICLE MODEL ANALYSIS

The purpose of this study is to develop techniques which can be employed in the analysis of vehicle motion once a model has been specified, rather than to analyze any specific vehicle model. To this end, Appendix C outlines the traditional methods for a lumped parameter vehicle representation and defines coordinate systems and transformation of coordinates. A general n-wheeled rigid body model is developed in Appendix C together with the analog computer network necessary for its simulation.

In order to implement and demonstrate the methods of analysis outlined below, a simple four wheeled vehicle model was chosen which is presented in Appendix C. Appendix D presents a frequency domain analysis of this model using transfer functions for a linear version and Appendix E presents a non-linear version analyzed in the time domain through analog computer simulation.

4.1 Frequency Domain Approach

A linear vehicle model is necessary to analyze vehicle motions using transfer function concepts in the frequency domain. The linear assumption necessitates a non-yielding surface (or at most, a linear yielding surface) and a vehicle speed below that which would cause surface-vehicle separation. While this approach places rather severe restrictions on model analysis, it does allow a convenient solution which yields a good deal of insight into vehicle behavior.

This output P.S.D. for a linear system with one input is given[16] by:

$$P_o(\omega) = |T(\omega)|^2 P_i(\omega) \tag{37}$$

That is, the output P.S.D. $P_o(\omega)$ is related to the input P.S.D. $P_i(\omega)$ through the square of the transfer function for a linear system. The phase information in the transfer function has thus

been ignored and only a "real" number function exists which represents the square of the magnitude amplification as a function of frequency, (i.e., the product of the transfer function and its complex conjugate).

If more than one random input is imposed on the linear system then the response P.S.D. $P_{aa}(\omega)$ at point a in the system for n inputs is given by:[7, 16]

$$P_{aa}(\omega) = \sum_{i=1}^{n} \sum_{k=1}^{n} T_{ai}\, T_{ak}^{*}\, P_{ik}(i\omega) \tag{38}$$

where T_{ai} is the transfer function between the $i^{\underline{th}}$ input and the output at a, T_{ai}^{*} is the complex conjugate of T_{ai} and $P_{ik}(i\omega)$ is the appropriate cross-spectral density. The cross-spectral density is a function which shows relationship between two functions in the frequency domain (see Appendix A). If the two functions are identical it becomes the usual P.S.D. which measures the variance of the function as a function of frequency. In general, however, if the functions are related, but not identical, it has both a real and an imaginary component. The real component (co-spectral density) measures the covariance of the "in phase" relationship of the functions as a function of frequency and the imaginary component (quadrature spectral density) measures the "out of phase" covariance. It should be noted that P_{ik} and P_{ki} are complex conjugates. If the functions in question are independent random functions then the cross-spectral density is zero.

Thus the phase relationships have been ignored in going to the random input approach, but the phase between inputs (wheels of the vehicle) cannot be ignored. If a certain phase predominately exists this will influence the motion. For example, if the front and rear wheels are predominately out of phase the pitch motion of the vehicle will be excited to a greater extent than the bounce motion.

4.1.1 Input Considerations

The P.S.D. of the slope input for a vehicle model analysis will now be chosen as the representative equation for an extraterrestrial surface as given by Equation 18 and reproduced below:

$$P_s(\Omega) = 4\pi^2 C \tag{39}$$

where C is the constant from Equation 2 which is a measure of surface roughness. The auto-covariance of an ideal white function (constant P.S.D. of Equation 38) can be defined in terms of the Dirac delta function by the following argument.

$$\phi(a) = 4\pi^2 C \delta(a) \tag{40}$$

$$P_s(\Omega) = \int_{-\infty}^{\infty} 4\pi^2 C \delta(a) e^{-i 2\pi \Omega a} da = 4\pi^2 C \tag{41}$$

Equation 39 states that the surface roughness correlates with itself only with zero space difference. Two parallel traces across the surface (inputs to left and right side of the vehicle) would therefore have no correlation and a zero cross-spectral density. (Appendix A shows an attempt to estimate the cross-spectral density between two parallel traces spaced approximately a vehicle tread width apart from available information of the lunar surface.) It can, therefore, be assumed for constant velocity straight line travel, that the inputs to the left and right sides of the vehicle are separate members of an ergodic set having the P.S.D. given by Equation 39.

For following in-line wheels, however, the situation is different. The same function acts as an input to the wheels with only a spacial difference (the distance between wheels d). Thus, with a space lag d the cross covariance of the two input functions is a Dirac delta function or:

$$\phi_{(1,2)}(a) = 4\pi^2 C \delta(a - d) \tag{42}$$

$$\text{or} \qquad C.S.D. = \int_{-\infty}^{\infty} 4\pi^2 C \, \delta(a - d) \, e^{-i 2\pi \Omega a} \, da$$

$$= 4\pi^2 C \, e^{-i 2\pi \Omega d} = 4\pi^2 C \left[\cos 2\pi \Omega d - i \sin 2\pi \Omega d\right] \tag{43}$$

4.1.2 *Vehicle Consideration*

Differential equations of motion are written for each degree of freedom of the linear model (See Appendix C). These equations are transformed (via Fourier Transform) to complex variable algebraic equations for frequency domain calculations. If more than 3 or 4 degrees of freedom are considered, it is necessary to employ a digital computer to obtain the appropriate transfer functions in numeric form. These transfer functions can be tabulated to give the magnitude and phase relationship between each input (wheel) and each output of interest (See Appendix D.)

The transfer function can be combined via Equation 38 by the arguments of Section 4.1.1 to give an output velocity P.S.D. at each point of interest in the vehicle. In the temporal frequency domain (cps or hertz) this yields Equation 44 for an n-wheeled vehicle.

$$P_v(f) \text{ at point } a = 4\pi^2 C V_x \sum_{i=1}^{n} \left[|T_{ai}|^2 \right. \tag{44}$$

$$\left. + \Re \left\{ 2 \sum_{k=1}^{i-1} \delta_{ik} \text{ (in line) } T_{ai} T_{ak}^{*} \left(\cos 2\pi f \frac{d_{ik}}{V_x} - i \sin 2\pi f \frac{d_{ik}}{V_x}\right) \right\} \right]$$

$P_v(f)$ = output velocity P.S.D. at point a $\left[(\text{meters/sec})^2 / \text{cps}\right]$

C = surface roughness coefficient [meters]

V_x = vehicle speed [meters/sec]

T_{ai} = Transfer function between i^{th} input and point a (dimensionless for translational output and having dimensions of radians/meter for angular output)

$\mathcal{R}$ = Symbol for "real part of"

δ_{ik} (in line)= 1 if inputs i and k are for in-line following wheels and zero otherwise.

T^*_{ak} = complex conjugate of T_{ak}

f = frequency (cps)

d_{ik} = horizontal distance between input i and k (meters)

The first term in Equation 44 is the square of the modulus of each transfer function times the input P.S.D. The second term is the interaction effects due to in-line following wheels. The two terms for interaction between each pair of in-line wheels (which are complex conjugates in Equation 38) have been combined to give twice the real part.

Equation 44 gives a velocity output P.S.D. for each degree of freedom (a) of interest in the vehicle. To compute a displacement or acceleration P.S.D. it is merely necessary to multiply the velocity P.S.D. at each frequency by $\frac{1}{4\pi^2 f^2}$ or $4\pi^2 f^2$ respectively.

4.1.3 Output Considerations

Since the input function is Gaussian, the output motions of the linear vehicle model will also be Gaussian. The variance and thus the standard deviation of the output can be calculated by integrating the appropriate P.S.D. over the desired frequency range. Knowing the standard deviation it is possible to calculate the probability of exceeding any predetermined value. These values might be the lunar g for lift-off, and static equilibrium angles for roll over and pitch over (See Appendix D).

4.2 Time Domain Approach

A time domain approach is used to analyze non-linear systems. Differential equations of motion are written for the system, to characterize the activity of various elements using Newton's Second Law (See Appendix C). These differential equations are programmed on an analog computer such that the various components in the computer behave in a manner analogous to the physical system. In order to compute the response of the system to a deterministic input it is necessary to have two surface profile traces properly spaced for the vehicle tread width recorded in continuous fashion on magnetic tape. Properly spaced tape heads allow reproduction of the signals at the proper time to excite the trailing wheels in the vehicle model. Vehicle speed is controlled by either changing the computer "time scaling" or by changing the playback speed of the tape.

If random inputs are employed the velocity input can be generated by a random Gaussian noise generator (See Appendix E.).

4.2.1 Input Considerations

The random surface profile Y_o is interposed between the vehicle rim mass and the effective soil mass, such that the wheel rim cannot be below the sum of the surface penetration and the profile input as shown in Figure 12. This effect is simulated by a high gain amplifier with a diode allowing surface-vehicle separation as shown in Figure 13.

A random Gaussian white noise generator is used for the velocity input for time domain analysis. The white noise velocity input is integrated to give a displacement input for insertion in the circuit of Figure 14. The integrator shown has a cut-off frequency $f = \frac{1}{2\pi\lambda}$ which is below any frequency of interest for vehicle motions. This is similar to the detrending (space

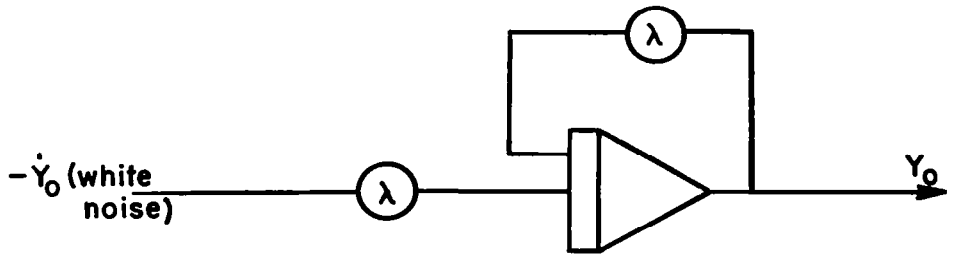

Figure 14 INTEGRATION WITH TIME DOMAIN SMOOTHING

domain smoothing) effects of the surface profile as discussed in Section II. While this integration does not adequately account for surface slope characteristics it is necessary to achieve drift free stability in the analog simulation. The static surface slope can be taken into account in the analysis of the output.

The method of determining the level of the white noise input is to filter the white noise between two frequencies f_1 and f_2, (values of 0.5 cps and 100 cps were used in Appendix E) and take the mean square value of the result using an analog computer circuit[12]. The gain can then be adjusted to give

$$\text{Mean Square input volts} = 4\pi^2 C V (f_2 - f_1) \left(\frac{\alpha}{\beta}\right)^2 \qquad (45)$$

C = surface roughness coefficient (meters)

V = vehicle speed (meters/sec)

f_2 = upper cut-off frequency (cps)

f_1 = lower cut-off frequency (cps)

α = computer voltage scaling (volts/meter)

β = computer time scaling (machine seconds/second)

If the inputs are for wheels which are not following in-line wheels (such as left and right side of a vehicle), then separate noise generators can be used, each adjusted to the proper level.

In order to account for the effect of a preceding wheel on a following in-line wheel two functions are time delayed for input to the following wheel. The first function is the surface profile which must be delayed and fed into the following in-line wheel-soil model. The second is the effect of the maximum surface penetration of the preceding wheel as an instantaneous value as discussed in Section 3.4.

4.2.2 Output Considerations

The outputs of the analog computer simulation are voltages which represent the displacement and its derivatives (velocity and acceleration) at each point in the vehicle model. These can be processed, using analog computer techniques, to give direct estimates of the P.S.D. or A.P.D. at the point in question (see reference 12 and Appendix E).

In addition, the probability of meeting limiting values can be easily estimated using analog circuitry. Hard limiters(or diodes) can be employed to give a pulse output at each time the roll or pitch displacement exceeds some static equilibrium limit. While in reality, the vehicle operator would normally employ an evasive action prior to roll-over, counting the number of roll-overs in a given distance traveled is a convenient method for vehicle comparison. The percent of time that lift-off occurs for any one wheel or any combination of wheels can be measured in a similar fashion (See Appendix E).

V. SUMMARY

A statistical analysis technique has been developed for the classification of virgin terrestrial and extraterrestrial surfaces. It has been demonstrated from available data that the power spectral density of profile height for a traverse across the lunar surface is equal to $C\Omega^{-2}$. C is the surface roughness coefficient and Ω is spacial frequency. A six db per octave, zero phase shift filter has been devised and implemented to detrend finite digital data samples and thus allow an accurate estimate of the surface roughness coefficient. Available information shows that the amplitude probability distribution of surface roughness is Gaussian. The variance can be computed by integrating the P.S.D. over the frequency range of interest and it is sufficient to predict the probability of exceeding any given level. Thus, the single parameter C completely specifies the surface roughness in a statistical sense (see Section II and Appendix A).

A dynamic non-linear yielding surface model has been developed from existing information of soil mechanics. This model includes the hysteresis due to initial soil compaction and effects of vehicle speed and loading area (see Section III and Appendix B).

Traditional analog computer techniques have been used to simulate lumped parameter models of typical lunar vehicles. An analog computer network, capable of accurately predicting the dynamic response of vehicles traversing yielding and non-yielding surfaces (see Appendix C) has been developed and implemented. A technique is included which allows a random surface profile to be introduced between the vehicle model and the yielding surface model and allows vehicle-surface separation. The probability of exceeding design limits can easily be predicted, from this model analysis, and used for vehicle design optimization.

An early NASA concept vehicle model was used to demonstrate the stochastic techniques of model analysis. Appendix D describes a linear frequency domain analysis of this vehicle model on a non-yielding surface using transfer function concepts. In this case a random input was determined from lunar surface roughness. The probability of exceeding design limits was predicted by computing the variance of vehicle motion and assuming a Gaussian output distribution based on the linear system model and Gaussian input.

Appendix E describes the time domain analysis for a non-linear version of the same vehicle model on a yielding surface using the analog network. In this case the prediction of meeting limiting constraints can be directly measured from analog output.

VI. CONCLUSIONS AND RECOMMENDATIONS

6.1 Conclusions

The following conclusions result from the general investigation and theoretical development reported herein.

(1) The properly interpreted variance of the surface profile is sufficient to completely specify, in a statistical sense, the surface roughness of a virgin terrestrial or extra-terrestrial surface.

(2) A statistical technique has been devised and implemented for analog computer solution which is considered the best available method for analyzing vehicle motions excited by rough yielding and non-yielding surfaces.

6.2 Recommendations

The following recommendations are made in the interest of aiding future research programs tailored toward surface classification and vehicle performance.

(1) A generalized digital computer program should be written to allow statistical analysis of digital profile height and slope information and classification of surface roughness.

(2) Statistical techniques should be developed and implemented in the form of computer prediction of vehicle power requirement, mobility analysis, LEM landing site acceptability analysis, and other key engineering applications based on the surface roughness classification.

(3) Further study is needed to establish the validity of the yielding surface model and an experimental program should be undertaken with a typical vehicle on a yielding terrestrial surface.

(4) Complete statistical dynamic response analysis should be made using the latest lunar vehicle designs being developed, for the purpose of establishing more complete design criteria and design modifications.

REFERENCES

1. Bodeau, A. C., Bollinger, R. H., and Lippin, L.: "Passenger Car Suspension Analysis," S.A.E. Trans., Vol. 64, 1956, pp 273-283.

2. Kohr, R. H.: "Analysis and Simulation of Automobile Ride," S.A.E. Paper 144A, March 1960.

3. Grimes, C. K.: "Development of a Method and Instrumentation for Evaluation of Runway Roughness Effects on Military Aircraft, NATO AGARD," Report 119, 1957.

4. Thompson, W. E.: "Measurements and Power Spectra of Runway Roughness at Airports in Countries of the North Atlantic Treaty Organization," NACA TN 4303, 1958.

5. Silby, N. S.: "An Analytical Study of Effects of some Airplane and Landing Gear Factors on the Runway Roughness with Application to Supersonic Transports." NASA TN D-1492, December 1962.

6. Tung, C. C., Penzien, J., Horonjeff, R.: "The Effect of Runway Unevenness on the Dynamic Response of Supersonic Transports." NASA CR-119, October 1964.

7. Van Deusen, B. D.: "A Study of the Vehicle Ride Dynamics Aspects of Ground Mobility - MERS Project." Vol. I "Summary", April, 1965.

8. Kozin, F., Cote, L. J., Bogdanoff, J. L.: "Statistical Studies of Stable Ground Roughness," Land Locomotion Laboratory Report No. 8391, November 1963.

9. Eisenbaum, F., Schloss, M.: "Bi-Parameter Universal Random Surface," Bendix Systems Division Research Report, No. 1082, January, 1965.

10. Van Deusen, B. D.: "A Study of the Vehicle Ride Dynamics Aspects of Ground Mobility - MERS Project." Vol. IV "Field Measurements," April, 1965.

11. Hutchinson, B. G.: "Analysis of Road Roughness Records by Power Spectral Density Techniques." Dept. of Highways, Ontario, Canada, Report No. 101.

12. Van Deusen, B. D.: "Data Acquisition and Statistical Analysis Using Analog Computer Techniques," 1963 S.A.E. Transactions, pp. 350-357.

13. Blackman and Tukey: "The Measurement of Power Spectra." Dover Publications, Inc., New York, 1958.

14. Van Deusen, B. D.: "Preliminary Lunar Vehicle Dynamics Study." Technical Report No. 18114.1, Engineering Staff, Chrysler Corporation, July, 1964.

15. Watts, D. G.: "Practical Averaging Circuits," Mathematics Research Center, United States Army, The University of Wisconsin, MRC Technical Summary Report No. 518, October, 1964.

16. Aseltine, J. A.: "Transform Method in Linear Systems Analysis," McGraw-Hill (Electric and Electronic Series), 1958.

17. Rindfleisch, T.: "A Photometric Method for Deriving Lunar Topographic Information." Technical Report No. 32-786. Jet Propulsion Laboratory, California Institute of Technology, Pasadena, California, Sept. 16, 1965.

18. Kemeny, J. G. and Krutz, T. E.: "Basic," Dartmouth College Computation Center, June, 1965.

19. Bekker, M. G.: Theory of Land Locomotion. University of Michigan Press, Ann Arbor, Mich., 1956.

20. Wismer, R. D., and Smith, M. E.: Discussion of "An Analysis of Pneumatic Tire Performance in Deformable Soils - Z. Janosi." Proceedings First International Conference Soil Vehicle Mechanics, Turin, Italy, 1961.

21. Reece, A. R.: "Problems of Soil Vehicle Mechanics." Report 8470 (LL 97), U. S. Army Tank-Automotive Center, Warren, Michigan, March, 1964.

22. Assur, A.: "Locomotion Over Soft Soil and Snow." Paper No. 782F, Automotive Engineering Congress, Society of Automotive Engineers, Detroit, Michigan, January, 1964.

23. Barkan, D. D.: "Dynamics of Bases and Foundations." Chapter 1, Elastic Properties of Soil , McGraw-Hill, 1962.

24. Hall, J. R., Jr., and Richart, F. E., Jr.: "Dissipation of Elastic Wave Energy in Granular Soils." Proceedings American Society of Civil Engineers, Vol. 89, No. SM6, pp. 27-56, 1963.

25. Weissman, G. F., and Hart, R. R.: "The Damping Capacity of some Granular Soils, American Society Testing Materials, Special Technical Publication No. 305, pp 45-54, 1961.

26. Whitman, R. V.: "Analaysis of Foundation Vibrations." Massachusetts Institute of Technology, Department of Civil Engineering. Paper presented at Symposium on Man-Made Vibrations in Civil Engineering, British National Section, International Association for Earthquake Engineering, London, April, 1965.

27. Reissner, E.: "Stationare, axialsymmetrische durch eine schuttelnde Masse erregte Schwingungen eines homogenen elastischen Halbraumes." Ingenieur-Archiv, Vol. 7, pp 381-396, December, 1936.

28. Sung, T. Y.: "Vibrations in Semi-Infinite Solids due to Periodic Surface Loading." American Society Testing Materials, Special Technical Publication No. 156, pp. 35-68, 1953.

29. Bycroft, G. N.: "Forced Vibrations of a Rigid Circular Plate on a Semi-Infinite Elastic Space and an Elastic Stratum" Philosophical Transactions Royal Society of London, Series A, Vol. 248, pp. 327-368, 1956.

30. Hsieh, T. K.: "Foundation Vibrations." Proceedings Institution of Civil Engineers, Vol. 22, pp. 211-226, 1962.

31. Lysmer, L.: "Vertical Motion of Rigid Footings." U. S. Army Engineer Waterways Expediment Station, Contract Report No. 3-115, Vicksburg, Mississippi, June, 1965.

32. Bycroft, G. N.: "Machine Foundation Vibrations." Proceedings Institution Mechanical Engineers, Vol. 173, No. 18, pp. 469-473, 1959.

33. Liston, R. A., and Hegedus, E.: "Dimensional Analysis of Load Sinkage Relationships in Soils and Snow." Technical Report 8692 (LL 100), U. S. Army Tank-Automotive Center, Warren, Michigan, December, 1964.

34. Bussman, Dr. Dale R.: "Vibrations of a Multi-Wheeled Vehicle," Systems Research Group, Department of Industrial Engineering, The Ohio State University, Columbus, Ohio, Systems Research Group Report No. RF-573 TR 64-1 (U) August 1964.

35. Kozin, F. and Bogdanoff, J. L.: "On the Statistical Analysis of the Motion of Some Simple Two Dimensional Linear Vehicles Moving on a Random Track," Land Locomotion Laboratory, Research Division Report No. RR-19 LL-66, April 1960.

36. Crafton, P. A., "Shock and Vibration in Linear Systems," Harper and Brothers, Publishers, New York.

37. Guillemin, E. A., "Theory of Linear Physical Systems," John Wiley and Sons, Inc., New York.

38. Van Deusen, B. D.: "A Study of the Vehicle Ride Dynamics Aspect of Ground Mobility - MERS Project." Vol. III "Theoretical Dynamics Aspects of Vehicle Systems", April, 1965.

APPENDIX A

ANALYSIS OF LUNAR SURFACE ROUGHNESS

ANALYSIS OF LUNAR SURFACE ROUGHNESS

By: G. E. McCarron and V. J. Borowski

This appendix is a development of the mathematical concepts necessary to characterize surface roughness in a statistical fashion and a presentation of the analysis of some of the available data from Ranger photographs.

A.1 Theory

This section is a development of the theory and mathematical concepts as applied to the processing of Ranger data and classification of the lunar surface roughness.

A.1.1 Determination of Spectral Density

The power spectral density (P.S.D.) is the second moment or variance density spectrum. In order to determine the P.S.D. for a surface, the profile record must be a sample function from a stationary random process.[13] Stationarity implies that the mean value and higher moments are space invariant. P.S.D. of a random function, f(x), is defined as the Fourier transform of its autocovariance. The average height of the profile function f(x) is expressed in Equation A-1.

$$\overline{f(x)} = \underset{X\to\infty}{\text{Limit}} \frac{1}{2X} \int_{-X}^{X} f(x)\, dx \qquad (A-1)$$

In order to compute a meaningful autocovariance the average must be zero. This can be achieved by subtracting the average value from each of the points in the original function.

$$F(x) = f(x) - \overline{f(x)} \qquad (A\text{-}2)$$

The autocovariance, $\phi(a)$, is defined by Equation A-3.

$$\phi(a) = \underset{X \to \infty}{\text{Limit}} \frac{1}{2X} \int_{-X}^{X} F(x)\ F(x + a)\, dx \qquad (A\text{-}3)$$

The P.S.D. is defined by Equation A-4.

$$P(\Omega) = 2 \int_{-\infty}^{\infty} \phi(a)\, e^{i 2\pi \Omega a}\, da \qquad (A\text{-}4)$$

The factor of 2 in Equation A-4 is due to the convention adopted in this report, that the integral on frequency from 0 to ∞ of the P.S.D. is the variance. The P.S.D. can be obtained by direct substitution of Equation A-3 into Equation A-4.

$$P(\Omega) = 2 \int_{-\infty}^{\infty} \left\{ \underset{X \to \infty}{\text{Limit}} \frac{1}{2X} \int_{-X}^{X} F(x)\, F(x + a)\, dx \right\} e^{-i 2\pi \Omega a}\, da \qquad (A\text{-}5)$$

If $F(x)$ is a well behaved function, in the mathematical sense, the above expression may be written as:

$$P(\Omega) = \underset{X \to \infty}{\text{Limit}} \frac{1}{X} \int_{-\infty}^{\infty} \left\{ \int_{-X}^{X} F(x)\, F(x + a)\, dx \right\} e^{-i 2\pi \Omega a}\, da \qquad (A\text{-}6)$$

It is now convenient to define a new function $H(x)$ such that

$$H(x) = \begin{cases} F(x) & \text{for} \quad x \leq |X| \\ 0 & \text{for} \quad x > |X| \end{cases}$$

By changing the order of integration Equation A-6 may be written: (A-7)

$$P(\Omega) = \underset{X \to \infty}{\text{Limit}} \frac{1}{X} \int_{-\infty}^{\infty} \left\{ \int_{-\infty}^{\infty} H(x + a)\, e^{-i 2\pi \Omega (x + a)}\, da \right\} H(x)\, e^{i 2\pi \Omega x}\, dx$$

The Fourier transform $S(\Omega)$ of $H(x)$ is defined as:

$$S(\Omega) = \int_{-\infty}^{\infty} H(x)\, e^{-i 2\pi \Omega x} dx = \int_{-\infty}^{\infty} H(x + a)\, e^{-i 2\pi \Omega (x + a)} dx \qquad (A-8)$$

Substituting Expression A-8 into Equation A-7 gives

$$P(\Omega) = \underset{X\to\infty}{\text{Limit}} \frac{1}{X} S(\Omega)\, S(-\Omega) = \underset{X\to\infty}{\text{Limit}} \frac{1}{X} \left| S(\Omega) \right|^2 \qquad (A-9)$$

$$= \underset{X\to\infty}{\text{Limit}} \frac{1}{X} \left| \int_{\infty}^{\infty} H(x)\, e^{-i 2\pi \Omega x} dx \right|^2 = \underset{X\to\infty}{\text{Limit}} \frac{1}{X} \left| \int_{-X}^{X} F(x)\, e^{-i 2\pi \Omega x} dx \right|^2$$

Equation A-9 states that the P.S.D. of a random function $F(x)$, is the average of the square of the modulus of its finite Fourier transform in the limit as the averaging time goes to infinity.

Using Euler's theorem the final form of Equation A-9 can be expanded to yield.

$$P(\Omega) = \underset{X\to\infty}{\text{Limit}} \frac{1}{X} \left| \int_{X}^{X} F(x) \cos(2\pi\Omega x)\, dx - i \int_{-X}^{X} F(x) \sin(2\pi\Omega x)\, dx \right|^2 \qquad (A-10)$$

The two functions $A(\Omega)$ and $B(\Omega)$ will now be introduced and defined as follows:

$$A(\Omega) = \frac{1}{X} \int_{-X}^{X} F(x) \cos(2\pi\Omega x)\, dx \qquad (A-11)$$

$$B(\Omega) = \frac{1}{X} \int_{-X}^{X} F(x) \sin(2\pi\Omega x)\, dx \qquad (A-12)$$

Substituting Expressions A-11 and A-12 into Equation A-10 yields:

$$P(\Omega) = \underset{X\to\infty}{\text{Limit}}\ X \left| A(\Omega) - i B(\Omega) \right|^2 = \underset{X\to\infty}{\text{Limit}}\ X \left[A(\Omega)^2 + B(\Omega)^2 \right] \qquad (A-13)$$

A similar relationship between Fourier transforms and cross-spectral density of two related functions, F_1 and F_2, is

$$C(i\Omega) = \underset{X\to\infty}{\text{Limit}} \frac{1}{X}\left[\int_{-X}^{X} F_1(x)\, e^{-i\,2\pi\Omega x}dx\right]\left[\int_{-X}^{X} F_2(x)\, e^{i\,2\pi\Omega x}dx\right] \qquad (A-14)$$

Substituting the Expressions A-11 and A-12 for the functions $F_1(x)$ and $F_2(x)$ into Equation A-14 gives:

$$C(i\Omega) = \underset{X\to\infty}{\text{Limit}}\; X\left\{A_1(\Omega)\,A_2(\Omega) + B_1(\Omega)\,B_2(\Omega) + i\left[A_1(\Omega)\,B_2(\Omega) - A_2(\Omega)\,B_1(\Omega)\right]\right\} \qquad (A-15)$$

The real part of $C(i\Omega)$ is the cospectral density and the imaginary part is the quadrature spectral density.

A.1.2 Estimation of Power Spectral Density

If the profile height Y_i is available at equal increments Δx over a finite length the autocovariance function ϕ_a can then be approximated by the relationship:

$$\phi_a = \frac{1}{n-a}\sum_{i=1}^{n-a} Y_i\, Y_{i+a} \qquad (A-16)$$

The P.S.D. estimate is: (p. 53 Ref. 13)

$$P'(n) = 2\Delta X\left[\phi_o + 2\sum_{a=1}^{m-1}\phi_a \cos\frac{n\,a\,\pi}{m} + \phi_m \cos n\pi\right] \qquad (A-17)$$

Another method of estimation from a finite data sample of length $L = 2X$ is to use Equation A-13 and neglect the limiting process.

$$P(\Omega) = \frac{L}{2}\left[A(\Omega)^2 + B(\Omega)^2\right] \qquad (A-18)$$

The functions $A(\Omega)$ and $B(\Omega)$ are defined in Equation A-11 and A-12 as continuous functions of Ω. These definitions are identical to the Fourier series coefficients

at the discrete frequencies where $\Omega_n = n/L$ and n is a positive integer. Thus, at these discrete frequencies an estimate of the P.S.D. can be defined by Equation A-19.

$$P(n) = \frac{L}{2}\left[A(n)^2 + B(n)^2\right] \qquad (A-19)$$

Due to the inability to accurately resolve any frequency in a finite sample, it is necessary to smooth the spectral estimates from Equation A-17 or A-19 over neighboring frequencies.

$$\overline{P(n)} = \sum_{k=-\infty}^{\infty} A_k P(n-k) \qquad (A-20)$$

The A_k coefficients define a particular spectral window. Table A-1 lists the coefficients for five spectral windows where the first three have been previously published. The last two are linear and exponential windows developed for analysis of lunar surface profiles since it was deemed necessary to smooth the P.S.D. estimates over a wider frequency range for the limited amount of available data. A digital computer program (FOR-5) based on an implementation of Equations A-19 and A-20 is presented at the end of this Appendix.

A.1.3 Stationarity and Space Domain Smoothing

A stationary random process is defined as one whose statistical properties are unaffected by a shift in the scale of the independent variable of the process. Since the length of a data sample determines a lower limit on frequency resolution it is not possible to prove stationarity from a data sample of finite length. Any component of the process with a frequency less than the limiting value appears as a trend or

Table A-1 COEFFICIENTS OF SPECTRAL WINDOWS

Coefficient	Hamming Values	Hanning Values	Akaike Values	Linear Values	Exponential Values
A_o	.54	.50	.42	.11111	.29395
$A_1 = A_{-1}$	.23	.25	.25	.11111	.10531
$A_2 = A_{-2}$	0	0	.04	.11111	.07546
$A_3 = A_{-3}$	0	0	0	.11111	.05407
$A_4 = A_{-4}$	0	0	0	.11111	.03874
$A_5 = A_{-5}$	0	0	0	0	.02776
$A_6 = A_{-6}$	0	0	0	0	.01989
$A_7 = A_{-7}$	0	0	0	0	.01425
$A_8 = A_{-8}$	0	0	0	0	.01212
$A_9 = A_{-9}$	0	0	0	0	.00732
All others	0	0	0	0	0

non-stationary component which will contaminate P.S.D. estimates computed from the data. Two types of common trends found in surface profile traces are shown in Figure A-1. In order to reliably process data it is necessary to eliminate the trends from the data and analyze the results, with the realization that low frequency components have been removed. A numerical filter based on a moving two sided exponentially weighted average was developed to compute the trend for digital data. The data trend $\overline{F(x)}$ at point X as a function of the original data F(x) is given by:

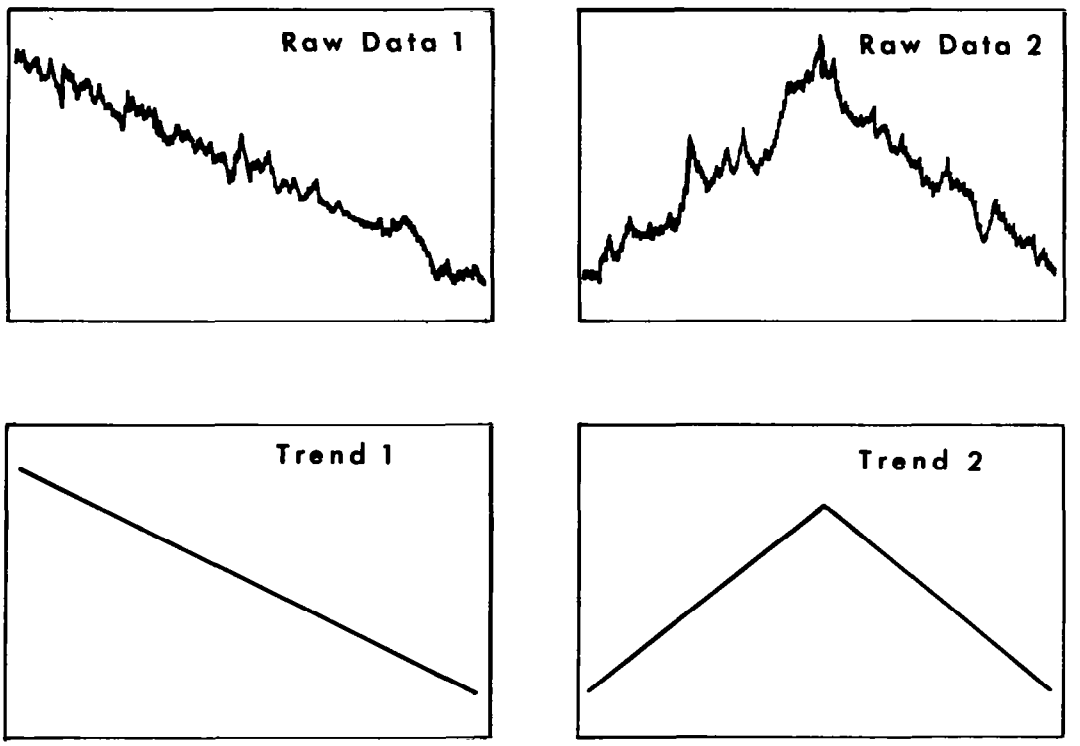

Figure A-1 TWO DATA TRENDS

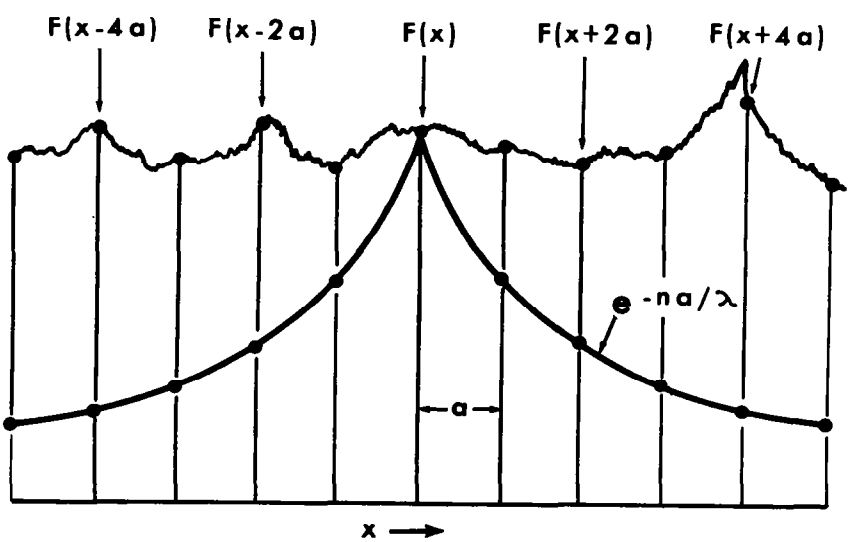

Figure A-2 EXPONENTIAL DETRENDING OF DATA POINTS

$$\overline{F(x)} = \frac{\sum_{n=o}^{\infty} \left[F(x + na) + F(x - na)\right] e^{-na/\lambda}}{2 \sum_{n=o}^{\infty} e^{-na/\lambda}} \qquad (A\text{-}21)$$

Where the notation is explained in Figure A-2.

The detrended or filtered data $F_d(x)$ is then given by the relation:

$$F_d(x) = F(x) - \overline{F(x)} \qquad (A\text{-}22)$$

This type of filtering is similar to an analog electrical high pass filter with the exception that two sided averaging (both past and future) can be performed on digital data to remove phase shift characteristics. To demonstrate this effect consider Equation A-21 in the limit as $n \longrightarrow \infty$ and a becomes a continuous variable. In this limit, Equation A-21 becomes:

$$\overline{F(x)} = \frac{1}{2\lambda} \int_{o}^{\infty} \left[F(x + a) + F(x - a)\right] e^{-a/\lambda} da \qquad (A\text{-}23)$$

If F(x) is now considered to be a continuous signal of the form $\sin(2\pi \Omega x)$, then $F_d(x)$ is:

$$F_d(x) = \frac{\sin(2\pi \Omega x)}{1 + \left(\frac{1}{2\pi \Omega \lambda}\right)^2} \qquad (A\text{-}24)$$

Thus, the detrending filter effects only amplitude of the input and not phase. Equation A-24 affords an insight into the interactions and influences between detrending, the weighting constant λ, and frequency. It can be seen that the amplitude of the detrended function approaches that of the original data for large values of $\Omega\lambda$. That is, for high frequencies or for broad based exponentials, the detrended

function is approximately equal to the original function and little attenuation at this frequency is apparent. Conversely, if the product of $\Omega\lambda$ is very small the amplitude of the detrended function approaches zero and this frequency component is highly attenuated.

From Equation A-24 the transfer function as a function of frequency Ω, and weighting constant λ is:

$$\text{Amp. ratio} = \frac{1}{1 + \left(\frac{1}{2\pi\Omega\lambda}\right)^2} \qquad \text{(A-25)}$$

In practice a finite averaging interval must be used. For this case the transfer function is given by:

$$\text{Amp Ratio} = 1 - \frac{\left[1 + e^{-n}\left\{2\pi\Omega\lambda \sin(2\pi n\Omega\lambda) - \cos(2\pi n\Omega\lambda)\right\}\right]}{(1 - e^{-n})\left[1 + (2\pi\Omega\lambda)^2\right]} \qquad \text{(A-26)}$$

The averaging interval is $-n\lambda$ to $n\lambda$, where n is any positive number and λ is the exponential weighting constant. A weighting over 3λ is reasonable for most practical applications.

Since the sample length is finite, some attention must be given to those points for which the averaging interval extends beyond the end points of the data sample. In order to account for this, the data was extended for a length 3λ beyond each of the end-points by mirror reflection. If the original data is defined as F(x) on the interval (0, L), then this reflection is given by:

$$\begin{aligned} F(x - a) &= F(a - x) \qquad \text{For } x - a < 0 \\ F(x + a) &= F(2L - X - a) \quad \text{For } x + a > L \end{aligned} \qquad \text{(A-27)}$$

This endpoint reflection is a method of estimating the expected value beyond the sample length. This estimate is exact for an even periodic function but causes a distortion near the endpoints for an odd periodic function. Figure A-3 shows the distortion for a unit amplitude sine wave which has been detrended with a weighting constant equal to one tenth the wave length.

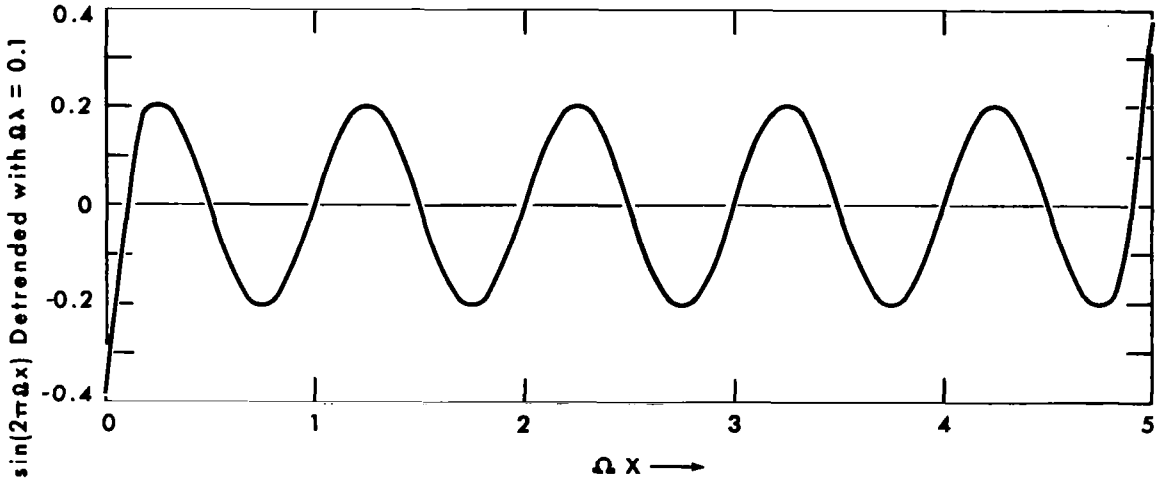

Figure A-3 EFFECT OF END POINT REFLECTION ON DETRENDED ODD FUNCTION

The frequency cut-off or half-power point $\Omega_{1/2}$ is the frequency at which the P.S.D. of the filtered function is one-half of that of the unfiltered function, and is defined as a function of λ by Equation A-28.

$$\Omega_{1/2} = \frac{1}{2\pi\lambda(\sqrt{2}-1)^{1/2}} \qquad \text{(A-28)}$$

The effect of an exponentially-weighted-average filter on an ideal P.S.D. predicted by Equation A-29 is shown in Figure A-4. If a trend is contained in the data sample it

$$P(\Omega) = C(\Omega)^{-2} \qquad \text{(A-29)}$$

is quite likely this trend will increase the estimated P.S.D. at each frequency as shown by the line marked Undetrended Estimate in Figure A-4. This, in effect, would raise the estimated value for the surface roughness constant coefficient C. The two finite data trends shown in Figure A-1 have a P.S.D. estimate similar to the ideal P.S.D. If a substantial trend such as either of these exist in the data it might obscure the real data of interest. Thus, before an accurate estimate of surface roughness can be made the data must be detrended. The effect of detrending on the ideal P.S.D. is also shown in Figure A-4. Here it is noted that detrending removes the lower frequencies.

This figure also indicates the importance of selecting an appropriate exponential weighing factor λ. Excessively large weighting factors will fail to remove the trend completely and the resulting estimates of surface roughness will be high. As the weighting factor is reduced the detrended P.S.D. approaches the ideal and reasonable estimates of surface roughness can be made. As the weighting factor is further reduced, higher frequencies are filtered out, and the estimate of surface roughness can be contaminated by statistical errors in resolving higher frequencies from digital data.

A.1.4 Amplitude Probability Distribution

The amplitude probability distribution (A.P.D.) of a continuous random variable F(x) as given by Equation A-30 defines the probability that F(x) will exceed the level Y.

$$\text{A.P.D. } (Y) = \lim_{X \to \infty} \frac{1}{2X} \int_{-X}^{X} \delta[F(x) > Y]\, dx \qquad \text{(A-30)}$$

where $\delta[F(x) > Y]$ is a delta function defined by Equation A-31.

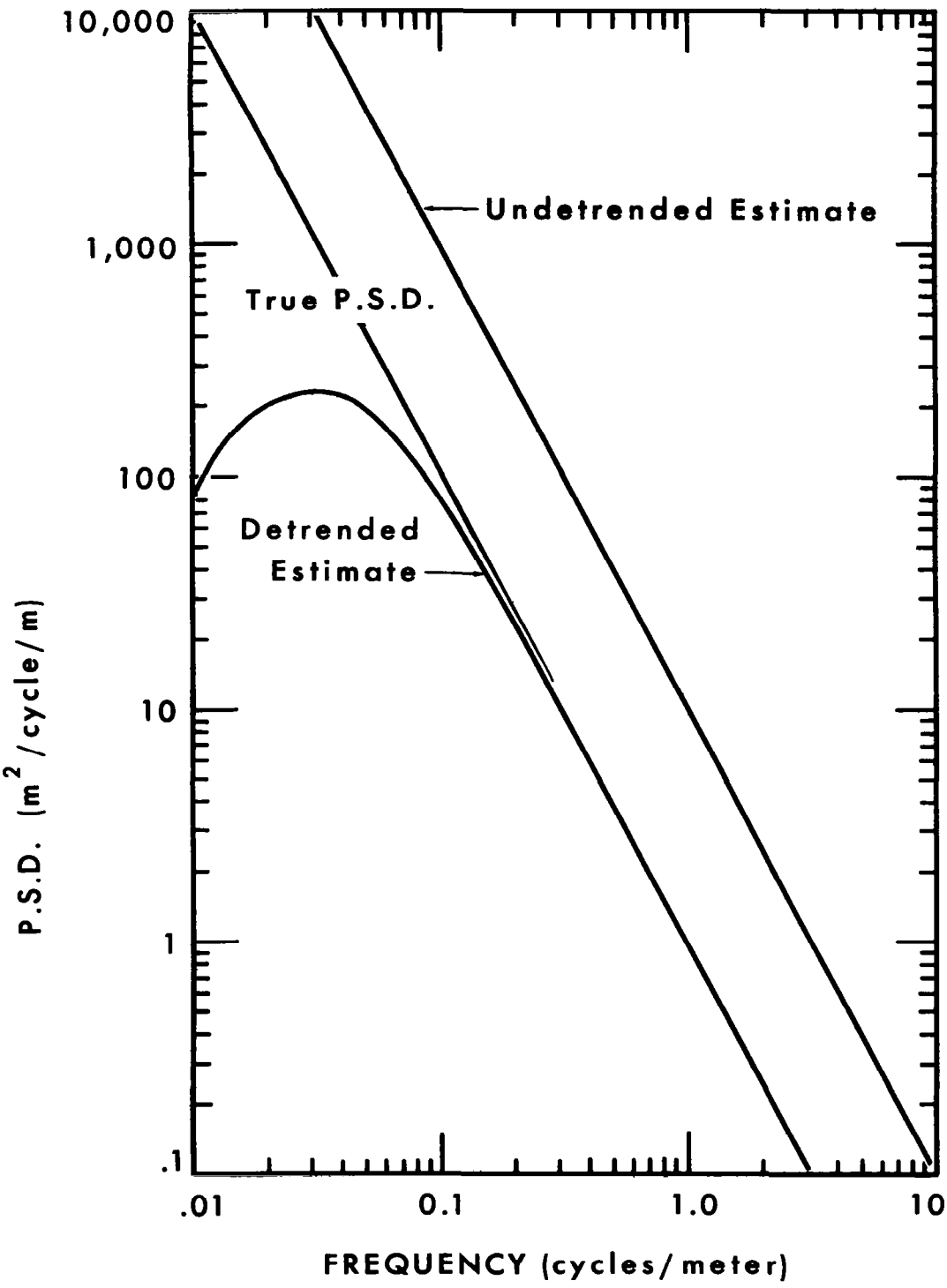

Figure A-4 EFFECT OF EWA FILTER ON P.S.D. ESTIMATE

$$\delta[F(x) > Y] = \begin{cases} 1 \text{ if } F(x) \geq Y \\ 0 \text{ if } F(x) < Y \end{cases} \qquad (A\text{-}31)$$

An estimate of the A.P.D. can be obtained from a finite continuous signal by dropping the limit of Equation A-30 as shown in Equation A-32:

$$A.P.D.\ (Y) = \frac{1}{2X} \int_{-X}^{X} \delta[F(x) > Y]\ dx \qquad (A\text{-}32)$$

where 2X is the data length. For a discrete digital data sample the integration in Equation A-32 is replaced by summation as given by Equation A-33:

$$A.P.D.\ (Y) = \frac{1}{N} \sum_{i=1}^{N} \delta[F(x_i) > Y] \qquad (A\text{-}33)$$

where N is the total number of data points. Equation A-33 was used to calculate the A.P.D. of the Ranger VIII data and the computer program AMPDIS is given at the end of this appendix. In the preceding section it was shown that the presence of a trend in the data sample could lead to erroneous estimations of the P.S.D. It is reasonable to expect that the same is true in the case of A.P.D. Figure A-5 shows the A.P.D. of a linear trend plotted on probability paper. The straight line in the figure is a plot of a Gaussian distribution whose standard deviation is equal to that of the linear trend. Figure A-5 clearly shows that the existence of a trend in the data could indeed lead to misleading estimates of the A.P.D. Thus, as in the case of the P.S.D., the data must be detrended before an accurate estimate of the A.P.D. is possible.

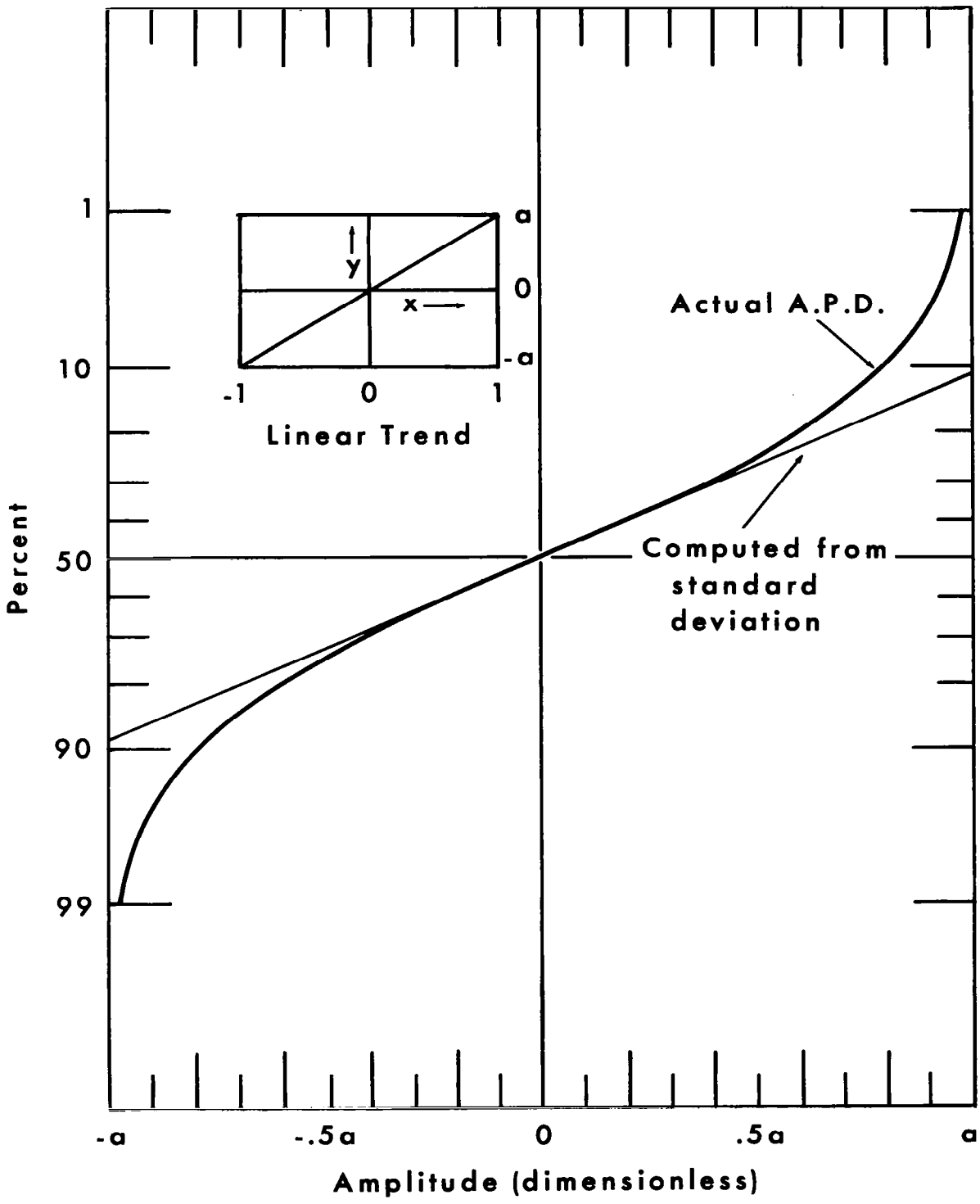

Figure A-5 AMPLITUDE PROBABILITY DISTRIBUTION OF A LINEAR TREND

The effect of detrending on the A.P.D. and the P.S.D. of an actual surface profile is shown in Figure A-6. This figure shows the A.P.D. and P.S.D. of the undetrended profile and of the same profile after it had been detrended, with λ's of 5 and 2 meters respectively.

A.1.5 Variance and Calculation of C

The P.S.D. of a virgin terrestrial or extraterrestrial surface can be closely approximated by Equation A-34.

$$P_d(\Omega) = C\,\Omega^{-2} \qquad \text{(A-34)}$$

The variance of the surface is equal to the P.S.D. integrated over all frequency, or expressed mathematically

$$VAR = \int_0^\infty C\,\Omega^{-2}\, d\Omega \qquad \text{(A-35)}$$

The above integral does not exist due to the singularity at $\Omega = 0$. If a surface profile with a P.S.D. given by Equation A-34 is detrended, the P.S.D. of the filtered function is given by:

$$P_d(\Omega) = \frac{C\,\Omega^{-2}}{\left[1 + \frac{1}{(2\pi\Omega\lambda)^2}\right]^2} \qquad \text{(A-36)}$$

To show this, consider the P.S.D. defined in terms of the Fourier transform as given by Equation A-37.

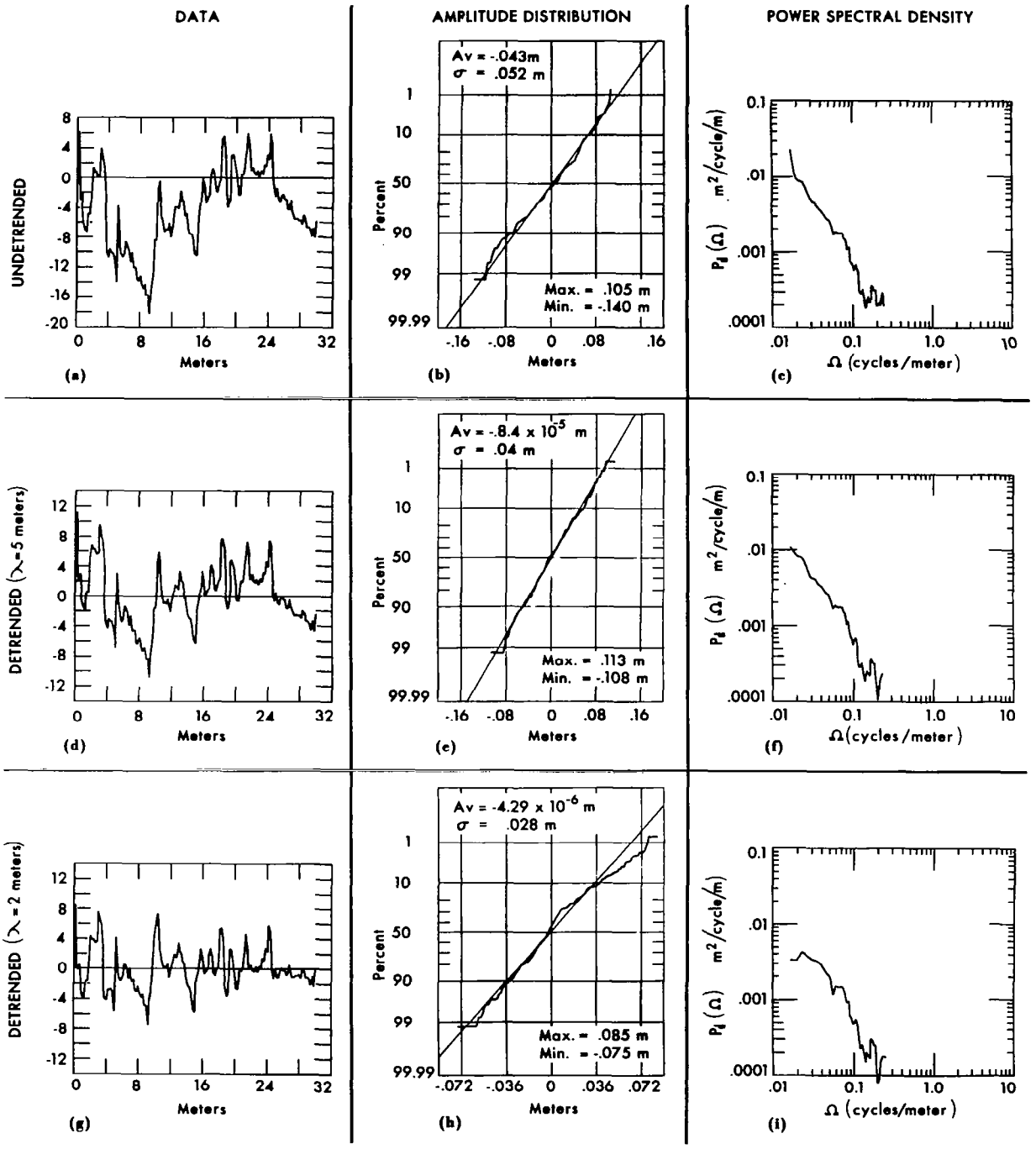

Figure A-6 EFFECT OF DETRENDING ON A.P.D. AND P.S.D.

$$P.S.D. = \underset{X\to\infty}{\text{Limit}} \frac{1}{X} \left| \int_{-X}^{X} F(x)\, e^{-i 2\pi \Omega x} dx \right|^2 = C\Omega^{-2} \qquad (A\text{-}37)$$

If the function F(x) is passed through the detrending filter, the filtered function is given by;

$$\frac{F(x)}{\left[1 + \frac{1}{(2\pi\Omega\lambda)^2}\right]} \qquad (A\text{-}38)$$

If this expression is substituted into Equation A-37 in place of F(x), the P.S.D. of the filtered function is then:

$$P.S.D. = \underset{X\to\infty}{\text{Limit}} \frac{1}{X} \left| \int_{-X}^{X} \frac{F(x)\, e^{-i2\pi\Omega x}}{\left[1 + \left(\frac{1}{2\pi\Omega\lambda}\right)^2\right]} dx \right|^2 \qquad (A\text{-}39)$$

Since the denominator of the integrand above is inherently positive and independent of x it may be factored out, so that Equation A-39 may be written as:

$$P.S.D. = \frac{1}{\left[1 + \left(\frac{1}{2\pi\Omega\lambda}\right)^2\right]^2} \underset{X\to\infty}{\text{Limit}} \frac{1}{X} \left| \int_{-X}^{X} F(x)\, e^{-i2\pi\Omega x} dx \right|^2$$

$$= \frac{C\Omega^{-2}}{\left[1 + \left(\frac{1}{2\pi\Omega\lambda}\right)^2\right]^2} \qquad (A\text{-}40)$$

The variance of the filtered function can now be written as:

$$VAR = \int_0^{\infty} \frac{C\,\Omega^{-2}\,d\Omega}{\left[1 + \left(\frac{1}{2\pi\,\Omega\,\lambda}\right)^{2}\right]^{2}} \qquad \frac{C\pi^2\lambda}{2} \qquad \text{(A-41)}$$

Equation A-41 gives the relationship for the variance of the detrended data, in terms of the filtering constant λ and the P.S.D. constant C. Since variance can be accurately estimated from a finite amount of data, Equation A-41 is a good means of estimating the surface roughness coefficient C and thus the P.S.D.

A.2 Application

In order to show the application of the techniques developed in the preceding section, some of the available information from the Ranger photographs has been processed. This processing was not intended to be a comprehensive analysis, but rather a verification of the techniques developed and allowed a preliminary estimate of the lunar surface roughness for an input to vehicle dynamic analysis.

A.2.1 Analysis of Jet Propulsion Laboratory Data

The Jet Propulsion Laboratory has processed and published[17] some of the available data from Ranger photographs. J.P.L. used the Ranger television scan lines to determine brightness of the lunar surface. The elevation height for a matrix of points covering the photographs, was then determined from this brightness information. A compensation (called a sine wave rectification filter (SWRF)), for camera angle was also attempted in the analysis. The lunar topographical data supplied to Chrysler Corporation

by the Jet Propulsion Laboratory was the elevation and the brightness print-outs (with and without (SWRF)) for the last two P-3 frames from Ranger VIII. The last frame covered an area of about 13,000 square meters. Estimates of surface elevation were provided in a 277 x 373 element matrix covering the surface of this frame. The horizontal distance between elevation points is .381 meters and the vertical definition was .09 meters. The next to last P-3 frame covered an area of about 103,000 square meters. It was decided to use arbitrary profile height traces from these photographs for analysis. Five data sets were analyzed from the last Ranger P-3 frame and one data set was analyzed for the second to the last Ranger P-3 frame. The relative locations and designation of each of these data sets is shown in Figure A-7. All of the data analyzed were compensated for the sine wave response fall-off of the camera (with SWRF). Data Sets 2 and 4 were analyzed prior to detrending to show the effects of detrending. Figure A-8 shows a plot of the raw data for trace 2, the computed trend, and the detrended profile. Figure A-9 shows the same information for Data Set 4. A substantial trend exists in Data Set 4 and, in fact, in all of the profile traces running parallel to this data set. Figure A-10 shows the amplitude probability distribution plots for Data Sets 2 and 4 before and after detrending. The effects of detrending can be seen here in Data Set 4. The trend has a significant influence on the data, making it appear non-Gaussian. The detrended data more nearly approximates a Gaussian distribution. In each case, the straight line on these plots is that of the Gaussian distribution calculated from the variance of the actual data.

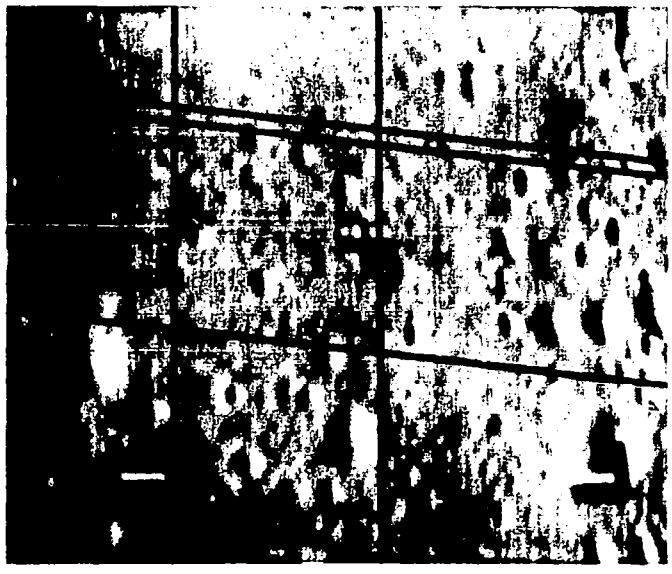

(a) Last P-3 Frame

(b) Next to the Last P-3 Frame

Figure A-7 TRACES ANALYZED FROM RANGER VIII PHOTOGRAPHS

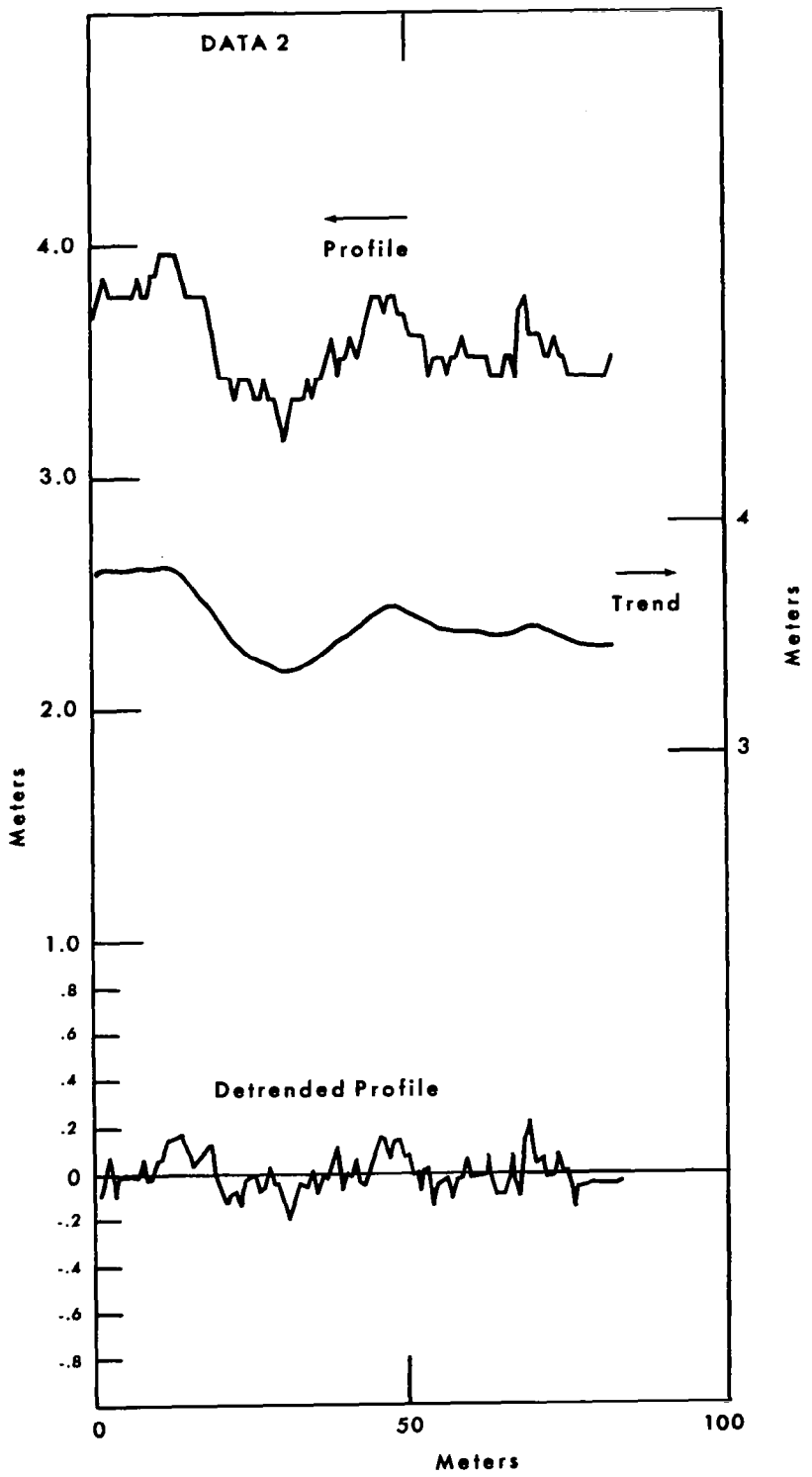

Figure A-8 EFFECT OF DETRENDING ON DATA SET 2

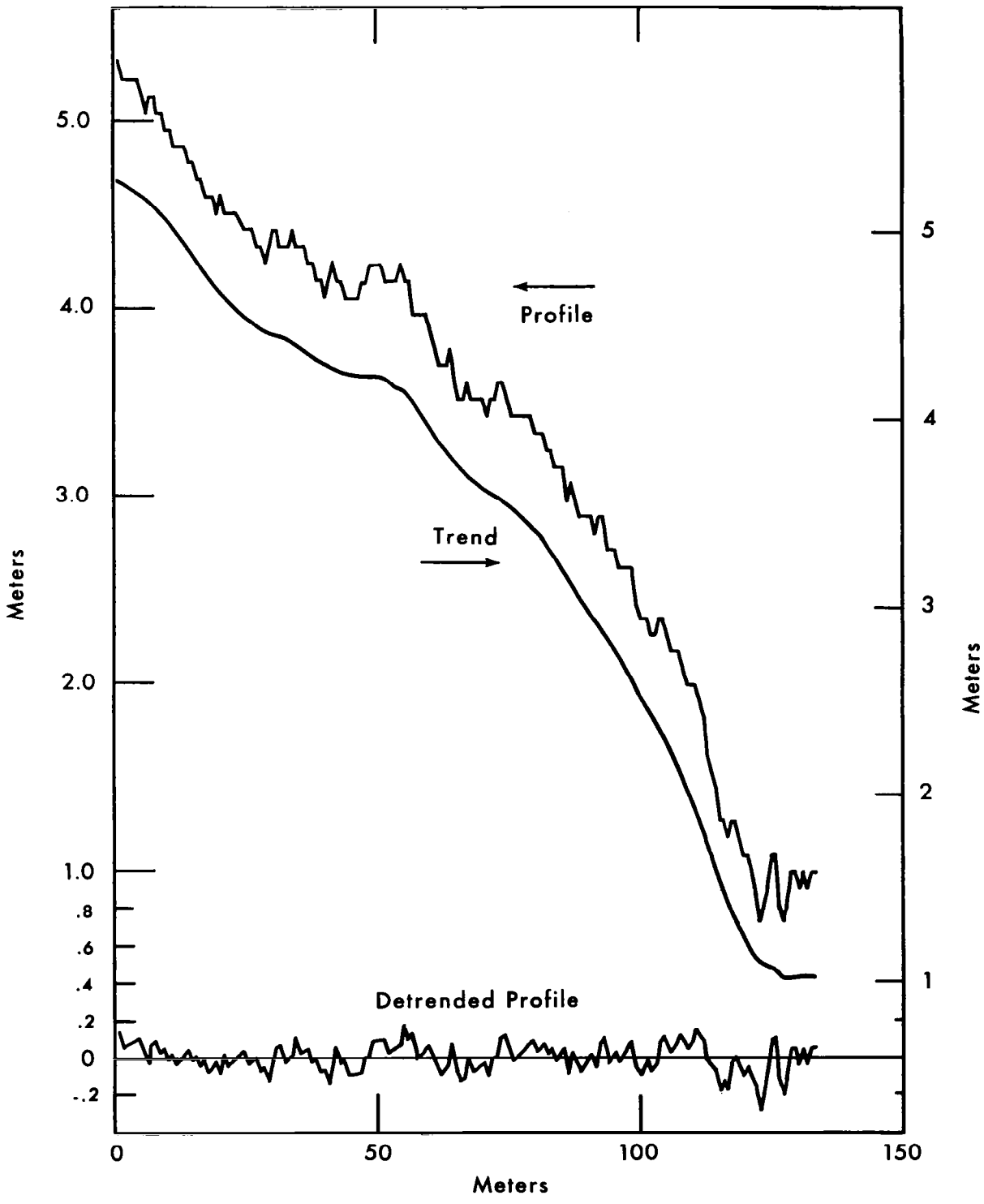

Figure A-9 EFFECT OF DETRENDING ON DATA SET 4

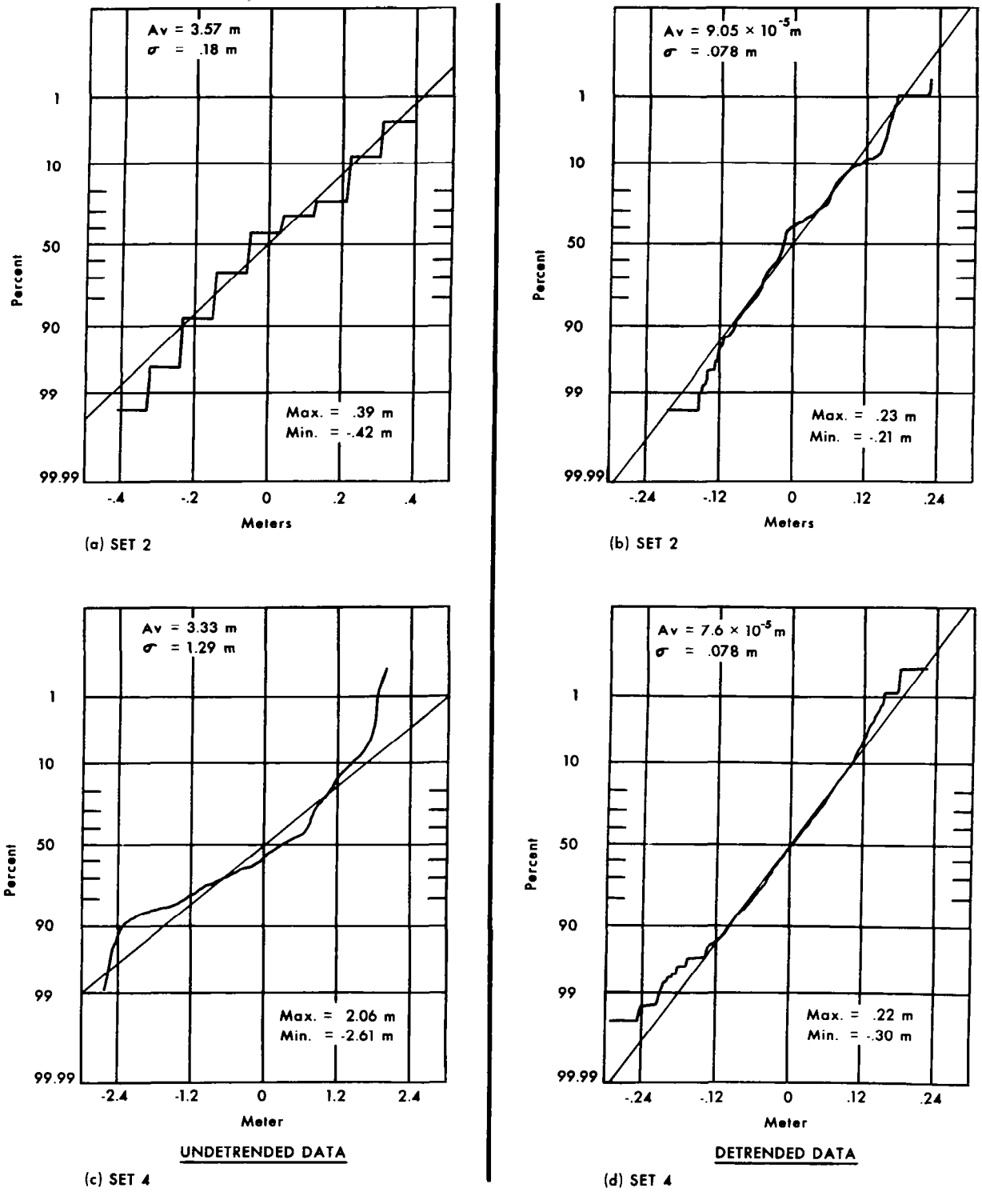

Figure A-10 A.P.D. PLOTS FOR DETRENDED AND UNDETRENDED DATA SETS 2 & 4

The effect of λ on the estimate of C for Data Set 4 is shown in Table A-2. A value of 5 meters for λ was chosen for the processing of the Ranger VIII data since this value was the largest one effective in detrending Data Set 4; which had the most substantial trend. In order to show the effect of this frequency cut-off on vehicle behavior consider the following argument. If F_{Min} is the lowest temporal frequency considered to have any effect on the vehicle's behavior and V_{Max} is the highest vehicle velocity, then

$$\Omega_{Min} = \frac{F_{Min}}{V_{Max}} \qquad (A-42)$$

Where Ω_{Min} is the lowest spacial frequency which will affect the vehicle's behavior. If 5 meters is then used for λ to calculate the half-power point of the detrending filter (See Equation A-28) and 4.77 meters/second (10 mph) is chosen as a top speed, this yields a value for F_{Min} of 0.5 Hertz (cps). This value is approximately one octave below the lowest resonant frequencies for most vehicles.

The amplitude probability distribution, variance, and standard deviation for each of the detrended data sets were calculated. Figure A-10 shows this information for Data Sets 2 and 4 and Figure A-11 shows the results for the detrended Sets 1, 3, 5, and 6. While the data available is very crude in a statistical sense it is possible to state that the amplitude probability distribution for the detrended data is Gaussian within the statistical accuracy of the data available.

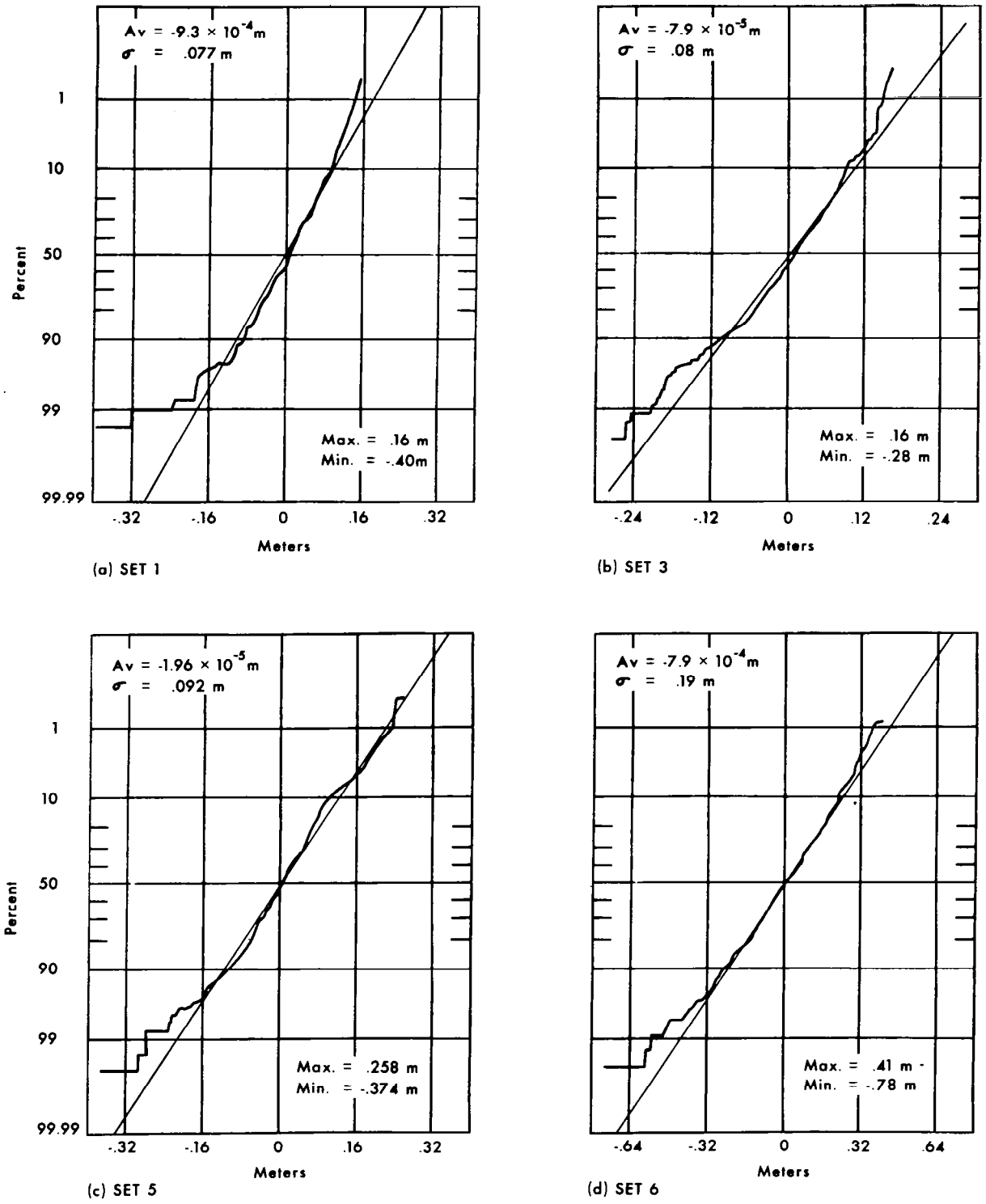

DETRENDED DATA

Figure A-11 A.P.D. PLOTS FOR DETRENDED SETS 1, 3, 5, & 6

Table A-2 EFFECT OF λ ON ESTIMATE OF C

DATA SET 4

λ Meters	Variance $(\text{Meters})^2$	Std. Dev. (Meters)	C $(\text{Meters})^2$ Cycle/Meter
1.00	0.00129	0.0359	2.61×10^{-4}
2.00	0.00252	0.0502	2.55×10^{-4}
3.00	0.00352	0.0593	2.37×10^{-4}
4.00	0.00473	0.0688	2.40×10^{-4}
5.00	0.00615	0.0784	2.49×10^{-4}
6.00	0.00780	0.0883	2.63×10^{-4}
7.00	0.00966	0.0984	2.80×10^{-4}
8.00	0.0117	0.108	3.00×10^{-4}
9.00	0.0142	0.119	3.19×10^{-4}
10.00	0.0171	0.131	3.47×10^{-4}
11.00	0.0206	0.143	3.79×10^{-4}

The P.S.D. of the lunar data was determined by means of Equation A-19. Linear and exponential spectral windows were employed for frequency domain smoothing, as given by Equation A-20 and Table A-1. The linearly smoothed P.S.D. is given in Equation (A-43).

$$P_d(\Omega_n) = \frac{L}{18} \sum_{i=n-4}^{n+4} (A_i^2 + B_i^2) \qquad \text{(A-43)}$$

The equation for the exponentially smoothed P.S.D. is:

$$P_d^{\sigma}(\Omega_n) = \frac{L}{2}\left\{ \frac{a_n^2 + b_n^2 + \sum_{i=n-9}^{n+9} (A_i^2 + B_i^2)\, e^{-i/3}}{\sum_{i=0}^{9} e^{-i/3}} \right. \qquad \text{(A-44)}$$

Figure A-12 shows the P.S.D. plots of the raw data for Data Sets 2 and 4 with both the exponential and linear smoothing. Figure A-13 shows the P.S.D. estimates of all six detrended sets with both linear and exponential smoothing. It can be seen in every case that the slope of minus two is approximately satisfied by each of these curves. The effect of detrending can be seen in some of these curves and is most obvious in Figure A-13 for Data Set 5. A value of C was determined for each of these data sets from the variance. A value of C was also calculated by taking 50 data points from the P.S.D. beyond the effective cut-off frequency of the filter, and computing this value. Table A-3 is a summary of the values of C calculated by these two methods. Data Set 4 was numerically differentiated to obtain the lunar slope information. It should be recognized that the available data is somewhat crude and numerical differentiation can lead to large errors. Nevertheless the P.S.D. of the slope was approximately constant over the frequency range and is shown in Figure A-14.

Data Sets 4 and 5 are parallel profiles across the surface separated by the approximate width of a typical MOLAB (2.5 meters). The cross-spectral density of these two data sets was calculated and is presented in Figure A-15. This cross-spectral density is normalized in such a fashion that perfect

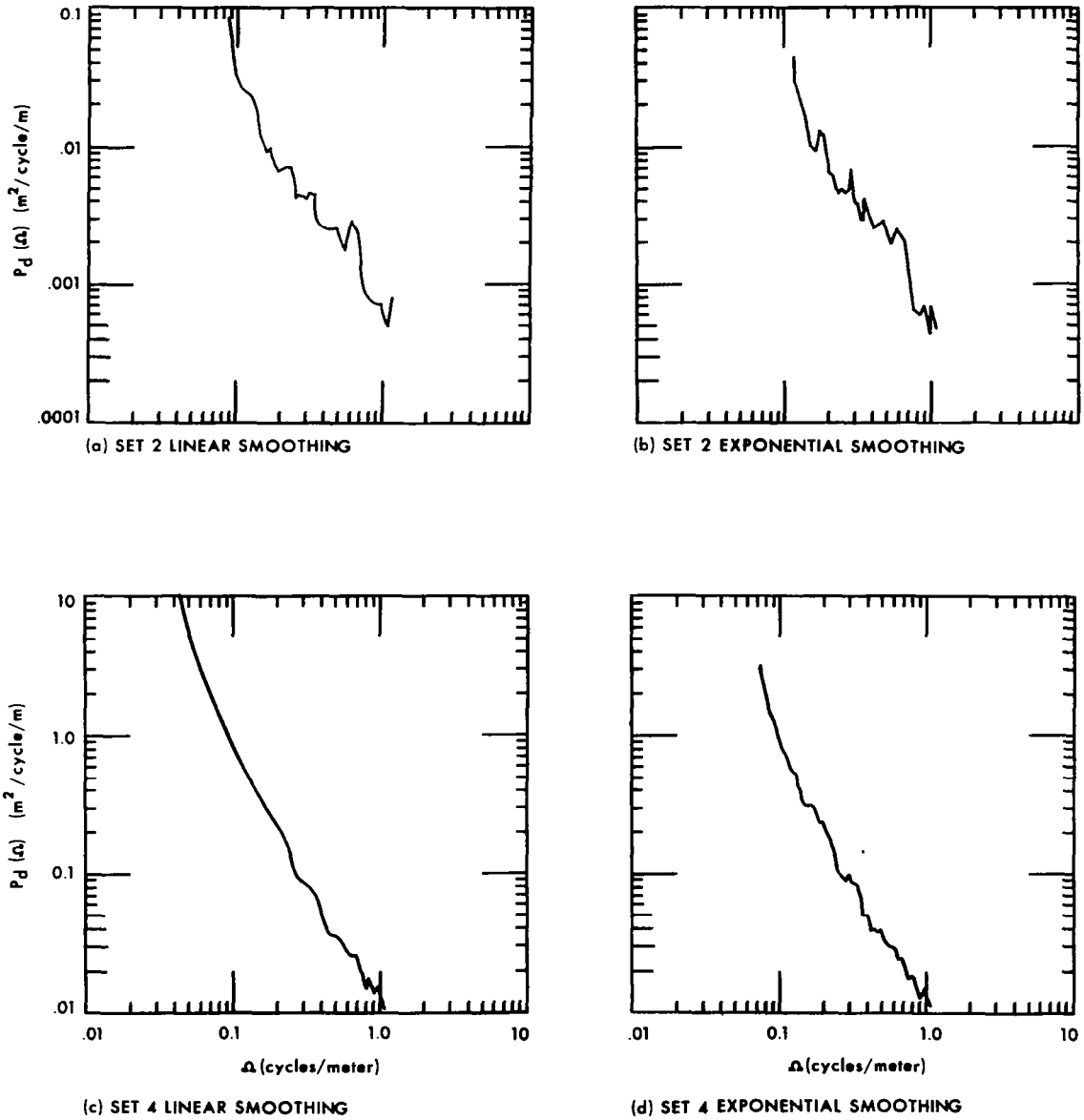

Figure A-12 P.S.D. OF UNDETRENDED SETS 2 & 4

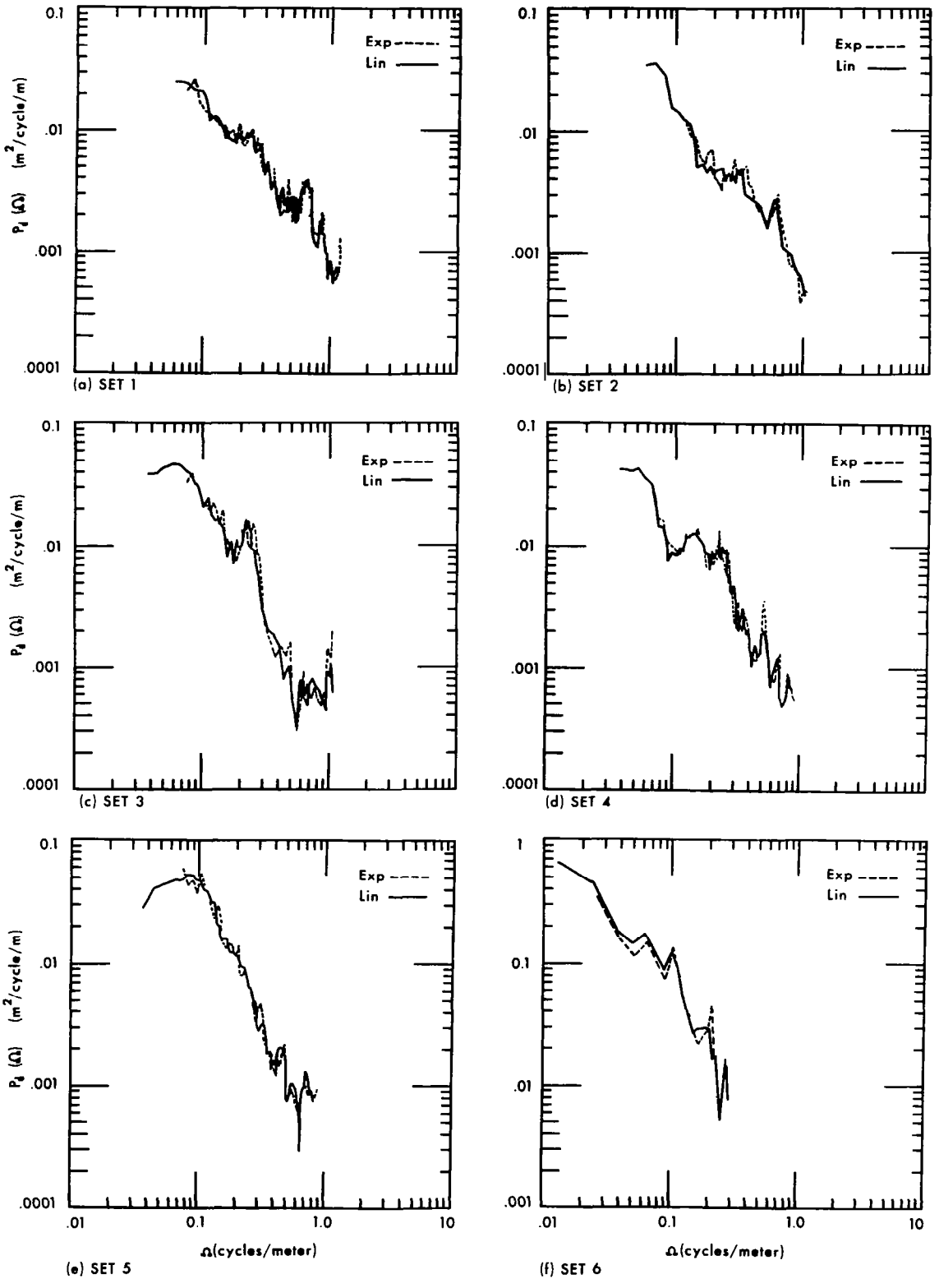

Figure A-13 P.S.D. OF DETRENDED LUNAR DATA

Table A-3 VALUES OF C FOR LUNAR SURFACE

DATA SET	STANDARD DEVIATION	FORMULA	VALUE OF C IN METERS CALCULATED FROM (σ)	CALCULATED FROM P.S.D.
Ranger VIII J.P.L. - 1 Last P-3 Frame	$\sigma = .077$	$C = \frac{2\sigma^2}{5\pi^2}$	2.4×10^{-4}	8.01×10^{-4}
Ranger VIII J.P.L. - 2 Last P-3 Frame	$\sigma = .078$	$C = \frac{2\sigma^2}{5\pi^2}$	2.4×10^{-4}	6.31×10^{-4}
Ranger VIII J.P.L - 3 Last P-3 Frame	$\sigma = .080$	$C = \frac{2\sigma^2}{5\pi^2}$	2.6×10^{-4}	2.49×10^{-4}
Ranger VIII J.P.L. - 4 Last P-3 Frame	$\sigma = .078$	$C = \frac{2\sigma^2}{5\pi^2}$	2.4×10^{-4}	3.67×10^{-4}
Ranger VIII J.P.L. - 5 Last P-3 Frame	$\sigma = .092$	$C = \frac{2\sigma^2}{5\pi^2}$	3.4×10^{-4}	3.48×10^{-4}
Ranger VIII J.P.L. - 6 Next to Last P-3 Frame	$\sigma = .190$	$C = \frac{2\sigma^2}{17.15\pi^2}$	4.3×10^{-4}	8.35×10^{-4}
Ranger VIII J.P.L.- 4 Slope	-------	$C = \frac{.011}{4\pi^2}$	-------	2.8×10^{-4}
Ranger VII U. S. G. S. Last P-3 Frame	$\sigma = .052$	$C = \frac{\Delta L \sigma^2}{2\pi^2}$	5.3×10^{-4}	-------

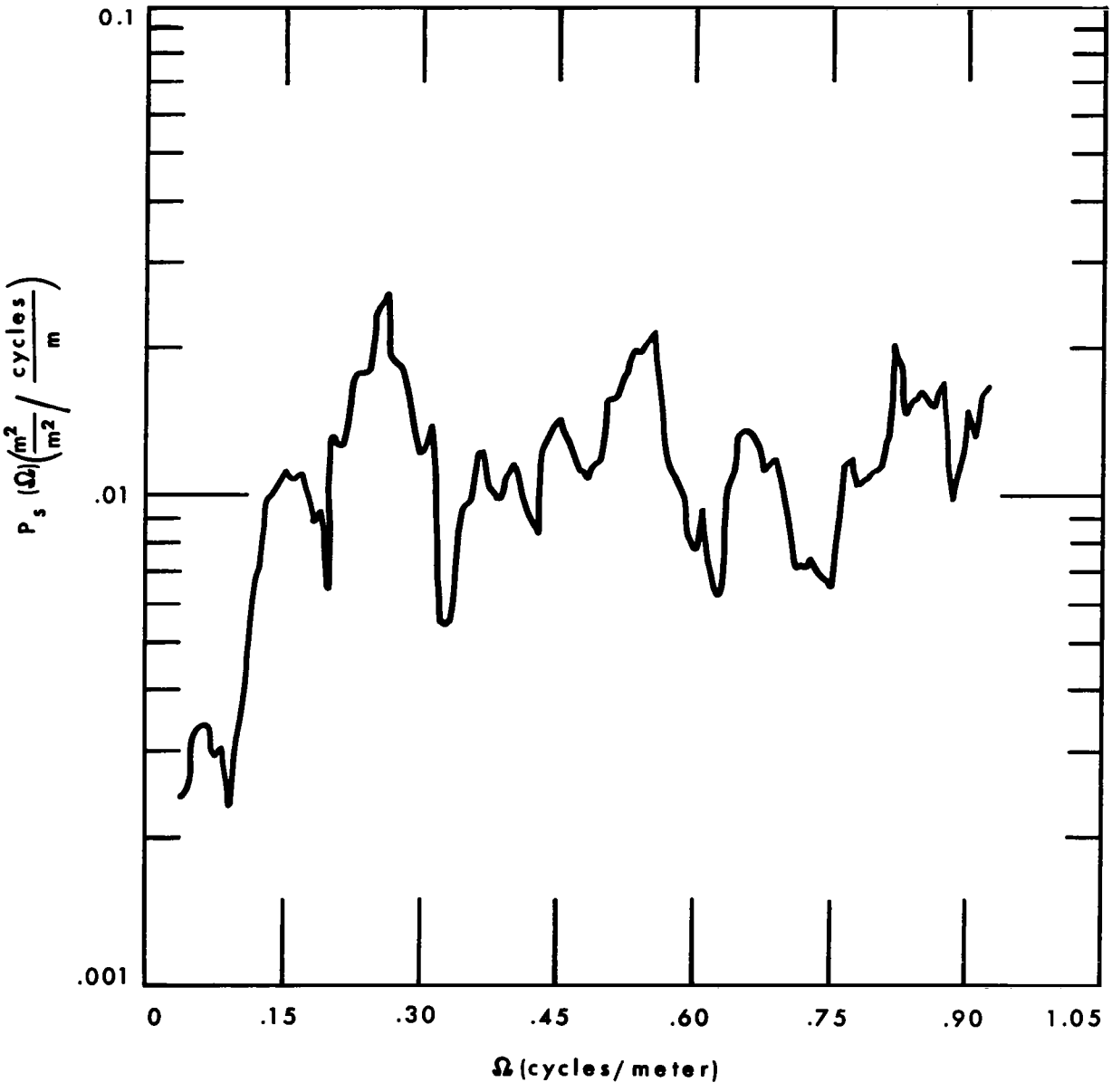

Figure A-14 SLOPE P.S.D. OF DETRENDED DATA SET 4

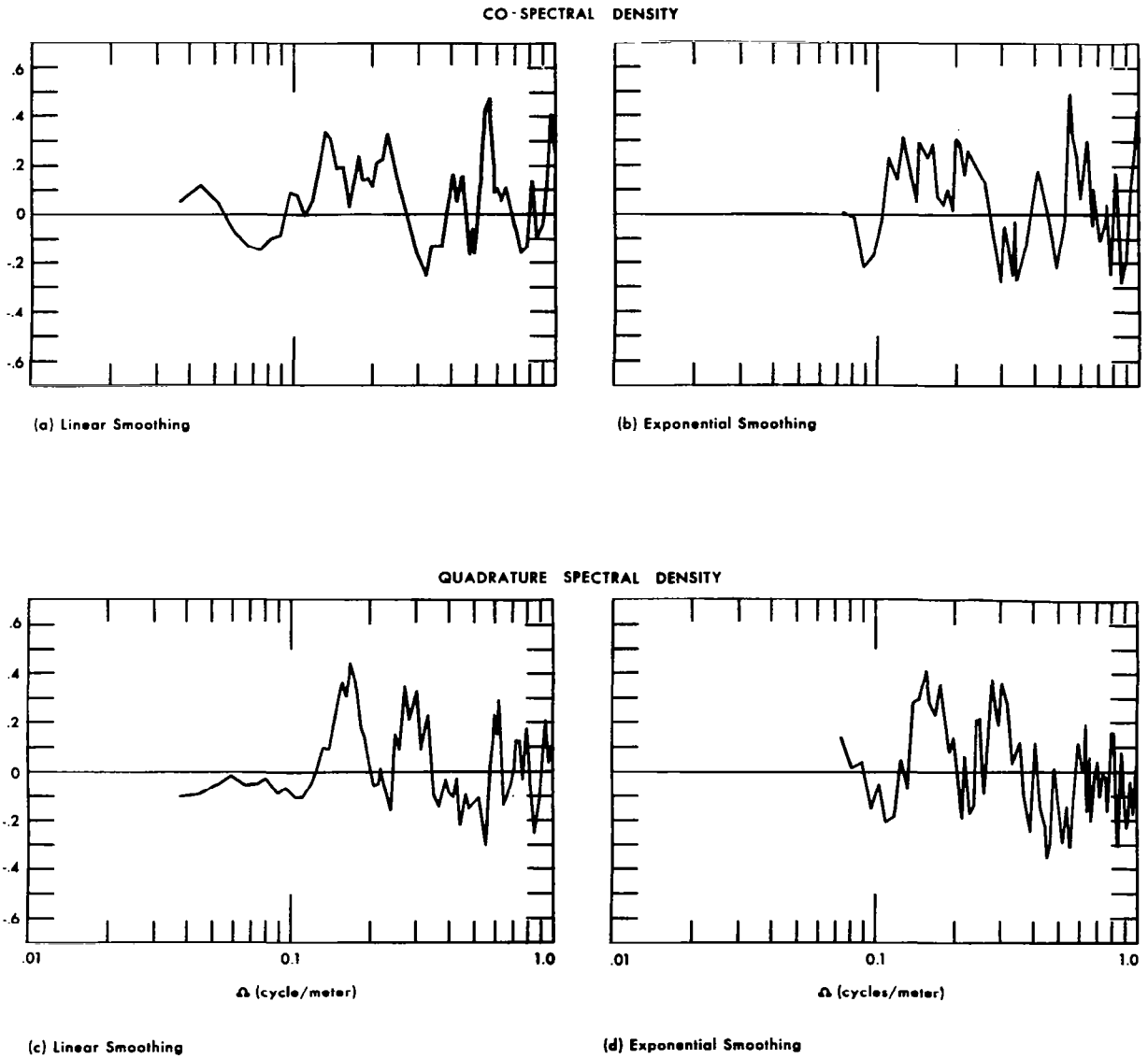

Figure A-15 CROSS SPECTRAL DENSITY BETWEEN DATA SETS 4 & 5

correlation would give a unit co-spectral density. It appears from these plots that the correlation between traces even this close together is negligible. There is no substantial trend of correlation between the plots, and the noise which does exist is considered to be due to statistical errors. While this data is not conclusive it points toward the validity of using separate members of the ergodic set predicted by the P.S.D. of one trace as inputs to the two sides of the vehicle.

A.2.2 Analysis of United States Geological Survey

Just prior to the end of this contract digital slope information from the U. S. Geological Survey was made available. This information was obtained from the last partial P-3 camera frame of Ranger VII. One set of slope information across the lunar surface was processed to give the amplitude probability distribution. This plot is shown in Figure A-16. It can be seen that the slope distribution is near Gaussian. A value for the constant C was computed from the variance of the slope information and is presented in Table A-3 together with estimates of C from the J.P.L. data.

A.3 Digital Computer Programs

Several digital computer programs were written to process the lunar data. In each case these are very direct approaches to the digital technique described in Section A.1. A list of each of the programs used is given on the following pages. The language (BASIC) is an elementary algebraic language used on a General Electric 235 computer in the time sharing mode. A description of the language is given in

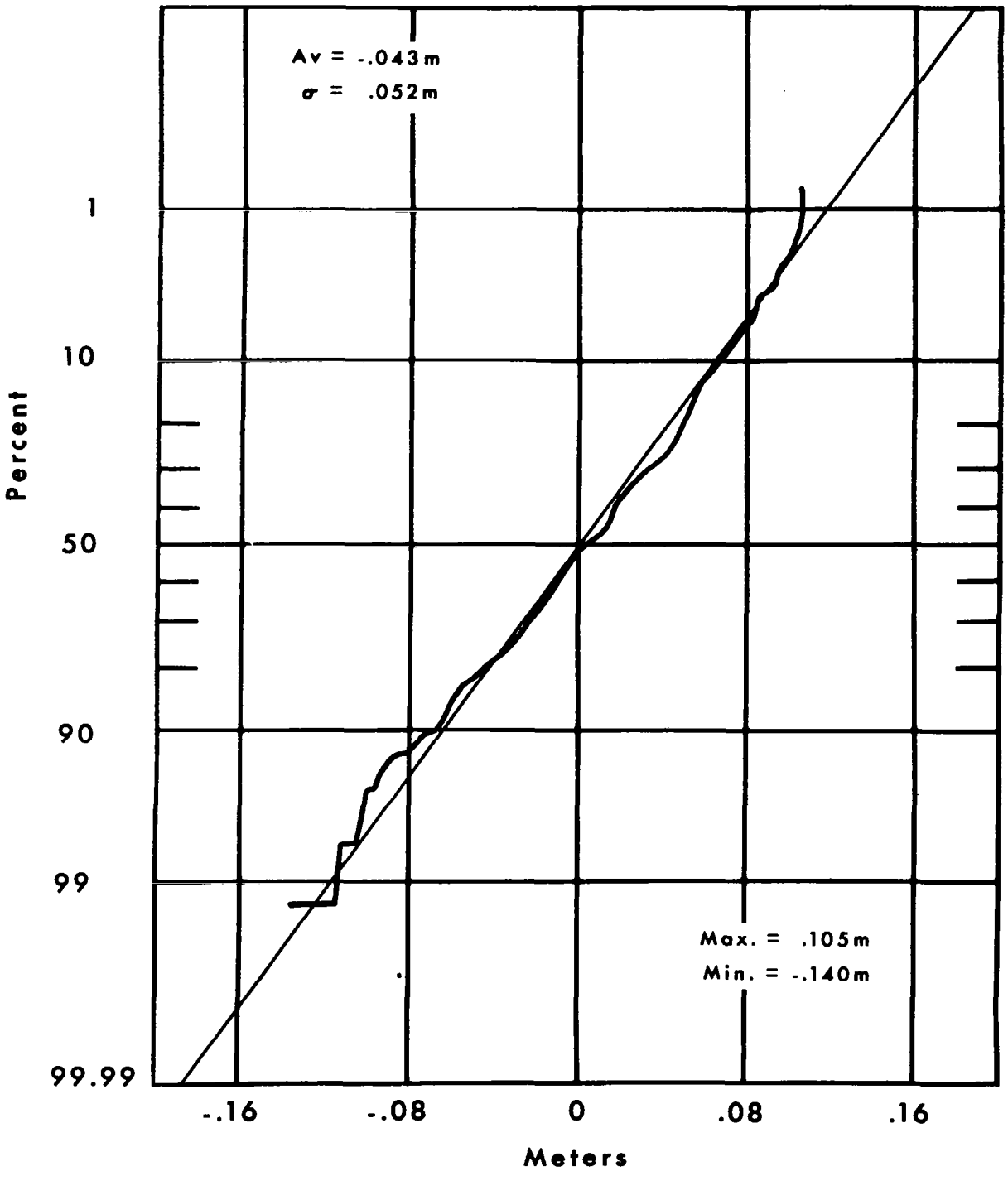

Figure A-16 A.P.D. PLOT FOR U.S.G.S. SLOPE DATA

Reference 18. The language is a very descriptive one and should allow analysis of these programs even by non-experienced computer programmers.

The first program listed, DETREN was developed to allow detrending of the raw data.

The second program, AMPDIS computed the average, maximum and minimum about the average, amplitude probability distribution, variance and standard deviation of the input data.

The third program listed, FORSER, computes the Fourier coefficients of the input data and then uses these coefficients to reconstruct the input data for validation. It also compares the reconstructed data to the input data and computes the percent error of the reconstruction.

The last program listed, FOR 5, computes the Fourier coefficients and their magnitude squared. It then smoothes the squares of the magnitudes in a linear and exponential fashion and prints out the smoothed values as the P.S.D.

DETREN

```
1 REM BRUCE VAN DEUSEN TIE LINE 860 EXT 24
2 REM XXX
10
80 LET E=0
90 LET P=0
100PRINT900;"DATA";
110 DIM F(500),K(200)
120 LET D=2
130 READ N,H,S,L
140 FOR X=1 TO N
150 READ F(X)
160 IF S*X/L>3 THEN 200
170 LET K(X)=EXP(-S*X/L)
180 LET D=D+K(X)*2
190 LET E=E+1
200 NEXT X
210 FOR X=1 TO N
220 FOR Y=0 TO E
230 LET Z=X+Y
240 IF Z<=N THEN 260
250 LET Z=2*N-Z
260 LET W=X-Y
270 IF W>0 THEN 290
280 LET W=-W+1
290 IF Y<>0 THEN 320
300 LET M=2*F(X)/D
310 GOTO 330
320 LET M=M+(F(W)+F(Z))*K(Y)/D
330NEXT Y
340 LET K=F(X)-M
350 LET K=10↑(-5)*INT(K*10↑5)
360 IF P=5 THEN 400
370 PRINTK;",";
380 LET P=P+1
390 GOTO 430
400 PRINT K
410 PRINT 900+X/6;"DATA";
420 LET P=0
430 NEXT X
9999 END
```

AMPDIS

```
1 REM BRUCE D. VAN DEUSEN-CHRYSLER CORP-DETROIT--VE6-4100--EXT24
2 REM XXX
5 GO TO 9000
10 LET A=0
20 LET V=0
30 DIM F(900)
40 READ N,H
50 FOR X=1 TO N
60 READ F(X)
70 IF X<>1 THEN 100
80 LET Q1=F(X)
90 LET Q2=Q1
100 LET A=A+F(X)
110 IF F(X)>Q1 THEN 130
120 LET Q1=F(X)
130 IF F(X)<Q2 THEN 150
140 LET Q2=F(X)
150 NEXT X
160 LET A=A*H/N
170 LET Q1=H*Q1-A
180 LET Q2=H*Q2-A
190 PRINT "AVE="A,"MAX="Q2,"MIN="Q1
200 LET L=Q2
210 IF Q2>-Q1 THEN 230
220 LET L=-Q1
230 LET K1=0
240LET K2=0
250 IF L>1 THEN 290
260 LET L=10*L
270 LET K1=K1+1
280 GO TO 250
290 IF L<10 THEN 330
300 LET L=.1*L
310 LET K2=K2+1
320 GO TO 290
330 LET L=1+INT(L)
340 LET L=L*(10↑K2)*(.1↑K1)
350 PRINT
360 PRINT"AMPLITUDE DISTRIBUTION"
370 PRINT"LEVEL","+0","+".01*L,"+".02*L,"+".03*L
375 PRINT
380 FOR Y=-L TO .96*L STEP L/25
390 LET C1=0
400 LET C2=0
410 LET C3=0
420 LET C4=0
430 FOR X=1 TO N
440 IF Y<>-L THEN 480
450 LET F(X)=H*F(X)-A
```


86

AMPDIS (CON'T.)

```
470 LET V=V+F(X)↑2
480 IF F(X)<Y THEN 560
490LET C1=C1+1
500 IF F(X)<.01*L+Y THEN 560
510 LET C2=C2+1
520 IF F(X)<Y+.02*L THEN 560
530 LET C3=C3+1
540 IF F(X)<Y+.03*L THEN 560
550 LET C4=C4+1
560 NEXT X
570 PRINT Y,C1/N,C2/N,C3/N,C4/N
580 NEXT Y
590 PRINT
600 PRINT "VARIANCE="V/N,"STANDARD DEVIATION="SQR(V/N)
8800 STOP
9000 PRINT"THIS PROGRAM CALCULATES THE AVERAGE,MAXIMUM,MINIMUM,"
9010 PRINT"(ABOUT THE AVERAGE) AND VARAINCE OF NUMERICAL DATA PLACED"
9020 PRINT"IN DATA STATEMENTS.  IT ALSO CALCULATES THE AMPLITUDE"
9030 PRINT"PROBABILITY DISTRIBUTION.  THIS IS THE INTEGRAL DISTRIBUTION"
9040 PRINT"THAT IS THE NUMBER OF DATA POINTS ABOVE LEVEL (L) VS (L)"
9050 PRINT"THE LIMITS ARE AUTOMATICALLY CALCULATED AND 100 EQUAL"
9060 PRINT"INTERVALS ARE CHOSEN FOR PLOTTING ON PROBABILITY PAPER"
9070 PRINT"IN ORDER TO RUN PRINT (5 DATA N,H) WHERE N IS THE NUMBER"
9080 PRINT"OF DATA POINTS AND H IS A MULTIPLICATION OR SCALE FACTOR"
9090 PRINT"I.E. IF THERE ARE 200 DATA POINTS AND NO SCALING IS DESIRED"
9100 PRINT"PRINT   5 DATA 200,1       -----THEN LOAD DATA IN DATA"
9110 PRINT"STATEMENTS STARTING WITH STATEMENT 700  --AND RUN"
9998 DATA 1
9999 END
```

FORSER

```
1 REM BRUCE D. VAN DEUSEN-CHRYSLER CORP-DETROIT--VE6-4100 EXT 24
2 REM XXX
10 GO TO 590
90 LET A=0
100 DIM F(351),S(351),C(351),A(150),B(150)
110 READ N,H,J
120 FOR X=1 TO N
130 READ F(X)
140 LET F(X)=H*F(X)
150 LET A=A+F(X)
160 LET S(X)=SIN(3.1415926*X/N)
170 LET C(X)=COS(3.1415926*X/N)
180 NEXT X
184 LET C(0)=1
186 LET S(0)=0
190 PRINT "FOURIER SERIES COEFFICIENTS"
200 PRINT"HARMONIC"," A"," B","MAG SQUARED"
210 PRINT" 0",A/N," 0",(A/N)↑2
220 FOR Y=1 TO J
222 LET A(Y)=0
224 LET B(Y)=0
230 FOR X=1 TO (N+1)/2
240 LET W=N+1-X
250 IF W=X THEN 300
260 GOSUB 490
270 LET A(Y)=A(Y)+C(Z)*(F(X)+F(W))
280 LET B(Y)=B(Y)+Q*S(Z)*(F(X)-F(W))
290 GOTO 310
300 LET I=(-1)↑Y
301 LET A(Y)=A(Y)+I*F(X)
310 NEXT X
320 LET A(Y)=A(Y)*2/N
330 LET B(Y)=B(Y)*2/N
340 PRINT Y,A(Y),B(Y),A(Y)↑2+B(Y)↑2
350 NEXT Y
360 PRINT "RECONSTRUCT DATA 1 OR 0";
370 INPUT M
380 IF M=0 THEN 480
390 PRINT "POINT NUMBER","TRUE VALUE","COMPUTED VALUE","PERCENT ERROR"
400 FOR X=1 TO N
410 LET P=A/N
420 FOR Y=1 TO J
430 GOSUB 490
440 LET P=P+A(Y)*C(Z)+Q*B(Y)*S(Z)
450 NEXT Y
460 PRINT X,F(X),P,ABS((F(X)-P)*100/F(X))
470 NEXT X
480 STOP
```

FORSER (CON'T.)

```
490 LET Z=Y*(2*X-1)
500 LET Q=1
510 IF Z<=N THEN 580
520 LET Z=2*N-Z
530 LET Q=-1*Q
540 IF Z>0 THEN 580
550 LET Z=-Z
560 LET Q=-1*Q
570 GOTO 510
580 RETURN
590 PRINT"PROGRAM PRINTS FOURIER SERIES COEFFICIENTS FROM DATA"
600 PRINT"PRINT  (10 DATA N,H,J)  WHERE N IS THE NUMBER OF DATA"
610 PRINT"POINTS,H IS A SCALE OR MULTIPLCATION FACTOR FOR RAW"
620 PRINT"DATA AND J IS THE NUMBER OF HARMONICS DESIRED------"
630 PRINT"LOAD DATA IN DATA STATEMENTS 700 AND FOLLOWING--AND RUN"
9998 DATA 1
9999 END
```

FOR 5

```
1 DATA 348,150
80 LET I=0
100DIMF(352),S(351),C(351),A(150)
110 READ N,J
120 FOR X=1 TO N
130 READ F(X)
160 LET S(X)=SIN(3.1415926*X/N)
170 LET C(X)=COS(3.1415926*X/N)
171 IF 2*X<>N+1THEN180
172LET I=F(X)
180 NEXT X
184 LET C(0)=1
186 LET S(0)=0
200 PRINT"HARMONIC"," A"," B","MAG SQUARED"
220 FOR Y=1 TO J
221LET I=-1*I
222LETK=I
224LETL=0
230FORX=1TON/2
240 LET W=N+1-X
241IFY<>1THEN490
242LETA=F(X)+F(W)
244LETF(W)=F(X)-F(W)
246LETF(X)=A
490 LET Z=Y*(2*X-1)
500 LET Q=1
510 IF Z<=N THEN 580
520 LET Z=2*N-Z
530 LET Q=-1*Q
540 IF Z>0 THEN 580
550 LET Z=-Z
560 LET Q=-1*Q
570 GOTO 510
580LETK=K+C(Z)*F(X)
590LETL=L+Q*S(Z)*F(W)
600NEXTX
605LETA(Y)=(K*K+L*L)*4/(N*N)
610PRINTY,2*K/NNN,2*L/N,A(Y)
620NEXTY
630PRINT"CY/CM","LINEAR","EWA"
640LETQ=0
645LETR=2
650FORX=1TO9
660LETQ=Q+A(X)
670LETQ(X)=EXP(-X/3)
680LETR=R+2*Q(X)
690NEXTX
700FORX=5TOJ-5
710PRINTX/(N*38.1),N*38.1*Q/18,
```

FOR 5 (CON'T.)

```
720LETT=X+5
730LETU=T-9
740LETQ=Q+A(T)-A(U)
750IFX<10THEN820
760 IF X>J-10 THEN 820
765LETW=2*A(X)
770FORY=1TO9
775LETZ=X+Y
777LETG=X-Y
780LETW=W+Q(Y)*(A(Z)+A(G))
790NEXTY
800PRINT(N*38.1*W)/(2*R)
810GOTO830
820PRINT"       "
830NEXTX
9998 DATA 1
9999 END
```

APPENDIX B

YIELDING SURFACE MODEL

YIELDING SURFACE MODEL

By: R. F. Hughes

Surface deformation can influence vehicle motion. The discussion which follows is concerned with the formulation of a dynamic yielding surface model. It is recognized that the representation presented is grossly approximate since a comprehensive theory for dynamic vehicle-soil interaction does not exist. However, the essential features of soil behavior are believed to be adequately described for estimating surface-layer property effects on vehicle motion. Only a motion caused by an unbalance of forces in the direction perpendicular to the soil surface is under examination.

Investigations of soil mechanics demonstrate a functional relationship between load penetration and soil response. Theory suggests that a portion of the reaction is dependent on the rate of penetration. This phenomenon is a damping action associated with the propagation of stress waves throughout the soil and soil viscosity in the form of friction or shear. Therefore, it is postulated that the dynamic soil reaction force acting on a vehicle may be represented by Equation B-1.

$$R_s = \phi_1(Z) + \phi_2(\dot{Z}) \qquad (B-1)$$

R_s is the soil reaction force, $\phi_1(Z)$ is a function dependent on soil penetration (Z), and $\phi_2(\dot{Z})$ is a function dependent on soil penetration rate ($\dot{Z}$).

The contact surface between the soil and the wheel is assumed to be a flat plate of fixed shape and area "A". From Figure B-1, the equation describing the wheel motion on a yielding surface is:

$$m_w \ddot{Z} + \phi_2(\dot{Z}) + \phi_1(Z) = F_v$$

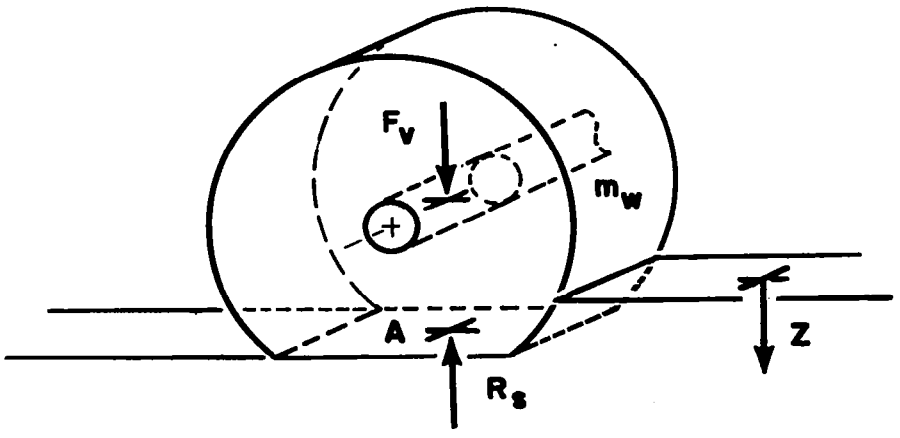

Figure B-1 WHEEL-SOIL INTERACTION MODEL

where m_w is wheel mass and F_v is the vertical force acting on the wheel. It now remains to determine the functions $\phi_1(Z)$ and $\phi_2(\dot{Z})$ from theory and the property of soils.

B.1 The Function $\phi_1(Z)$

Data from standard plate penetrometer tests of soil which are normally reserved for assessing vehicle trafficability are considered applicable to represent $\phi_1(Z)$ since this term as defined is time independent.

The pressure-sinkage relation which has received the most attention in recent years is that due to Bekker[19]. The Bekker relationship is given by the equation:

$$P = (k_\phi + k_c/b)\, Z^n \qquad \text{(B-3)}$$

where P = applied pressure; k_ϕ = frictional modulus of sinkage; b = least dimension of loading plate area; k_c = cohesive modulus of sinkage; n = empirical exponent; Z = sinkage

A serious deficiency of this relationship is the dimensional dependence of k_ϕ, and k_c on n. Wismer and Smith[20] have experienced difficulty in obtaining consistent values for k_ϕ, k_c and n. Reece[21] deplores the lack of a sound theoretical basis for Bekker's equation and recommends a new expression based on the bearing capacity theory of soil mechanics.

In view of the above arguments a relation due to Assur[22] has been adopted to represent soil deflection under load. Under the pressure of a rigid flat plate a soil will initially settle proportional to load.

$$P = K_s Z \tag{B-4}$$

K_s is the coefficient of subgrade reaction. If the load is continuously increased, the soil eventually exhibits a deviation from Equation B-4. According to Assur this deviation may be categorized into one of three fundamental traits shown below.

I Fluidization $$P = K_s Z \left[1 - (K_s Z/P_m)^2 + 2(K_s Z/P_m)^4 + \ldots\right] \tag{B-5}$$

II Compaction $$P = K_s Z/(1 - Z^2/Z_m^2) \tag{B-6}$$

III Collapse $$P = K_s Z/(1 + Z^2/Z_m^2) \tag{B-7}$$

where Z = plate sinkage, P_m = maximum bearing strength,

P = bearing pressure, Z_m = sinkage at maximum bearing strength

K_s = coefficient of subgrade reaction.

The characteristics of each type of deformation Z related to bearing pressure P is presented in Figure B-2. Category I is the most common soil reaction and is

representative of clay but not restricted to clay. It indicates a progressive deterioration of elemental particle bonding with load. Snow and very loose soils have been observed to respond according to Category II where bond strength increases with load. Category III, which is exhibited by densely compacted sand, is a typical behavior for a crust over a soft underlayer and predicts a collapse after a finite maximum bearing pressure. Figure B-2 illustrated soil reaction to continuous increasing load. Figure B-3 illustrates soil reaction to repetitive loading with the maximum load increasing with each cycle. A permanent plastic deformation of the soil remains following each loading (AC, CE, EG, etc.). The soil recovery (BC, DE, FG, etc.) may be approximately described by a series of parallel straight lines which suggests Hooke's Law. The initial load cycle may be conceived as a consolidation plus elastic compression, AB, followed by an elastic recovery, BC. Equation B-8 is an expression for recovery from the theory of elasticity.[23]

$$P = \frac{C E Z}{(1-\nu^2)\sqrt{A}} \qquad \text{(B-8)}$$

Where

P = bearing pressure

E = soil modulus of elasticity

A = area of load bearing plate

C = dimensionless coefficient dependent on plate shape

ν = Poissons ratio of the soil

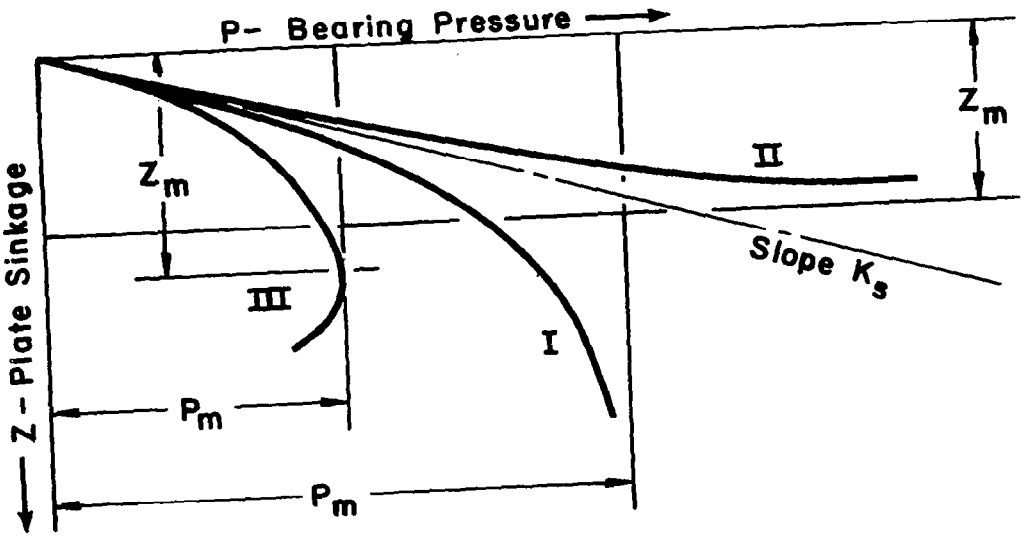

Figure B-2 PRESSURE-SINKAGE CHARACTERISTICS OF SOIL ACCORDING TO ASSUR

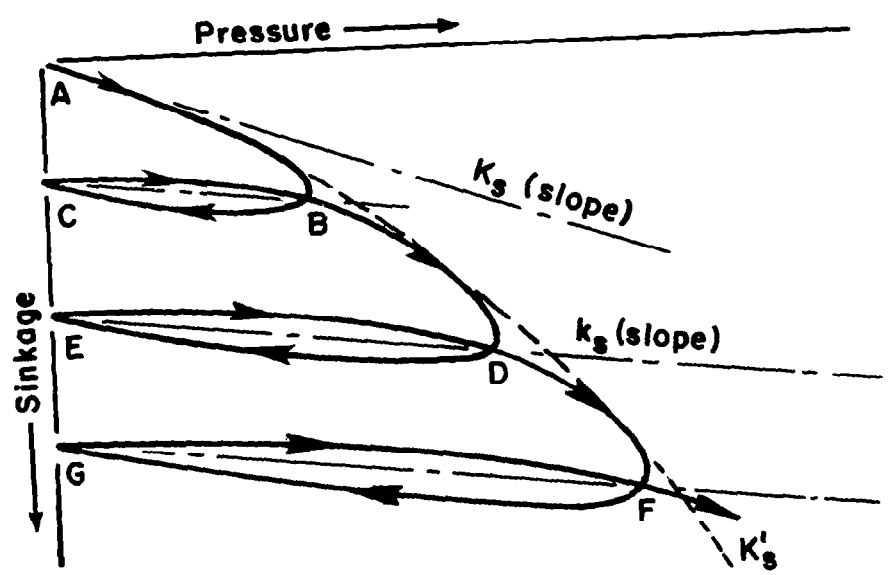

Figure B-3 SOIL RESPONSE TO REPETITIVE LOADING

Table B-1 presents values of the coefficient C related to bearing plate geometry.

Table B-1. VALUES FOR C FOR EQUATION B-8

PLATE GEOMETRY	PLATE CONDITION	
	Rigid	Flexible
Circle	1.13	1.04
Square	1.08	1.06
Rectangle (length to width ratio)		
3/2	1.09	1.07
2	1.10	1.09
3	1.15	1.13
5	1.24	1.22
10	1.41	1.41

Since $\phi_1(Z)$ is a force equal to P times A, it has the following form:

Consolidation and Elastic Compression

$\phi_1(Z)$ for fluidization is $K_s ZA\left[1 - (K_s Z/P_m)^2 + 2(K_s Z/P_m)^4 + \ldots\right]$ (B-9)

or for compaction is $K_s ZA/(1 - Z^2/Z_m^2)$ (B-10)

or for collapse is $K_s ZA/(1 + Z^2/Z_m^2)$ (B-11)

Elastic Recovery

$$\phi_1(Z) = \frac{C E Z \sqrt{A}}{(1-\nu^2)} \qquad \text{(B-12)}$$

B.2 The Function $\phi_2(\dot{Z})$

An expression for $\phi_2(\dot{Z})$ of Equation B-1 has been obtained from a model illustrated in Figure B-4 consisting of a vibrating disc in surface contact with an elastic, homogenous, isotropic, semi-infinite medium. Although this theoretical model is ideally elastic, radiation damping exists since energy is transported from the disturbance source throughout the medium via pressure waves and unavailable for resonant re-enforcement of the disc motion. This model contains no internal

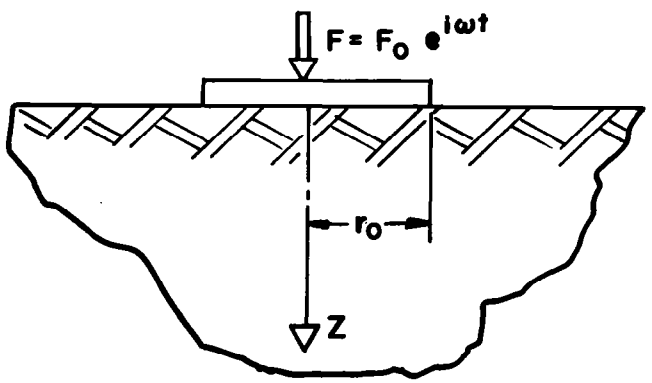

Figure B-4 WEIGHTLESS RIGID DISC SUPPORTED BY ELASTIC MEDIUM

damping which is related to the friction between soil particles or the process of soil shear. Experimental evidence indicates friction or shear is expressed by the hysteresis in the stress-strain cycle[24] [25] [26]. Since hysteresis is believed to be adequately accounted for by the form selected for $\phi_1(Z)$, no attempt is made to include this effect in $\phi_2(\dot{Z})$.

The above model has been the basis for the analytical study of vibrating foundations. The theory dates from the work of Reissner[27], 1936. A more recent development is accredited to Sung[28], Bycroft[29], Hsieh[30] and Lysmer[31]. The brief summary which follows is due to Hsieh[30], and Hall and Richart[24]. The vertical displacement Z of a weightless rigid disc resting upon an elastic semi-infinite medium and submitted to a periodic force $F = F_o e^{i\omega t}$ (see Figure B-4) is given by:

$$Z = - \frac{F_o}{G r_o} \left[f_1 + i f_2 \right] e^{i\omega t} \qquad (B-13)$$

where Z = displacement

F_o = amplitude of periodic force

$G = E/2(1+\nu)$ = shear modulus of medium

f_1; f_2 = dimensionless functions dependent on Poissons ratio ν and a_o

r_o = disc radius (for circular disk)

a_o = dimensionless quantity $- \omega r_o \sqrt{\rho/G}$

ρ = mass density of medium

ω = forcing frequency (radians/sec)

Differentiating Equation B-9 with respect to time yields

$$\dot{Z} = - \frac{\omega F_o}{G r_o} \left[i f_1 - f_2 \right] e^{i\omega t} \qquad (B-14)$$

Equations B-13 and B-14 may be combined to yield:

$$\omega Z f_1 - \dot{Z} f_2 = - \frac{\omega F_o}{G r_o} \left[f_1^2 + f_2^2 \right] e^{i\omega t} = - \frac{\omega F}{G r_o} \left[f_1^2 + f_2^2 \right] \qquad (B-15)$$

and therefore,

$$F = + \frac{G r_o}{\omega}\left[\frac{f_2}{f_1^2 + f_2^2}\right]\dot{Z} - G r_o\left[\frac{f_1}{f_1^2 + f_2^2}\right] Z \qquad \text{(B-16)}$$

$$\text{Setting } F_2 = \frac{f_2}{(f_1^2 + f_2^2)\, a_o} \quad \text{and } F_1 = -\frac{f_1}{(f_1^2 + f_2^2),} \qquad \text{(B-17)}$$

$$F = \sqrt{G \rho}\, r_o^2\, F_2\, \dot{Z} + G r_o F_1 Z = R_s \qquad \text{(B-18)}$$

where R_s is the reaction of the elastic medium.

Bycroft's calculated results for f_1 and f_2 related to Poissons ratio ν and $a_o = \omega r_o \sqrt{\rho / G}$ are presented in Figure B-5. From these graphs, Hsieh has determined approximations for F_1 and F_2 sufficiently accurate for practical calculations. These expressions are:

$$F_1 = c_o - c_1 a_o^2 \qquad F_2 = b_o + b_1 a_o \qquad \text{(B-19)}$$

where the values for the coefficients c_o, c_1, b_o, and b_1 are contained in Table B-2.

At $\omega = o$, a_o is zero and the second term of Equation B-18 is the elastic reaction to a rigid disc under static load. From Table B-1, $C = 1.13 = 2/\sqrt{\pi}$ for a circular plate and therefore

$$\underset{\text{(elastic)}}{\phi_1 (Z)} = \frac{2}{\sqrt{\pi}} \frac{E Z \sqrt{A}}{(1 - \nu^2)} = \frac{2 r_o 2 (1 + \nu) G Z}{(1 - \nu^2)} = \frac{4 G r_o Z}{(1 - \nu)}$$

Thus $F_1 = 4/(1 - \nu)$ for $a_o = 0$ which agrees with Hsieh's numerical values tabulated in Table B-2. Therefore $c_o = 4/(1 - \nu)$.

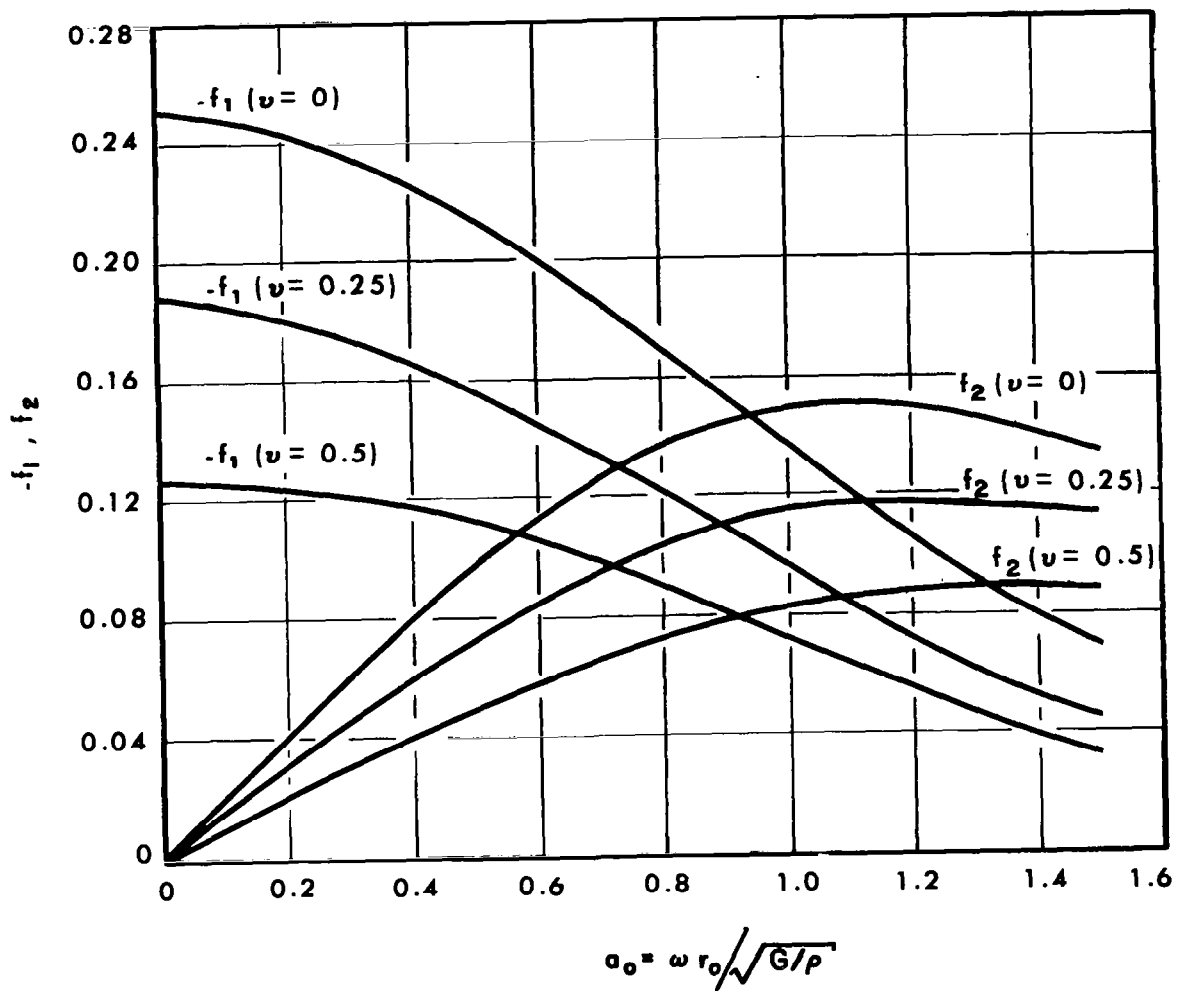

Figure B-5 BYCROFT'S DISPLACEMENT FUNCTION
VIBRATING RIGID DISC SUPPORTED BY ELASTIC MEDIUM
(Ref 32)

Table B-2. HSIEH'S VALUES FOR F_1, F_2

$0 < a_o < 3/2$

$F_1 = c_o - c_1 a_o^2$

$F_2 = b_o + b_1 a_o$

POISSONS RATIO ν	F_1		F_2	
	c_o	c_1	b_o	b_1
0	4.0	0.5	3.3	0.4
1/4	5.3	1.0	4.4	0.8
1/2	8.0	2.0	6.9	0

Hsieh's expression for F_1 is of the form $c_o - c_1 a_o^2$ where $c_o = 4/(1-\nu)$ and $a_o = \omega r_o \sqrt{\rho/G}$. Substituting these values into Equation B-18 yields:

$$\sqrt{G\rho}\ r_o^2 F_2 \dot{Z} + G r_o \left(\frac{4}{1-\nu} - \frac{c_1 \omega^2 r_o^2 \rho}{G}\right) Z = F \qquad \text{(B-21)}$$

Noting for a periodic motion of frequency ω that $\ddot{Z} = -\omega^2 Z$ Equation B-21 can be rewritten as:

$$(c_1 \rho r_o^3) \ddot{Z} + \sqrt{G\rho}\ r_o^2 F_2 \dot{Z} + \left(\frac{4 G r_o}{1-\nu}\right) Z = F \qquad \text{(B-22)}$$

The term $c_1 \rho r_o^3$ in Equation B-22 appears as an effective mass for the soil and represents a retardation to disc motion related to the inertia of soil in proximity to the disc.

Accepting a correspondence between soil reaction to the vibration of a foundation footing (disc) and soil reaction to the dynamic motion of a vehicle wheel, expressions for $\phi_2(\dot{Z})$ and soil effective mass m_e from Equation B-22 are:

SOIL REACTION FUNCTION		RADIATION DAMPING	(B-23)
$\phi_2(\dot{Z})$	$\longrightarrow$	$\frac{A}{\pi}(b_o + b_1 a_o)\sqrt{\frac{E\rho}{2(1+\nu)}}\,\dot{Z}$	

SOIL EFFECTIVE MASS		INERTIA	(B-24)
m_e	$\longrightarrow$	$c_1\rho\left(\frac{A}{\pi}\right)^{3/2}$	

For wheel-soil interaction, the surface contact dimension r_o of the disc theory has been generalized to $\left[A/\pi\right]^{1/2}$. The factor $b_o + b_1 a_o$ is the Hsieh representation of F_2 where the coefficients b_o and b_1 are dependent on Poissons ratio ν. It is seen that $\phi_2(\dot{Z})$ varies with the frequency of wheel motion through the parameter a_o. For most applications, however, it can be shown that the product $b_1 a_o$ may be neglected with respect to the value b_o. For example, at the wheel resonance of a typical vehicle (10 cps),

$$b_1 a_o = \frac{\omega r_o b_1}{\sqrt{G/\rho}} = \frac{10 \text{ cycle}}{\text{sec}} \times \frac{2\pi}{\text{cycle}} \times \frac{20 \text{ cm} \times 0.8}{5000 \text{ cm/sec}} = 0.20$$

In this case for values of b_o from Table B-2, $b_1 a_o \ll b_o$.

B.3 Assembling the Model

The various terms can now be collected and substituted into a form of Equation B-1 modified by the existence of a soil effective mass (Relation B-24).

$$m_e \ddot{Z} + C_s \dot{Z} + \phi(Z, Z_{max}) Z = F_v \qquad \text{(B-25)}$$

The form of Equation B-25 is similar to a mass-spring-damper system as shown in Figure B-6.

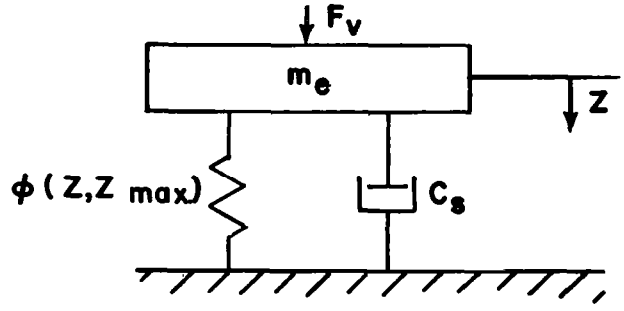

Figure B-6 SOIL MODEL

The soil "spring rate" $\phi(Z, Z_{max})$ is a complex non-linear function which includes hysteresis and the effects of soil shear. The "damper" has the form of a linear "viscous" damping coefficient and represents the energy dissipation due to radiation damping from elastic theory.

The procedure for determining $\phi(Z, Z_{max})$, C_s and m_e for simulation in an analog computer model is summarized on the following page. Information on properties of earth soils E, ν, ρ from Reference 23 is presented in Tables B-3, B-4, and B-5. Values for K_s and Z_m or P_m are normally obtained from standard plate penetrometer measurements of soil which record sinkage versus pressure, plate shape and size[21] [33]. In the case of extraterrestrial studies, it might be desirable at the present time to assign a range of arbitrary values and note the effect on computer prediction of

SUMMARY OF PROCEDURE

STEP	Soil Property Required	Reference
1. Select Vehicle-Soil Footprint (Area A)	-----	-----
2. Select Coefficient "C"	-----	Table B-1
3. Compute $\phi(Z, Z_{max}) = \frac{\phi_1(Z)}{Z}$ (Recovery)	E, ν	Equation B-12
4. Compute $\phi(Z, Z_{max}) = \frac{\phi_1(Z)}{Z}$ (Consolidation)	K_s, Z_m, or P_m	Equation B-9, B-10 or B-11
5. Select Coefficients b_o, b_1	ν	Table B-2
6. Compute $C_s = \frac{\phi_2(\dot{Z})}{\dot{Z}}$	E, ν, ρ	Equation B-23
7. Select Coefficient c_1	ν	Table B-2
8. Compute m_e	ρ	Equation B-24

Table B-3. YOUNG'S MODULUS E

SAND (Grain size, mm)	E kg/cm^2 *	SOIL TYPE	E kg/cm^2 *
1.25 - 1.55	450	Plastic Silty Clay with Sand	310
1.00 - 1.25	520	Saturated Silty Clay with Sand	440
0.60 - 0.80	620	Dense Silty Clay with Sand	2950
0.35 - 0.60	480	Medium Moist Sand	540
0.30 - 0.35	480	Gray Sand with Gravel	540
0.20 - 0.30	620	Fine Saturated Sand	850
		Medium Sand	830
		Loess	1000 - 1300
		Loessial Soil	1200

* Tabulated data and units are from Reference 23.

Table B-4. POISSONS RATIO ν

Clay	.50	Sand	.30 to .35
Clay with 30% Sand	.42		

Table B-5. DENSITY ρ

SOIL TYPE	kg sec^2/cm^4 X 10^{-6} *	SOIL TYPE	kg sec^2/cm^4 x 10^{-6}*
Moist Clay	1.80	Fine Grained Sand	1.65
Loess (Natural Moisture)	1.67	Medium Grained Sand	1.65
Dense Sand and Gravel	1.70	Medium Sized Gravel	1.80

* Tabulated data and units are from Reference 23.

APPENDIX C

VEHICLE MODELING

VEHICLE MODELING

By: J. M. Sneyd

C.1 Introduction

The traditional technique for the mathematical representation of a vehicle and its suspension system is to use a lumped rigid mass model with visco-elastic interconnections between the elements. At best, the model is an approximation of the physical system; this is due either to the shortcomings of the mathematics employed or the limitations imposed due to computing equipment. In establishing a model the above limitations must be kept in mind. To serve its purpose, however, the model must characterize the important features of the various motions and their intercouplings.

C.2 Requirements of the Mathematical Model

The investigation of the limiting conditions dictate that the model must at least include vertical translation, roll and pitch rotations for the vehicle body. From the standpoint of the vehicle model, it will be assumed that only a point contact exists at the wheel-surface interface. In references 34 and 35 it has been shown that under some conditions of speed and number of wheels a point contact is a valid assumption. The models chosen for examples of modeling techniques will be of two types; a solid axle model and an independently suspended model. Two variations for the independently suspended wheel are also considered; one with a trailing arm and one with a lateral arm.

Since the gross motions are the main concern the vehicle body is taken as a rigid frame. Articulated vehicle bodies have been mentioned in much of the literature. Although these body types are not considered here, the techniques discussed may be easily extended to include these configurations.

C.3 Approach to Derivations

The equations of motion for the various mass elements making up the vehicle system will be derived through Newton's second law ($F = ma$). Intercoordinate transformations for successive rotations will be defined in terms of Eulerian angles, using matrix notations for simplicity. First, a general case will be considered, then several example configurations will be discussed, followed by some considerations for simplification and linearization.

C.4 General Case

A six dimensional (three translation and three rotation) right hand Cartesian coordinate system is employed. The space fixed system (X, Y, Z) has the X axis horizontal with the positive direction along the vehicle body (statically) pointing to the rear. The Y axis is vertical with the positive direction upward, and the Z axis is perpendicular to the other two with the positive direction to the left of the vehicle. The body or mass fixed systems (ξ, ζ, η) in the undisturbed condition has the (ξ) axis parallel to the X axis, the (ζ) axis parallel to the Y axis and the (η) axis parallel to the Z axis. The transformation equations between space and body fixed are written with the order of rotations being yaw (angle ϕ), pitch angle ψ), and roll (angle θ) from the space fixed to the mass fixed coordinates (See Figure C-1).

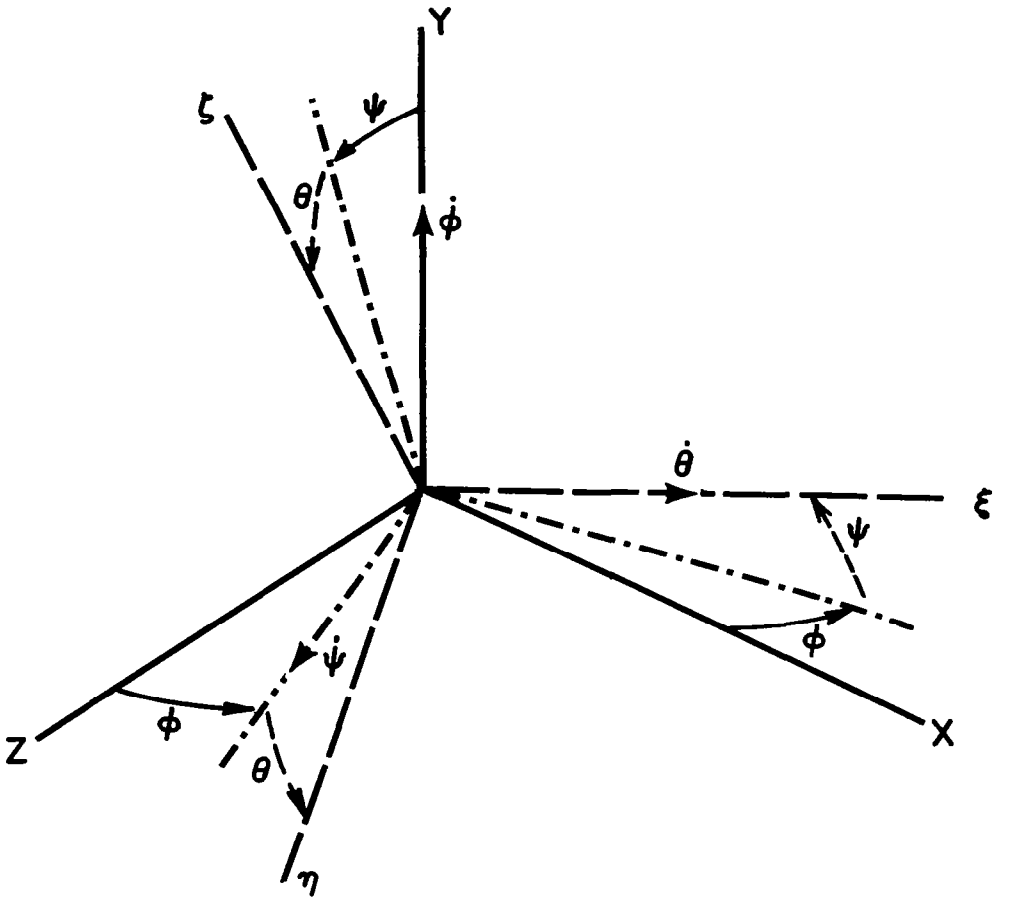

Figure C-1 ANGULAR ORIENTATION BETWEEN SPACE FIXED AND ROTATING COORDINATE SYSTEMS

The transformation matrix is given in Equation C-1

$$\begin{vmatrix} X \\ Y \\ Z \end{vmatrix} = \begin{vmatrix} C\phi C\psi & -C\phi S\psi C\theta + S\phi S\theta & C\phi S\psi S\theta + S\phi C\theta \\ S\psi & C\psi C\theta & -C\psi S\theta \\ -S\phi C\psi & S\phi S\psi C\theta + C\phi S\theta & -S\phi S\psi S\theta + C\phi C\theta \end{vmatrix} \begin{vmatrix} \xi \\ \varsigma \\ \eta \end{vmatrix} \qquad (C-1)$$

Where C has been written for cosine and S has been used for sine. Let S_o represent the space fixed vector (column matrix), B represent the mass fixed vector, and (M) be the transformation matrix. Equation C-1 can then be reduced to Equation C-2.

$$S_o = (M)\, B \qquad (C-2)$$

The components of angular velocity about the mass centered coordinates are defined in Equation C-3.

$$\begin{aligned} \omega_\xi &= \dot{\theta} + \dot{\phi} S\psi \\ \omega_\varsigma &= \dot{\phi} C\psi C\theta + \dot{\psi} S\theta \\ \omega_\eta &= -\dot{\phi} C\psi S\theta + \dot{\psi} C\theta \end{aligned} \qquad (C-3)$$

A set of equations such as Equations C-2 and C-3 can be written for each mass element in the system. If each mass element is considered to have complete freedom of motion then transformations (and angular velocities) for each mass can be denoted by equations similar to C-2 (and C-3), with the addition of subscripts, for example

$$S_1 = (M_1)\, B_1 \qquad (C-4)$$

where (M_1) has the same functional relationship as shown in Equation C-1 with a different angular measure. The transformation equations (Equations C-2 and C-4)

define the spatial orientation of each mass centered coordinate system. Since the space fixed system for each mass element is taken as parallel, the orientation of one mass centered system with respect to another is determined by equating the two;

$$(M)\,B = (M_1)\,B_1 \qquad (C\text{-}5)$$

or this may be written

$$B = (M)^{-1}\,(M_1)\,B_1 \qquad (C\text{-}6)$$

where $(M)^{-1}$ indicates the inverse, or since this is an orthogonal transformation, the transpose of (M).

Forces and moments between the various mass elements depend upon the relative displacements (for spring or stiffness elements) or velocities (for damping elements) at the attachment points in each mass element. Stiffness elements that are not co-linear with their centers of mass are affected by some component of the angular velocity or angular displacement. For these stiffness elements the relative velocities at the extremities must be used to determine the forces generated (angular displacements are not commutative). The total space fixed velocity of a point in a mass element is

$$\dot{S}_a = \dot{S}_o + (W)\,r \qquad (C\text{-}7)$$

where $\dot{S}_a$ is the total space fixed velocity of point a in the vehicle body, $\dot{S}_o$ is the column matrix of the space fixed translational velocity at the center of gravity, (W) is the angular velocity matrix (defined in Equation C-8), and r is the radius vector from the center of gravity to the point a.

$$(W) = \begin{vmatrix} 0 & -\omega_\eta & \omega_\varsigma \\ \omega_\eta & 0 & -\omega_\xi \\ -\omega_\varsigma & \omega_\xi & 0 \end{vmatrix} \qquad \text{(C-8)}$$

The opposite end of the stiffness element (one end of which is attached to the body at point a) at point α in another mass centered system (subscript 1), has a total space fixed velocity given by Equation C-9.

$$\dot{S}_\alpha = \dot{S}_1 + (W_1)\, r_1 \qquad \text{(C-9)}$$

The difference (Equation C-7 minus Equation C-9) is the total space fixed velocity of end one with respect to end two of the stiffness element. Transforming this difference into mass centered coordinates and pre-multiplying by a stiffness matrix of the form

$$K = \begin{vmatrix} C_\xi & 0 & 0 \\ 0 & C_\varsigma & 0 \\ 0 & 0 & C_\eta \end{vmatrix} \qquad \text{(C-10)}$$

determines the mass centered force components in the three orthogonal directions.

$$F = K(M)^{-1}(\dot{S}_a - \dot{S}_\alpha) \qquad \text{(C-11)}$$

Moments about the mass centered coordinate system are found by pre-multiplying by a position matrix as given in Equation C-12 . (The position matrix is formed in a manner analogous to the angular velocity matrix C-8).

$$r_a = \begin{vmatrix} 0 & -Z_a & Y_a \\ Z_a & 0 & -X_a \\ Y_a & -X_a & 0 \end{vmatrix} \qquad (C-12)$$

This gives for the moments about the mass centered system

$$T = r_a F \qquad (C-13)$$

In the above treatment the implicit assumption has been made that during the deflections the stiffness elements remain parallel to their static orientations. For rather small deflections this assumption holds, but if relative deflections between the various mass elements are large this assumption becomes invalid. Also, each mass element is considered to have freedom of motion in all axes. In those instances where the motion of a mass element is linearly related to the motion of another mass element, a constraining equation can be written. Each equation of constraint reduces by one the number of degrees of freedom for the total system.

In the following sections different versions of the "typical" vehicle will be examined to indicate how these techniques can be applied.

C.5 Solid Axle Model

A rigid framed vehicle with four wheels and two solid axles is now considered. Attention is confined to motions in the X, Y plane making the assumption that the yaw and lateral translations are zero. Figure C-2 is a skeleton drawing showing only spring stiffness elements. Stiffness elements attached to the vehicle body at points a, b, c, and d and to the two axles at points α, β, γ, and δ are shown as the body

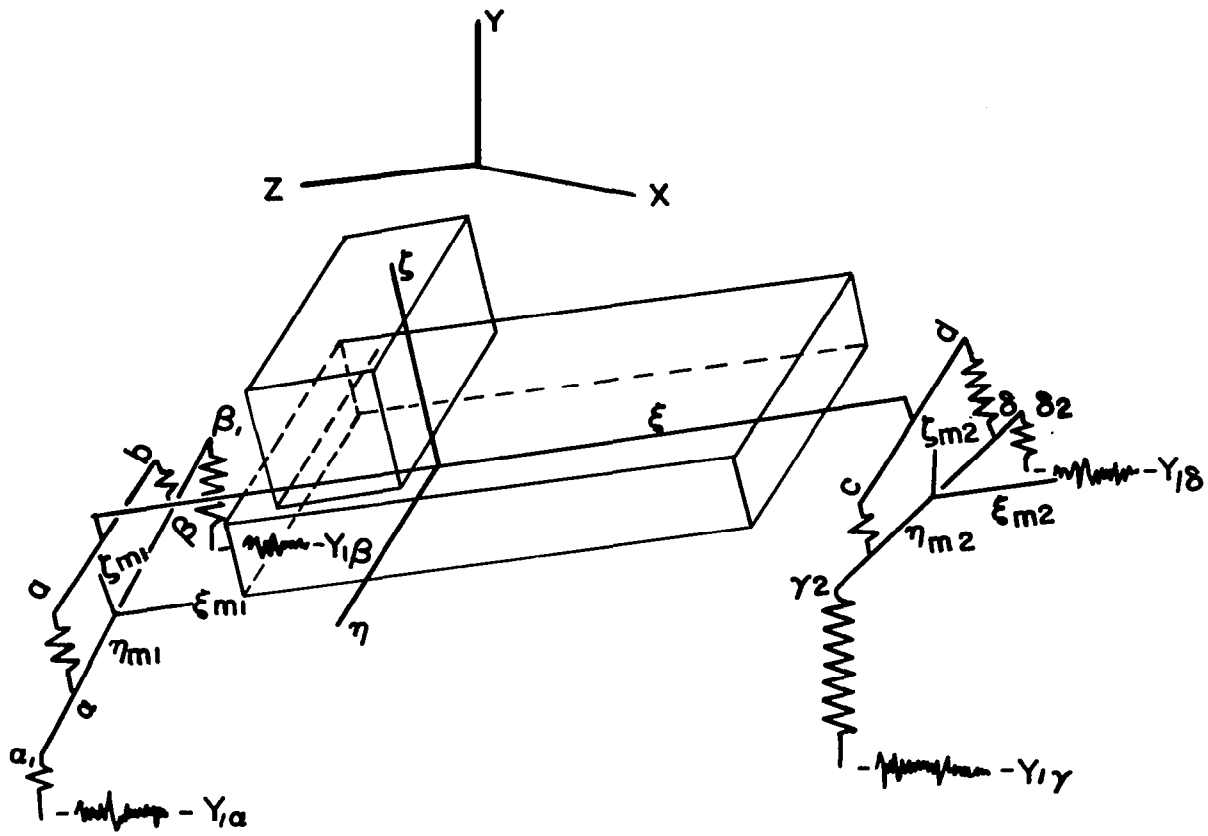

Figure C-2 SCHEMATIC OF SOLID AXLE VEHICLE MODEL

suspension system. The wheel rates are represented by stiffnesses connecting the hub of each wheel to the surface. Also indicated in the figure are the various coordinate systems (i.e., spaced fixed and mass centered systems). It is assumed that the stiffness elements are attached to the two axles in such a way that moments about the roll and pitch axes are zero. These assumptions reduce the number of degrees of freedom to seven: body vertical translations, body roll, body pitch, plus vertical translation and roll for each axle. The transformation matrices for the three mass elements are given in Equation C-14.

$$\begin{vmatrix} X_n \\ Y_n \\ Z_n \end{vmatrix} = \begin{vmatrix} C\psi & -S\psi C\theta_n & S\psi S\theta_n \\ S\psi & C\psi C\theta_n & -C\psi S\theta_n \\ 0 & S\theta_n & C\theta_n \end{vmatrix} \begin{vmatrix} \xi_n \\ \varsigma_n \\ \eta_n \end{vmatrix} \qquad (C-14)$$

$$n = 1, 2, 3$$

where yaw has been assumed to be zero.

The orientation between the axle mass systems and the body mass centered system is given in Equation C-15

$$\begin{vmatrix} \xi \\ \varsigma \\ \eta \end{vmatrix} = \begin{vmatrix} 1 & 0 & 0 \\ 0 & C(\theta_m - \theta_1) & -S(\theta_m - \theta_1) \\ 0 & S(\theta_m - \theta_1) & C(\theta_m - \theta_1) \end{vmatrix} \begin{vmatrix} \xi_m \\ \varsigma_m \\ \eta_m \end{vmatrix} \qquad (C-15)$$

$$m = 2, 3$$

The angular velocities about the body mass centered system are given in Equation C-16

$$\begin{aligned} \omega_{\xi_1} &= \dot{\theta}_1 \\ \omega_{\varsigma_1} &= \dot{\psi} S\theta_1 \\ \omega_{\eta_1} &= \dot{\psi} C\theta_1 \end{aligned} \qquad (C-16)$$

The axles have rotational freedom about the roll axis only. The angular velocities about the pitch and yaw axes are related to the body mass as shown in Equation C-15

$$\omega_{\xi m} = \omega_{\xi 1}\, C(\theta_m - \theta_1) + \omega_{\eta 1}\, S(\theta_m - \theta_1)$$

$$\omega_{\eta m} = -\omega_{\xi 1}\, S(\theta_m - \theta_1) + \omega_{\eta 1}\, C(\theta_m - \theta_1) \qquad (C-17)$$

$$m = 2, 3$$

From this set of defining equations (Equations C-14 through C-17) the forces and moments acting on each mass element can be derived. Equating these forces and moments to the inertial forces establishes a set of seven simultaneous second order differential equations.

C.6 Independent Suspension Systems

A sketch of the left front wheel and accompanying suspension system is shown in Figure C-3. For this model lateral translations and yaw rotations are again taken to be zero, and the wheel is assumed to have freedom only in the roll direction (rotation about the ξ axis). Allowing the vehicle body to have freedom in vertical translation, roll, pitch rotations, and each wheel in roll only, results in a seven degree of freedom system. The differential equations for this system are similar to those for the solid axle model with the additional condition that the motion at the wheel pivot point (point b in Figure C-3) is constrained. This constraining equation is written by equating the total space fixed displacement of point b as measured in the body centered system to that measured in the wheel centered system (Equation C-18).

$$\dot{S}_1 + (W_1)\, r_1 = \dot{S}_2 + (W_2)\, r_2 \qquad (C-18)$$

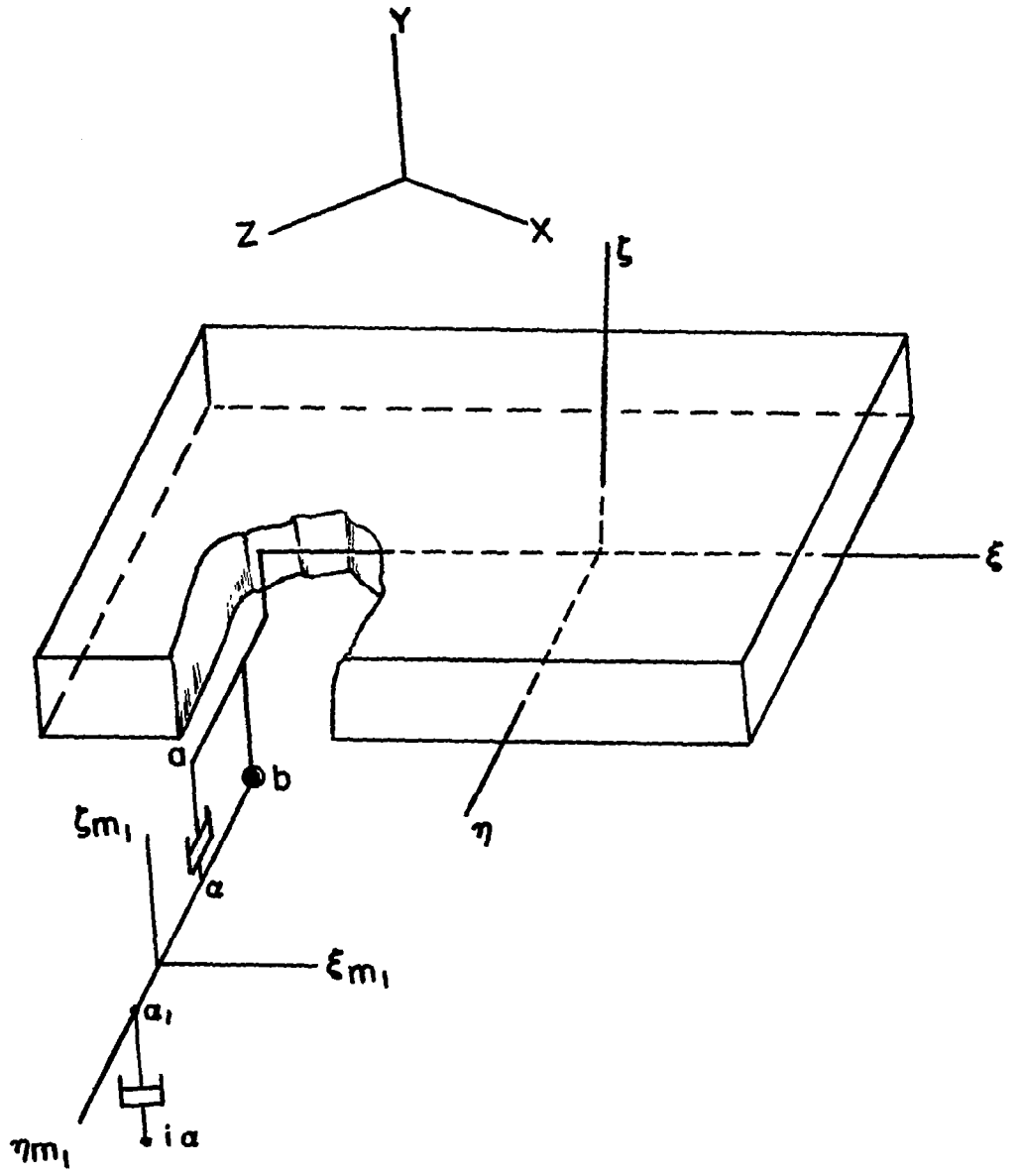

Figure C-3 SCHEMATIC OF A TYPICAL INDEPENDENTLY SUSPENDED WHEEL

where $\dot{S}_n$ is the space fixed translational velocity, (W_n) is the angular velocity matrix, and r_n is the radius vector from the center of gravity to the pivot point.

A second example of an independently suspended wheel is shown in Figure C-4. Here there is a trailing arm suspension, providing freedom of rotation of the wheel mass about the pitch axis. If the order of the successive rotations are held in deriving the Eulerian angles (that is yaw, pitch, then roll), then the defining equations for the coordinate transformations are given in Equation C-19 .

$$\begin{vmatrix} X_n \\ Y_n \\ Z_n \end{vmatrix} = \begin{vmatrix} C\psi\, C(\psi_n - \psi) & C\psi\, S(\psi_n - \psi) & S\psi\, S\theta \\ -S\psi\, S(\psi_n - \psi)\, C\theta & S\psi\, C(\psi_n - \psi)\, C\theta & \\ S\psi\, C(\psi_n - \psi) & -S\psi\, S(\psi_n - \psi) & -C\psi\, S\theta \\ +C\psi\, S(\psi_n - \psi)\, C\theta & C\psi\, C(\psi_n - \psi)\, C\theta & \\ S(\psi_n - \psi)\, S\theta & C(\psi_n - \psi)\, S\theta & C\theta \end{vmatrix} \begin{vmatrix} \xi_n \\ \varsigma_n \\ \eta_n \end{vmatrix} \qquad (C\text{-}19)$$

In the above equation yaw angle has been taken as zero; the defining transformations between body mass centered and wheel mass centered coordinate systems is shown in Equation C-20.

$$\begin{vmatrix} \xi \\ \varsigma \\ \eta \end{vmatrix} = \begin{vmatrix} C(\psi_n - \psi) & -S(\psi_n - \psi) & 0 \\ S(\psi_n - \psi) & C(\psi_n - \psi) & 0 \\ 0 & 0 & 1 \end{vmatrix} \begin{vmatrix} \xi_n \\ \varsigma_n \\ \eta_n \end{vmatrix} \qquad (C\text{-}20)$$

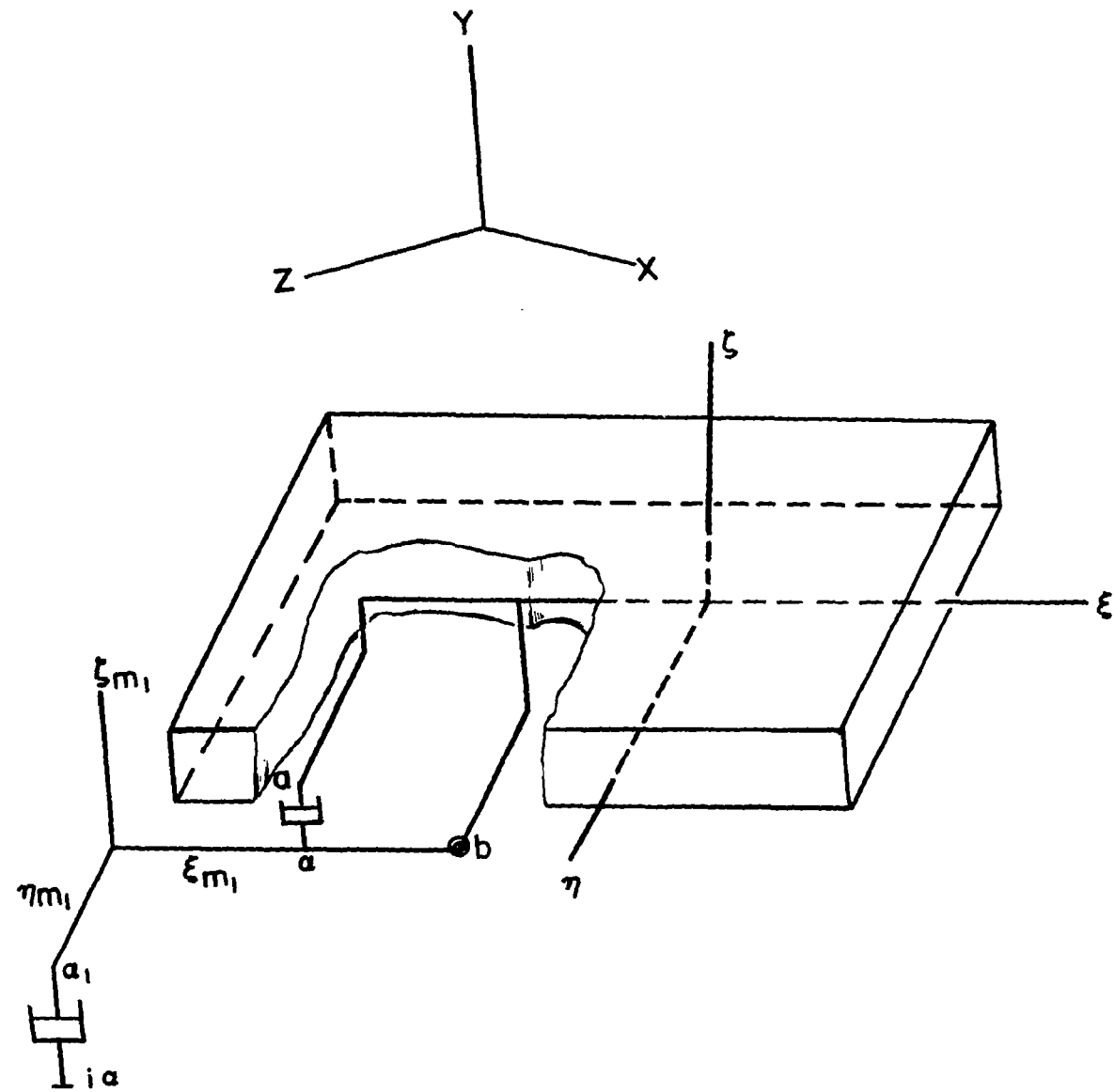

Figure C-4 SCHEMATIC OF A TYPICAL TRAILING ARM INDEPENDENTLY SUSPENDED WHEEL

The angular velocities about the body centered system (Equation C-21)

$$\begin{aligned} \omega_\xi &= \dot{\theta} \\ \omega_\zeta &= \dot{\psi} S\theta \\ \omega_\eta &= \dot{\psi} C\theta_1 \end{aligned} \qquad \text{(C-21)}$$

are related to the angular velocities about the wheel centered systems through Equation C-20 which are equations of constraint. This gives

$$\begin{aligned} \omega_{\xi_n} &= \omega_\xi C(\psi_n - \psi) + \omega_\zeta S(\psi_n - \psi) \\ \omega_{\zeta_n} &= -\omega_\xi S(\psi_n - \psi) + \omega_\zeta C(\psi_n - \psi) \end{aligned} \qquad \text{(C-22)}$$

for the rotational motions.

In all cases the equations of motion, translation and rotation, have been written about the center of mass of each element. In the case of the independently suspended wheels the center of mass does not coincide with the center of rotation, so that care must be taken to define the moment of inertia for each wheel mass in the proper context. A recommended method of analysis is to use Lagrangian mechanics.

C.7 Simplification of the System of Equations

The models that have been discussed each represents a simplified description of the vehicle suspension system, yet the programming and solution is difficult. It is, therefore, of interest to investigate further simplifications or linearizations to produce a more tractable problem. Perhaps the most justifiable simplification is in the rotational freedom of the wheel masses. The defining equations for the wheel rotational motion include terms

in which the difference in two angles appear, such as the difference between the body roll and the wheel or axle roll. This angular difference can be linearized (small angle assumption) on the basis that the suspension system has but a limited range of free travel. For the independent suspension this can be carried further, approximating the small rotational motion by translational motion (such as the linear approach to the simple pendulum). Linearizations of the vehicle body rotational motion can only be justified for low amplitude input functions and/or for certain types of inputs. For a deterministic input the magnitude of the response may be approximated prior to solution in the same fashion that an analog problem is scaled.

Another simplifying approach that may be taken as an "initial investigation" is a two dimensional model. If a symmetric vehicle body is assumed, roll and pitch motions are uncoupled and the vehicle motion in bounce and pitch can be studied with a "bicycle model", or bounce and roll investigations made with a "two wheeled cart model".

In establishing the degree of sophistication for the vehicle model, the particular dynamic characteristics under study, the type of input, and the kind of computing equipment to be used must be considered.

C.8 Linear n-Wheeled Vehicle and Yielding Surface Model

For the purpose of illustration, equations of motion and an analog computer circuit are presented for a typical n-wheel rigid body vehicle where the body axes are assumed to be principle axes of inertia. The wheels are represented by the axle-hub mass (m_{w_i}) and a rim mass (m_{r_i}). The rim masses are in contact with a yielding surface represented by the effective soil mass (m_{s_i}). The surface profile is inserted between the soil and the rim. A mass (m_f) is attached to the body by a spring and a damper which may represent

a piece of on-board equipment that could be used as a vibration damper. Equations C-23 through C-28 are the equations of motion for this model and the symbols are defined in Table C-1.

Body Vertical

$$m\ddot{Y} = -\sum_{j=1}^{n}\left[k_{sj}\left(Y + x_{kj}\psi - z_{kj}\theta - Y_{wj}\right) + c_{sj}\left(\dot{Y} + x_{cj}\dot{\psi} - z_{cj}\dot{\theta} - \dot{Y}_{wj}\right)\right] - mg - k_f\left(Y + x_k\psi - z_k\theta - Y_f\right) - c_f\left(\dot{Y} + x_c\dot{\psi} - z_c\dot{\theta} - \dot{Y}_f\right) \quad \text{(C-23)}$$

Body Roll

$$I_x\ddot{\theta} = \sum_{j=1}^{n}\left[z_{kj}\,k_{sj}\left(Y + x_{kj}\psi - z_{kj}\theta - Y_{wj}\right) + z_{cj}\,c_{sj}\left(\dot{Y} + x_{cj}\dot{\psi} - z_{cj}\dot{\theta} - \dot{Y}_{wj}\right)\right] + z_k\,k_f\left[Y + x_k\psi - z_k\theta - Y_f\right] + z_c\,c_f\left[\dot{Y} + x_c\dot{\psi} - z_c\dot{\theta} - \dot{Y}_f\right] \quad \text{(C-24)}$$

Body Pitch

$$I_Z\ddot{\psi} = -\sum_{j=1}^{n}\left[x_{kj}\,k_{sj}\left(Y + x_{kj}\psi - z_{kj}\theta - Y_{wj}\right) + x_{cj}\,c_{sj}\left(\dot{Y} + x_{cj}\dot{\psi} - z_{cj}\dot{\theta} - \dot{Y}_{wj}\right)\right] - x_k\,k_f\left[Y + x_k\psi - z_k\theta - Y_f\right] - x_c\,c_f\left[\dot{Y} + x_c\dot{\psi} - z_c\dot{\theta} - \dot{Y}_f\right] \quad \text{(C-25)}$$

Vibration Damper-Body Mounted-Vertical

$$m_f\ddot{Y}_f = k_f\left[Y + x_k\psi - z_k\theta - Y_f\right] + c_f\left[\dot{Y} + x_c\dot{\psi} - z_c\dot{\theta} - \dot{Y}_f\right] - m_f\,g \quad \text{(C-26)}$$

Typical j^{th} Wheel Vertical

$$m_{wj}\ddot{Y}_{wj} = -k_{wj}\left[Y_{wj} - Y_{rj}\right] - c_{wj}\left[\dot{Y}_{wj} - \dot{Y}_{rj}\right] + k_{sj}\left[Y + x_{kj}\psi - z_{kj}\theta - Y_{wj}\right] + c_{sj}\left[\dot{Y} + x_{cj}\dot{\psi} - z_{cj}\dot{\theta} - \dot{Y}_{wj}\right] - m_{wj}\,g \quad \text{(C-27)}$$

Typical j^{th} Rim Vertical

$$m_{rj}\ddot{Y}_{rj} = -k_{wj}\left[Y_{wj} - Y_{rj}\right] + c_{wj}\left[\dot{Y}_{wj} - \dot{Y}_{rj}\right] - m_{rj}\,g - k_{rj}\left[Y_{rj} - (Y_{pj} + Y_{sj})\right] \quad \text{(C-28)}$$

Equivalent Soil Mass at j^{th} Wheel Vertical

$$m_{sj}\ddot{Y}_{sj} = \emptyset\,Y_{sj} - C_s\,\dot{Y}_{sj} + k_{rj}\left[Y_{rj} - (Y_{pj} + Y_{sj})\right] \quad \text{(C-29)}$$

Table C-1 LIST OF SYMBOLS FOR GENERAL EQUATIONS OF MOTION OF AN INDEPENDENTLY SUSPENDED VEHICLE WITH N-WHEELS ON YIELDING SOIL.

m	Sprung mass of the vehicle
$\ddot{Y}, \dot{Y}, Y$	Vertical motion of the c.g. of the sprung mass of the vehicle in acceleration, velocity, and displacement.
k_{sj}	Suspension spring constant connecting the j^{th} wheel to the vehicle.
c_{sj}	Suspension damping constant connecting the j^{th} wheel to the vehicle.
x_{kj}, z_{kj} x_{cj}, z_{cj}	Distances from mass center of vehicle to the point of connection between j^{th} wheel suspension component (K - spring, C-damper) and the vehicle. They carry with them the sign as determined from the body fixed axes.
$\ddot{\psi}, \dot{\psi}, \psi$	Pitch acceleration, Pitch velocity, and Pitch displacement of the vehicle, respectively.
$\ddot{\theta}, \dot{\theta}, \theta$	Roll acceleration, roll velocity, and roll displacement of the vehicle, respectively.
I_x, I_z	Mass moments of inertia of the sprung mass about the roll and pitch axes, respectively.
n	Number of wheels on the vehicle.
$\ddot{Y}_{wj}, \dot{Y}_{wj}, Y_{wj}$	The j^{th} wheel center acceleration, velocity and displacement.
m_{wj}	Mass of the j^{th} wheel
k_{wj}	Wheel spring constant for the j^{th} wheel.
c_{wj}	Wheel damping constant for the j^{th} wheel.
m_{rj}	Mass of the rim in contact with the soil for the j^{th} wheel.
$\ddot{Y}_{rj}, \dot{Y}_{rj}, Y_{rj}$	Vertical acceleration, velocity, and displacement of rim mass connected to the j^{th} wheel.

Table C-1 (CONT.)

$\ddot{Y}_{sj}$, $\dot{Y}_{sj}$, Y_{sj}	Vertical acceleration, velocity, and displacement of the soil under the j^{th} wheel.
m_{sj}	The effective mass of the soil under the j^{th} wheel.
C_s	Soil damping constant
k_{rj}	An imaginary spring rate between rim mass and the soil mass under the j^{th} wheel which has the property, $k_{rj} = \begin{cases} 0 \text{ if } Y_{rj} \geq Y_{pj} + Y_{sj} \\ \infty \text{ if } Y_{rj} < Y_{pj} + Y_{sj} \end{cases}$
g	Gravitational constant determined by where the vehicle is located.
$\emptyset$	Non-linear spring constant in soil model (See Appendix B).
Y_{pj}	Profile height under the j^{th} wheel

In this model angular motions have been linearized. The included non-linearities are the lift-off capability of the rim mass and the non-linear soil model of Appendix B. For the purpose of analog simulation it has been assumed here that the consolidation phase of soil response is represented by the linear coefficient of sub-grade reaction K_s. Function generators can be used in place of the potentiometers if actual loading curves are available for the soil in question (See Appendix B). The effects of the linear consolidation soil rate K_s and elastic recovery spring constant k_s in Equation C-29 are given in Equation C-30.

$$m_{sj} \ddot{Y}_{sj} = - K_s Y_{sj} - C_s \dot{Y}_{sj} + k_{rj} \left[Y_{rj} - (Y_{pj} + Y_{sj}) \right] - (k_s - k_s)(Y_{sj} - Y_{sj\ max}) \quad \text{(C-30)}$$

where $Y_{sj\ max}$ is the time dependent maximum deflection that the soil under the j^{th} wheel has experienced due to the loading of the j^{th} and preceding wheels. The subscript "max" as used here is defined in Equation C-31.

$$Y_{max} = \begin{cases} Y' e^{-2Vt'/R_j} & \text{for } Y < Y_{max} \\ Y & \text{otherwise} \end{cases} \qquad \text{(C-31)}$$

where Y' is the latest value for which $Y = Y_{max}$ and t' is a time measure which is reset to zero whenever Y' takes on a new value. The vehicle velocity and the wheel radius are represented by V and R_j respectfully. The maximum soil deflection at the j^{th} wheel is defined in the following manner.

$$Y_{sj\ max} = Y_{sk\ max} - \left[Y_{sj} - Y_{sk\ max}\right]_{max} \qquad \text{(C-32)}$$

where $Y_{sk\ max}$ is the properly time delayed maximum soil deflection due to the preceding in-line k^{th} wheel.

Figures C-5a and C-5b show an analog computer network for simulation of the general n-wheeled vehicle model without the body mounted vibration damper. Figure C-5a is the network for the three degrees of freedom (vertical pitch, and roll) of the vehicle body with inputs from each of the n-wheels. Figure C-5b is a typical j^{th} wheel computer network which must be repeated n times for the n-wheels with appropriate coefficients and time delays. While this vehicle model is linear it is possible to easily incorporate non-linearities of wheel travel limits with diodes around the appropriate amplifiers, or non-linearities of spring rates and damping coefficients with diode function generators replacing the appropriate potentiometers.

C.9 MOLAB Concept Model

A simple MOLAB Concept model was chosen to implement and demonstrate techniques. The same model was previously used for analysis to step inputs[14] and is based on the early conceptional MOLAB drawing made by NASA-MSFC shown in Figure C-6. A schematic

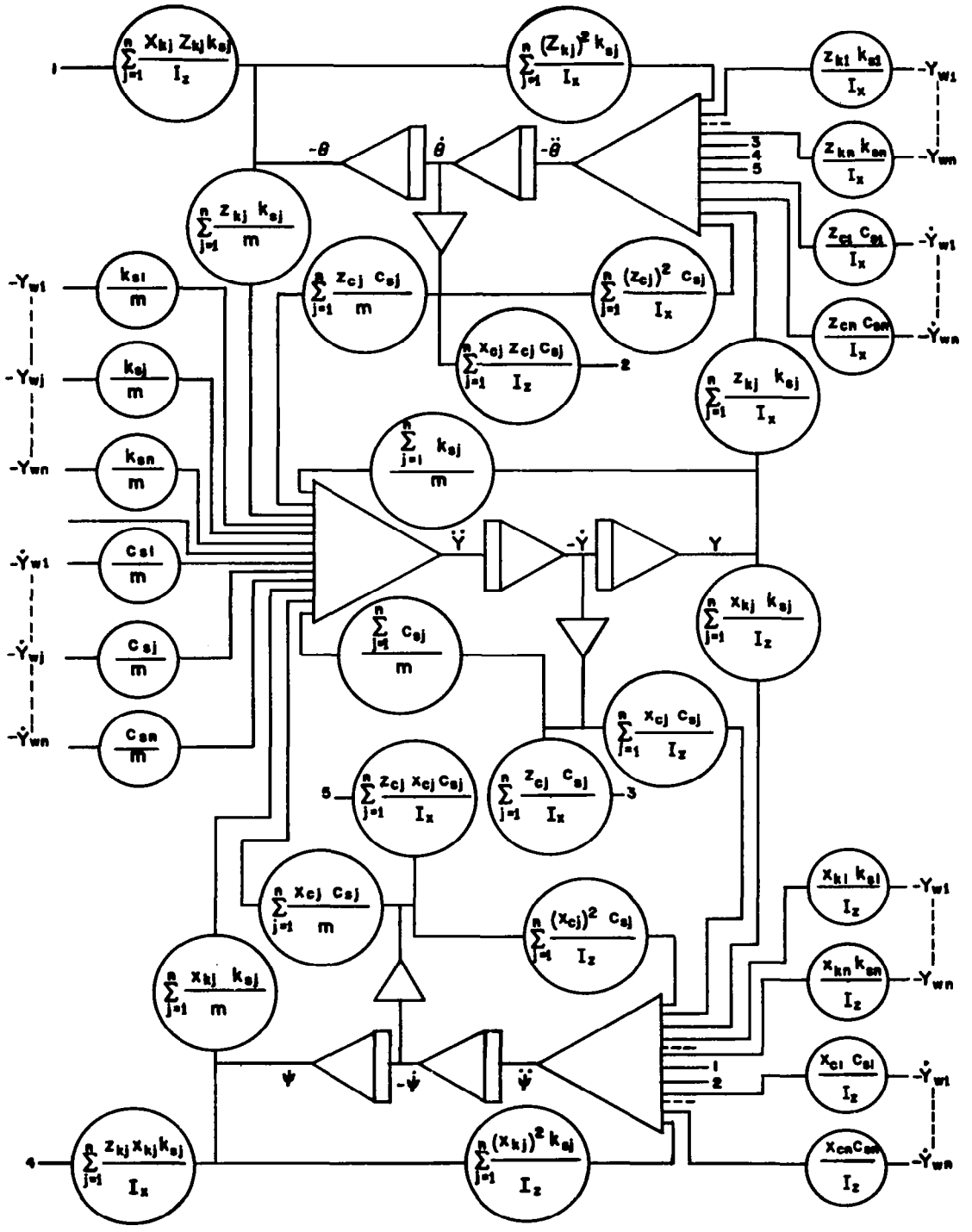

Figure C-5a GENERAL "n" WHEELED VEHICLE BODY COMPUTER CIRCUIT

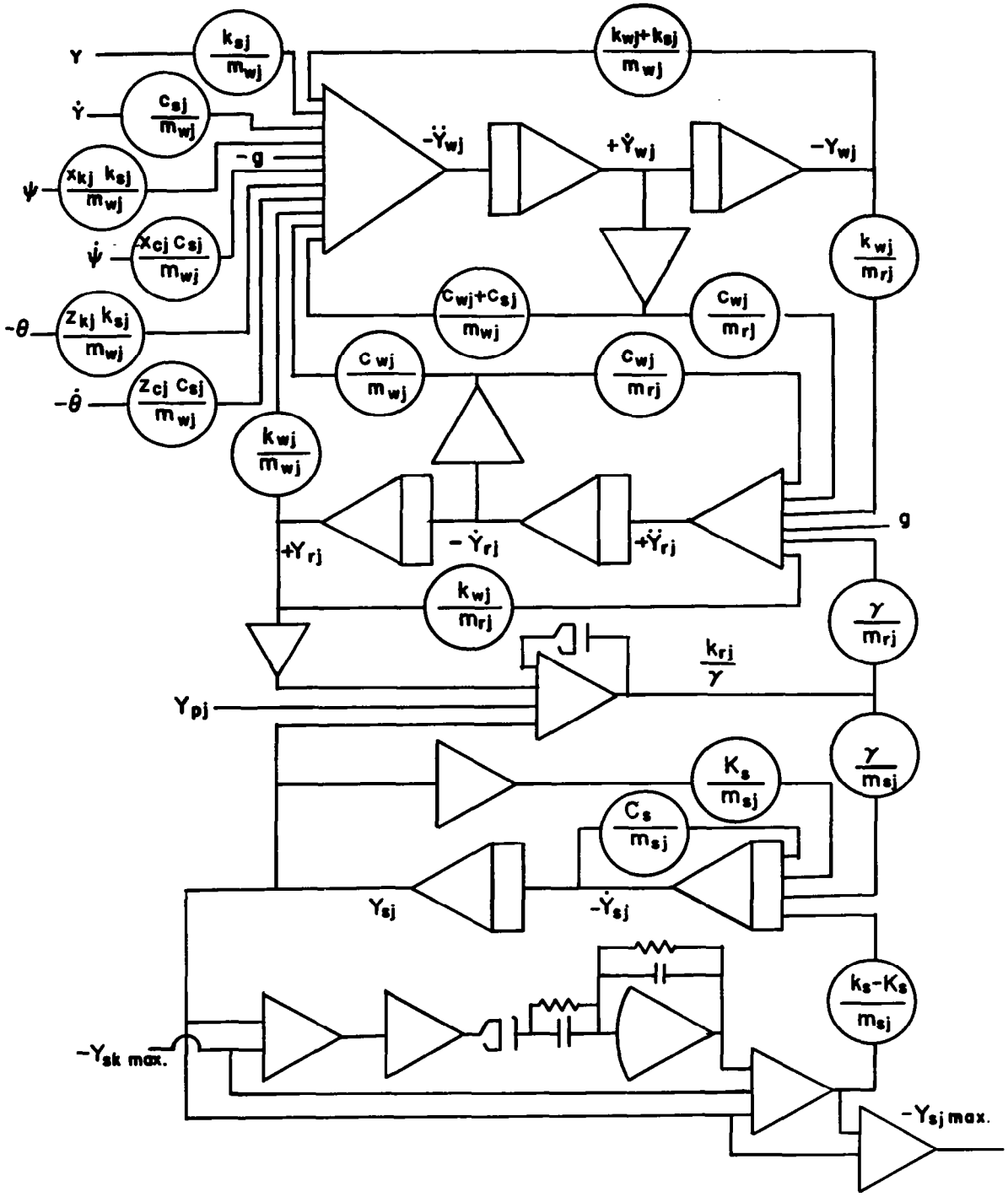

Figure C-5b COMPUTER CIRCUIT FOR jth WHEEL AND SOIL

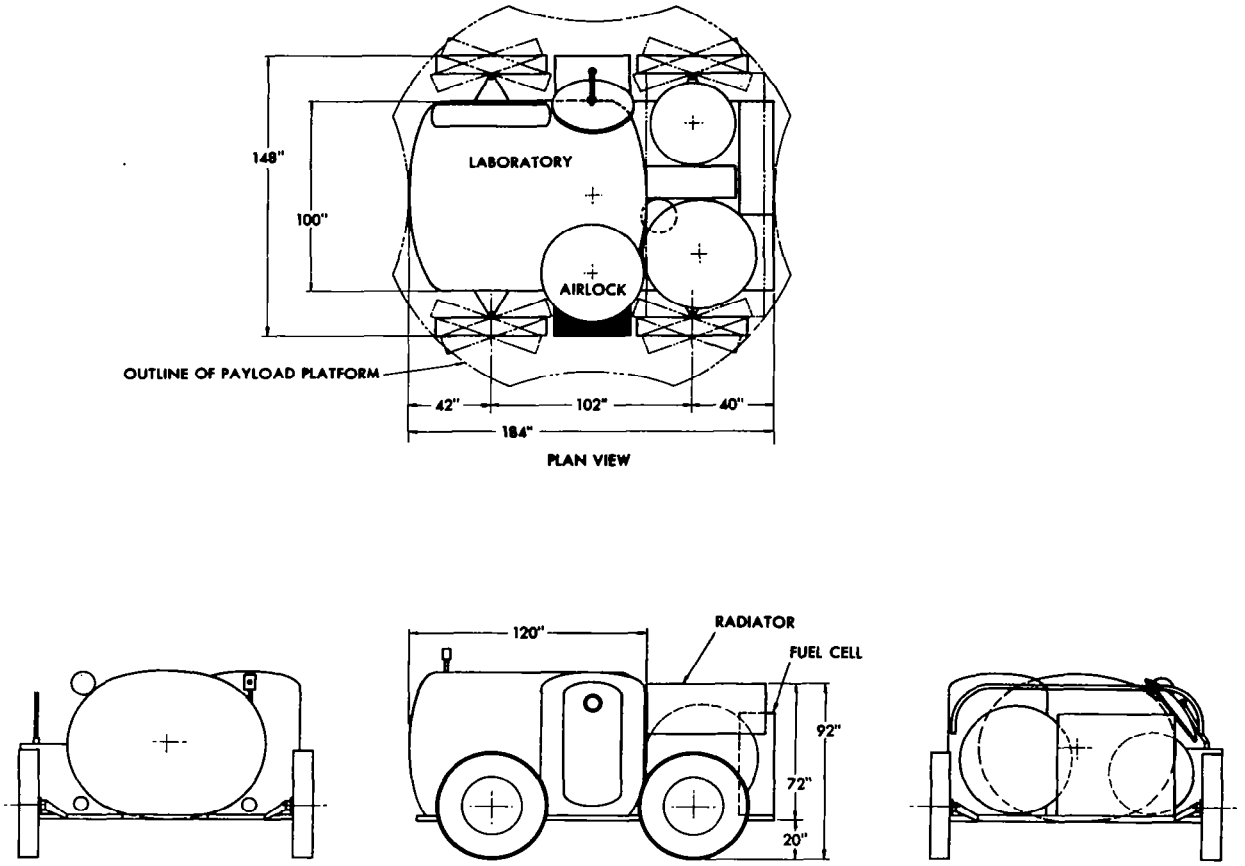

Figure C-6 MOLAB CONCEPT II

model for analysis based on the conceptional drawing is shown in Figure C-7. This model is a rigid body model with four independently suspended wheels that have identical coefficients. The values for the physical constants used in model analysis are shown in Table C-2.

Appendix D gives the results of a linear frequency domain analysis of this model on a non-yielding soil, where vehicle-surface separation was not allowed. Three different versions were investigated and compared:

1. Independent suspension
2. Independent suspension with on-board vibration damper.
3. Solid axle suspension.

Table C-3 gives the list of changes and additions to the physical constants of Table C-2 which were used for the analysis with an on-board vibration damper.

Appendix E gives the results of a non-linear time domain analysis of this model using an analog computer with white noise input. The equations of motion (Equations C-23 through C-32) were modified to represent the MOLAB model and the analog computer circuit was implemented from the circuit shown in Figures C-5a and C-5b. Table C-4 lists the physical constants for the yielding soil simulation. The time domain analysis included the effects of both yielding and non-yielding soil effects and in each case vehicle-surface separation was permitted and measured.

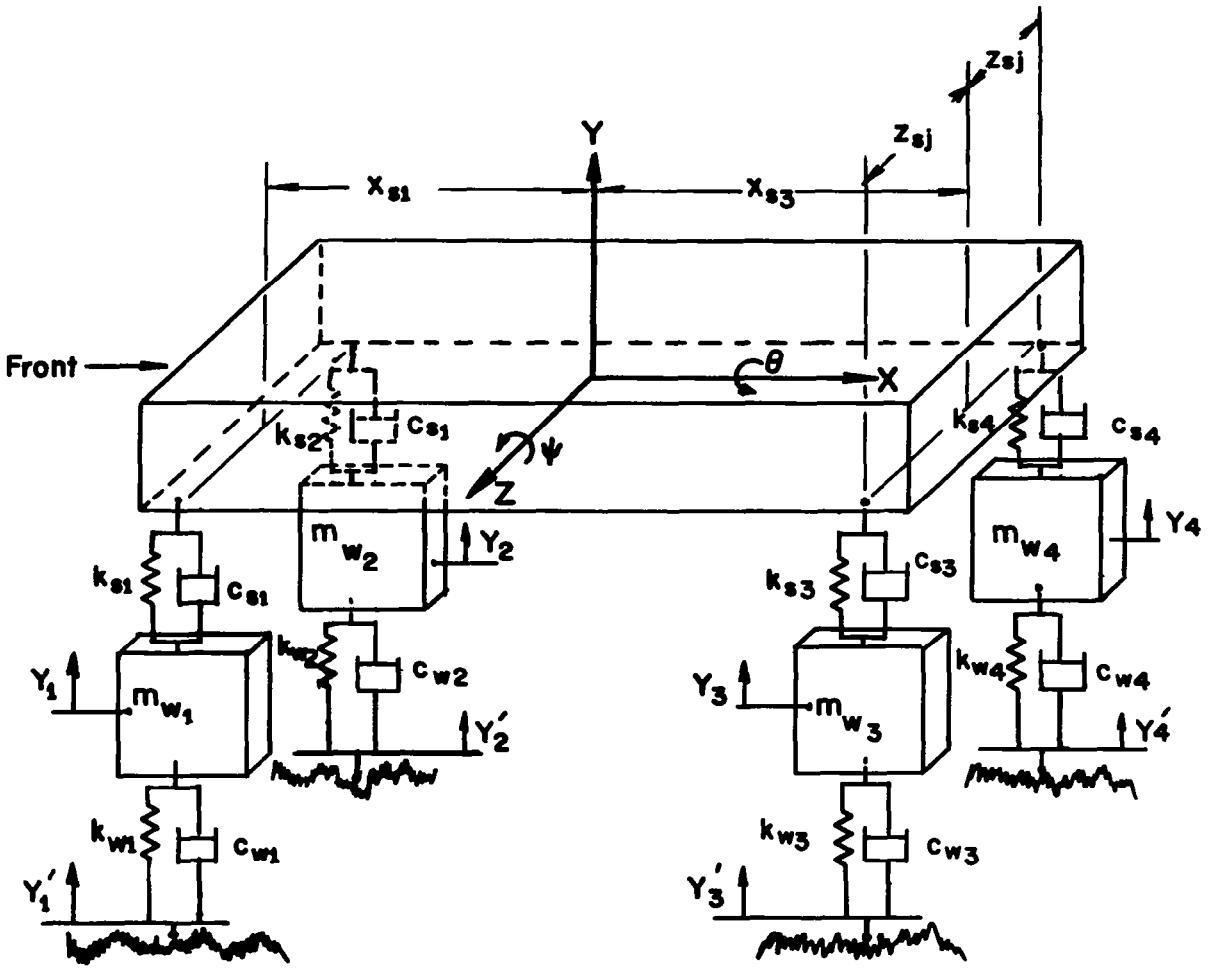

Figure C-7 SCHEMATIC MODEL OF VEHICLE USED FOR NON-YIELDING SURFACE

Table C-2 PHYSICAL CONSTANTS FOR MOLAB VEHICLE

Symbol	Description	Value M.K.S. Units	Value English Units
m	Body Mass	2950 kilograms	202 slugs
I_x	Roll moment of inertia	3145 kilograms (meters)^2	2320 slugs (ft)^2
I_z	Pitch moment of inertia	6240 kilograms (meters)^2	4600 slugs (ft)^2
m_{wj}	Wheel mass	22.8 kilograms	1.87 slugs
k_{sj}	Suspension spring rate	29200 newtons/meter	2000 pounds/ft.
C_{sj}	Suspension damping	700 newton sec./meter	48 pounds sec./ft.
k_{wj}	Wheel spring rate	78100 newton/meter	5350 pounds/ft.
c_{wj}	Wheel damping	35 newton sec./meter	2.4 pound sec./ft.
X_{s1}	Distance C.G. to front	1.27 meters	4.17 ft.
X_{s3}	Distance C.G. to rear	1.32 meters	4.33 ft.
Z_{sj}	Distance C.G. to side	1.75 meters	5.57 ft.

Table C-3 CHANGES AND ADDITIONS TO TABLE C-2 FOR ON-BOARD VIBRATION DAMPER

Symbol	Description	Value M.K.S. Units	Value English Units
m	Body mass	2723 kilograms	186.48 slugs
m_f	Vibration damper mass	226 kilograms	15.48 slugs
I_x	Body roll moment of inertia	2965 kilograms (meters)^2	2187 slugs (ft)^2
I_Z	Body pitch moment of inertia	5862 kilograms (meters)^2	4324 slugs (ft)^2
k_f	Spring rate vibration damper	895272 newtons/meter	61,320 pounds/ft
c_f	Damping constant vibration damper	70 newtons sec./meter	4.8 pounds sec./ft.
x_f	Distance of vibration damper behind body C.G.	1.5 meters	5.0 ft.
z_f	Distance of vibration damper to the left of body C.G.	0.7 meters	2.5 ft.

Table C-4 PHYSICAL CONSTANTS FOR YIELDING SOIL SIMULATION

Symbol	Description	Value M.K.S. Units	Value English Units
k_s	Elastic recovery spring rate of soil	328600 newton/meter	22533 pounds/ft.
K_s	Coefficient of subgrade reaction	16430 newton/meter	1127 pounds/ft
C_s	Damping coefficient of soil	3263 newton sec./meter	224 pounds sec./ft.
m_s	Effective soil mass	10 kilograms	0.686 slugs
m_{ri}	Rim mass of wheel	7 kilograms	0.48 slugs
R_i	Radius of wheel	0.7 meter	2.5 ft.

APPENDIX D

FREQUENCY DOMAIN ANALYSIS

FREQUENCY DOMAIN ANALYSIS

By: J. M. Sneyd and R. G. Gergle

D.1 Introduction

Equations of motion were derived for a general n-wheeled vehicle model in Appendix C and a specific four wheeled independent suspension model was described. In this appendix a linear version of this model is analyzed using a frequency domain approach. The differential equations of motion are converted to algebraic complex number equations via the Fourier transform and transfer functions are obtained on a digital computer. These transfer functions are combined, by the superposition theorem to predict the system response to random signal inputs. It is shown that for inputs (in this case lunar surface profiles) which can be statistically characterized by a power spectral density, the system response can be statistically analyzed and a prediction of the probability of exceeding limiting conditions can be made.

D.2 Description of Linearized Model

A schematic drawing of the vehicle is discussed in Appendix C. The total sprung mass is made up of the vehicle body mass and the mass of an on-board vibration damper, say the fuel cell. The fuel cell is attached to the body by a spring and damper. The body mass is assumed to have three degrees of freedom: vertical translation (bounce), roll and pitch rotations. The fuel cell is restricted to vertical translation, as are each of the wheels. The suspension springs and dampers have been assumed to be co-linear with the center of gravity of the wheel masses: the same is true for the springs and dampers representing the wheels.

The equations of motion for this eight degree of freedom system are given below as Equations D-1 through D-8. The notation employed in these equations is as follows: Subscripts

$$
\begin{aligned}
m_1(\ddot{Y}_1) = & -K_1\left[(Y_1) + (X_1)_1(\psi_1) - (Z_1)_1(\theta_1) - (Y_2)\right] \\
& -K_2\left[(Y_1) + (X_1)_2(\psi_1) - (Z_1)_2(\theta_1) - (Y_3)\right] \\
& -K_3\left[(Y_1) + (X_1)_3(\psi_1) - (Z_1)_3(\theta_1) - (Y_4)\right] \\
& -K_4\left[(Y_1) + (X_1)_4(\psi_1) - (Z_1)_4(\theta_1) - (Y_5)\right] \\
& -K_9\left[(Y_1) + (X_1)_9(\psi_1) - (Z_1)_9(\theta_1) - (Y_9)\right] \\
& -C_1\left[(\dot{Y}_1) + (X_1)_1(\dot{\psi}_1) - (Z_1)_1(\dot{\theta}_1) - (\dot{Y}_2)\right] \\
& -C_2\left[(\dot{Y}_1) + (X_1)_2(\dot{\psi}_1) - (Z_1)_2(\dot{\theta}_1) - (\dot{Y}_3)\right] \\
& -C_3\left[(\dot{Y}_1) + (X_1)_3(\dot{\psi}_1) - (Z_1)_3(\dot{\theta}_1) - (\dot{Y}_4)\right] \\
& -C_4\left[(\dot{Y}_1) + (X_1)_4(\dot{\psi}_1) - (Z_1)_4(\dot{\theta}_1) - (\dot{Y}_5)\right] \\
& -C_9\left[(\dot{Y}_1) + (X_1)_9(\dot{\psi}_1) - (Z_1)_9(\dot{\theta}_1) - (\dot{Y}_9)\right]
\end{aligned}
\qquad (D\text{-}1)
$$

$$
\begin{aligned}
I_{\theta 1}(\ddot{\theta}_1) = & \quad (Z_1)_1 K_1\left[(Y_1) + (X_1)_1(\psi_1) - (Z_1)_1(\theta_1) - (Y_2)\right] \\
& +(Z_1)_2 K_2\left[(Y_1) + (X_1)_2(\psi_1) - (Z_1)_2(\theta_1) - (Y_3)\right] \\
& +(Z_1)_3 K_3\left[(Y_1) + (X_1)_3(\psi_1) - (Z_1)_3(\theta_1) - (Y_4)\right] \\
& +(Z_1)_4 K_4\left[(Y_1) + (X_1)_4(\psi_1) - (Z_1)_4(\theta_1) - (Y_5)\right] \\
& +(Z_1)_9 K_9\left[(Y_1) + (X_1)_9(\psi_1) - (Z_1)_9(\theta_1) - (Y_9)\right]
\end{aligned}
\qquad (D\text{-}2)
$$

$$+ (Z_1)_1 C_1 \left[(\dot{Y}_1) + (X_1)_1 (\dot{\psi}_1) - (Z_1)_1 (\dot{\theta}_1) - (\dot{Y}_2) \right]$$

$$+ (Z_1)_2 C_2 \left[(\dot{Y}_1) + (X_1)_2 (\dot{\psi}_1) - (Z_1)_2 (\dot{\theta}_1) - (\dot{Y}_3) \right]$$

$$+ (Z_1)_3 C_3 \left[(\dot{Y}_1) + (X_1)_3 (\dot{\psi}_1) - (Z_1)_3 (\dot{\theta}_1) - (\dot{Y}_4) \right]$$

$$+ (Z_1)_4 C_4 \left[(\dot{Y}_1) + (X_1)_4 (\dot{\psi}_1) - (Z_1)_4 (\dot{\theta}_1) - (\dot{Y}_5) \right]$$

$$+ (Z_1)_9 C_9 \left[(\dot{Y}_1) + (X_1)_9 (\dot{\psi}_1) - (Z_1)_9 (\dot{\theta}_1) - (\dot{Y}_9) \right] \qquad \text{(D-2) (Cont.)}$$

$$I_{\psi_1} (\ddot{\psi}_1) = - (X_1)_1 K_1 \left[(Y_1) + (X_1)_1 (\psi_1) - (Z_1)_1 (\theta_1) - (Y_2) \right]$$

$$- (X_1)_2 K_2 \left[(Y_1) + (X_1)_2 (\psi_1) - (Z_1)_2 (\theta_1) - (Y_3) \right]$$

$$- (X_1)_3 K_3 \left[(Y_1) + (X_1)_3 (\psi_1) - (Z_1)_3 (\theta_1) - (Y_4) \right]$$

$$- (X_1)_4 K_4 \left[(Y_1) + (X_1)_4 (\psi_1) - (Z_1)_4 (\theta_1) - (Y_5) \right]$$

$$- (X_1)_9 K_9 \left[(Y_1) + (X_1)_9 (\psi_1) - (Z_1)_9 (\theta_1) - (Y_9) \right] \qquad \text{(D-3)}$$

$$- (X_1)_1 C_1 \left[(\dot{Y}_1) + (X_1)_1 (\dot{\psi}_1) - (Z_1)_1 (\dot{\theta}_1) - (\dot{Y}_2) \right]$$

$$- (X_1)_2 C_2 \left[(\dot{Y}_1) + (X_1)_2 (\dot{\psi}_1) - (Z_1)_2 (\dot{\theta}_1) - (\dot{Y}_3) \right]$$

$$- (X_1)_3 C_3 \left[(\dot{Y}_1) + (X_1)_3 (\dot{\psi}_1) - (Z_1)_3 (\dot{\theta}_1) - (\dot{Y}_4) \right]$$

$$- (X_1)_4 C_4 \left[(Y_1) + (X_1)_4 (\psi_1) - (Z_1)_4 (\theta_1) - (Y_5) \right]$$

$$- (X_1)_9 C_9 \left[(\dot{Y}_1) + (X_1)_9 (\dot{\psi}_1) - (Z_1)_9 (\dot{\theta}_1) - (\dot{Y}_9) \right]$$

$$m_2(\ddot{Y}_2) = -K_1\left[(Y_1) + (X_1)_1(\psi_1) - (Z_1)_1(\theta_1) - (Y_2)\right] \qquad \text{(D-4)}$$
$$- K_5\left[(Y_2) - (Y_{11})\right] + C_1\left[(\dot{Y}_1) + (X_1)_1(\dot{\psi}_1) - (Z_1)_1(\dot{\theta}_1) - (\dot{Y}_2)\right]$$
$$- C_5\left[(\dot{Y}_2) - (\dot{Y}_{11})\right]$$

$$m_3(\ddot{Y}_3) = K_2\left[(Y_1) + (X_1)_2(\psi_1) - (Z_1)_2(\theta_1) - (Y_3)\right] \qquad \text{(D-5)}$$
$$- K_6\left[(Y_3) - (Y_{12})\right] + C_2\left[(\dot{Y}_1) + (X_1)_2(\dot{\psi}_1) - (Z_1)_2(\dot{\theta}_1) - (\dot{Y}_3)\right]$$
$$- C_6\left[(\dot{Y}_3) - (\dot{Y}_{12})\right]$$

$$m_4(\ddot{Y}_4) = K_3\left[(Y_1) + (X_1)_3(\psi_1) - (Z_1)_3(\theta_1) - (Y_4)\right] \qquad \text{(D-6)}$$
$$- K_7\left[(Y_4) - (Y_{13})\right] + C_3\left[(\dot{Y}_1) + (X_1)_3(\dot{\psi}_1) - (Z_1)_3(\dot{\theta}_1) - (\dot{Y}_4)\right]$$
$$- C_7\left[(\dot{Y}_4) - (\dot{Y}_{13})\right]$$

$$m_5(\ddot{Y}_5) = K_4\left[(Y_1) + (X_1)_4(\psi_1) - (Z_1)_4(\theta_1) - (Y_5)\right] \qquad \text{(D-7)}$$
$$- K_8\left[(Y_5 - (Y_{14})\right] + C_4\left[(\dot{Y}_1) + (X_1)_4(\dot{\psi}_1) - (Z_1)_4(\dot{\theta}_1) - (\dot{Y}_5)\right]$$
$$- C_8\left[(\dot{Y}_5) - (\dot{Y}_{14})\right]$$

$$m_9(\ddot{Y}_9) = K_9\left[(Y_1) + (X_1)_9(\psi_1) - (Z_1)_9(\theta_1) - (Y_9)\right] \qquad \text{(D-8)}$$
$$- C_9\left[(\dot{Y}_1) + (X_1)_9(\dot{\psi}_1) - (Z_1)_9(\dot{\theta}_1) - (\dot{Y}_9)\right]$$

within the brackets denotes a mass centered coordinate system, subscripts outside the brackets denotes a dimension or a length from the mass center to a point in the mass element. For example (Y_1) is the vertical deflection of the body center of gravity and is a problem variable, while $(Z_1)_9$ is the distance in the Z direction measured in the body centered system to the point of attachment of mass element 9, and is a constant.

If the input functions (Y_{11}), (Y_{14}) are expressible in closed form, a solution to these equations could be obtained in a formal way by taking the Laplace transform, (with zero for the initial conditions) solving for the roots of the resulting polynomials and finding the inverse transforms. The Fourier transform may be obtained from the Laplace transform by setting $s = j\omega$, if the Fourier transform exists.[16] The transformed equations for this model are presented in matrix form, in Equation D-9 where A is the mechanical impedance.

$$\begin{vmatrix} A_{11} & A_{12} & A_{13} & A_{14} & A_{15} & A_{16} & A_{17} & A_{18} \\ A_{21} & A_{22} & A_{23} & A_{24} & A_{25} & A_{26} & A_{27} & A_{28} \\ A_{31} & A_{32} & A_{33} & A_{34} & A_{35} & A_{36} & A_{37} & A_{38} \\ A_{41} & A_{42} & A_{43} & A_{44} & 0 & 0 & 0 & 0 \\ A_{51} & A_{52} & A_{53} & 0 & A_{55} & 0 & 0 & 0 \\ A_{61} & A_{62} & A_{63} & 0 & 0 & A_{66} & 0 & 0 \\ A_{71} & A_{72} & A_{73} & 0 & 0 & 0 & A_{77} & 0 \\ A_{81} & A_{82} & A_{83} & 0 & 0 & 0 & 0 & A_{88} \end{vmatrix} \begin{vmatrix} \dot{Y}_1 \\ \dot{\theta}_1 \\ \dot{\psi}_1 \\ \dot{Y}_2 \\ \dot{Y}_3 \\ \dot{Y}_4 \\ \dot{Y}_5 \\ \dot{Y}_9 \end{vmatrix} = \begin{vmatrix} 0 \\ 0 \\ 0 \\ B_{41}\dot{Y}_{11} \\ B_{51}\dot{Y}_{12} \\ B_{61}\dot{Y}_{13} \\ B_{71}\dot{Y}_{14} \\ 0 \end{vmatrix} \quad \text{(D-9)}$$

The outputs and inputs are velocity column matrices. The impedance matrix A is a symmetrical matrix defined by the relationship that $A_{mn} = A_{nm}$.

Equations D- 9-1 through D- 9-30 define each intercoordinate impedance in terms of physical dimensions and quantities.

$$A_{11} = i\omega m_1 + C_1 + C_2 + C_3 + C_4 + C_9 + [1/i\omega][K_1 + K_2 + K_4 + K_9] \quad \text{(D-9-1)}$$

$$A_{12} = -[C_1(Z_1)_1 + C_2(Z_1)_2 + C_3(Z_1)_3 + C_4(Z_1)_4 + C_9(Z_1)_9] - [1/i\omega][K_1(Z_1)_1 + K_2(Z_1)_2 + K_3(Z_1)_3 + K_4(Z_1)_4 + K_9(Z_1)_9] \quad \text{(D-9-2)}$$

$$A_{13} = C_1(X_1)_1 + C_2(X_1)_2 + C_3(X_1)_3 + C_4(X_1)_4 + C_9(X_1)_9 + [1/i\omega][K_1(X_1)_1 + K_2(X_1)_2 + K_3(X_1)_3 + K_4(X_1)_4 + K_9(X_1)_9] \quad \text{(D-9-3)}$$

$$A_{14} = -C_1 - [1/i\omega][K_1] \quad \text{(D-9-4)}$$

$$A_{15} = -C_2 - [1/i\omega][K_2] \quad \text{(D-9-5)}$$

$$A_{16} = -C_3 - [1/i\omega][K_3] \quad \text{(D-9-6)}$$

$$A_{17} = -C_4 - [1/i\omega][K_4] \quad \text{(D-9-7)}$$

$$A_{18} = -C_9 - [1/i\omega][K_9] \quad \text{(D-9-8)}$$

$$A_{22} = i\omega(I_{\theta 1}) + C_1(Z_1)_1(Z_1)_1 + C_2(Z_1)_2(Z_1)_2 + C_3(Z_1)_3(Z_1)_3 + C_4(Z_1)_4(Z_1)_4 + C_9(Z_1)_9(Z_1)_9 + [1/i\omega][K_1(Z_1)_1(Z_1)_1 + K_2(Z_1)_2(Z_1)_2] + [1/i\omega][K_3(Z_1)_3(Z_1)_3 + K_4(Z_1)_4(Z_1)_4 + K_9(Z_1)_9(Z_1)_9] \quad \text{(D-9-9)}$$

$$A_{23} = - C_1 (X_1)_1 (Z_1)_1 + C_2 (X_1)_2 (Z_1)_2 \qquad \text{(D-9-10)}$$
$$+ C_3 (X_1)_3 (Z_1)_3 + C_4 (X_1)_4 (Z_1)_4 + C_9 (X_1)_9 (Z_1)_9$$
$$- [1/i\omega][K_1 (X_1)_1 (Z_1)_1 + K_2 (X_1)_2 (Z_1)_2 + K_3 (X_1)_3 (Z_1)_3]$$
$$+ [1/i\omega][K_4 (X_1)_4 (Z_1)_4 + K_9 (X_1)_9 (Z_1)_9]$$

$$A_{24} = C_1 (Z_1)_1 + [1/i\omega][K_1 (Z_1)_1] \qquad \text{(D-9-11)}$$

$$A_{25} = C_2 (Z_1)_2 + [1/i\omega][K_2 (Z_1)_2] \qquad \text{(D-9-12)}$$

$$A_{26} = C_3 (Z_1)_3 + [1/i\omega][K_3 (Z_1)_3] \qquad \text{(D-9-13)}$$

$$A_{27} = C_4 (Z_1)_4 + [1/i\omega][K_4 (Z_1)_4] \qquad \text{(D-9-14)}$$

$$A_{28} = C_9 (Z_1)_9 + [1/i\omega][K_9 (Z_1)_9] \qquad \text{(D-9-15)}$$

$$A_{33} = i\omega(I_{\psi 1}) + C_1 (X_1)_1 (X_1)_1 + C_2 (X_1)_2 (X_1)_2 \qquad \text{(D-9-16)}$$
$$+ C_3 (X_1)_3 (X_1)_3 (X_1)_3 + C_4 (X_1)_4 (X_1)_4 + C_9 (X_1)_9 (X_1)_9$$
$$+ [1/i\omega][K_1 (X_1)_1 (X_1)_1 + K_2 (X_1)_2 (X_1)_2 + K_3 (X_1)_3 (X_1)_3]$$
$$+ [1/i\omega][K_4 (X_1)_4 (X_1)_4 + K_9 (X_1)_9 (X_1)_9]$$

$$A_{34} = - C_1 (X_1)_1 - [1/i\omega][K_1 (X_1)_1] \qquad \text{(D-9-17)}$$

$$A_{35} = - C_2 (X_1)_2 - [1/i\omega][K_2 (X_1)_2] \qquad \text{(D-9-18)}$$

$$A_{36} = - C_3 (X_1)_3 - [1/i\omega][K_3 (X_1)_3] \qquad \text{(D-9-19)}$$

$$A_{37} = - C_4 (X_1)_4 - [1/i\omega][K_4 (X_1)_4] \qquad \text{(D-9-20)}$$

$$A_{38} = - C_9 (X_1)_9 - [1/j\omega][K_9 (X_1)_9] \quad (D\text{-}9\text{-}21)$$

$$A_{44} = j\omega m_2 + C_1 + C_5 + [1/j\omega][K_1 + K_5] \quad (D\text{-}9\text{-}22)$$

$$A_{55} = j\omega m_3 + C_2 + C_6 + [1/j\omega][K_2 + K_6] \quad (D\text{-}9\text{-}23)$$

$$A_{66} = j\omega m_4 + C_3 + C_7 + [1/j\omega][K_3 + K_7] \quad (D\text{-}9\text{-}24)$$

$$A_{77} = j\omega m_5 + C_4 + C_8 + [1/j\omega][K_4 + K_8] \quad (D\text{-}9\text{-}25)$$

$$A_{88} = j\omega m_9 + C_9 + [1/j\omega][K_9] \quad (D\text{-}9\text{-}26)$$

$$B_{41} = C_5 + [1/j\omega][K_5] \quad (D\text{-}9\text{-}27)$$

$$B_{51} = C_6 + [1/j\omega][K_6] \quad (D\text{-}9\text{-}28)$$

$$B_{61} = C_7 + [1/j\omega][K_7] \quad (D\text{-}9\text{-}29)$$

$$B_{71} = C_8 + [1/j\omega][K_8] \quad (D\text{-}9\text{-}30)$$

The acceleration and displacement in terms of the velocity variables are:

Displacement = Velocity / $j\omega$; Acceleration = Velocity ($j\omega$) (D-10)

In matrix notation Equation D-9 can be written:

$$A(j\omega)\, 0(j\omega) = I(j\omega) \quad (D\text{-}11)$$

where $A(j\omega)$ is the impedance matrix, $0(j\omega)$ is the output column matrix and $I(j\omega)$ is the input column matrix. The matrix solution for the outputs is:

$$0(j\omega) = A^{-1}(j\omega)\, I(j\omega) \quad (D\text{-}12)$$

where $A^{-1}(j\omega)$ is the inverse of $A(j\omega)$.

Equations D-10 and D-12 allow the outputs to be determined for any time derivative with any time derivative as the input, such as acceleration output for a displacement input, etc. From this array the output can be determined for one input at a time or for all four inputs (four wheels) simultaneously, each having an arbitrary phase angle.

The impedance matrix $A(j\omega)$ in Equation D-9 has the following properties:

1. It is symmetrical
2. The off-diagonal terms define the cross-coupling between the various modes of motion.
3. The imaginary part of the diagonal terms, when equated to zero give the uncoupled, undamped natural frequency for that mode.

D.3 Statistical Approach and Power Spectral Density

In Appendix A the statistical classification of surface profiles has been discussed, and the power spectral density was defined. In the literature (References 16, 36 and 37) it is shown that the power spectral density of the output for a linear system with a single input is the product of the square of the system transfer function and the power spectral density of the input.

$$P_o(\omega) = |T(j\omega)|^2 P_i(\omega) \qquad (D-13)$$

For the vehicle system described by Equations D-9, which has four inputs, the response P.S.D. $P_o(\omega)$ is given by:

$$P_o(\omega) = \sum_{m=1}^{4} \sum_{k=1}^{4} T_{om}(j\omega)\, T^*_{ok}(j\omega)\, P_{mk}(j\omega) \qquad (D-14)$$

where T_{om} is the transfer function between the output motion in question and the m^{th} input, T^*_{om} is the complex conjugate of T_{om} and P_{mk} is the cross-spectral density between the m^{th} and the k^{th} inputs which becomes the usual P.S.D. for $m = k$. It was shown in Appendix A that the

vertical velocity power spectral density of the lunar surface is "white", and may be expressed by Equation D-15.

$$P_v(f) = 4\pi^2 V C \tag{D-15}$$

where V is the horizontal velocity of the vehicle and C is a measure of the surface roughness. Converting Equation D-14 from circular frequency (rad/sec) to cps and substituting Equation D-15 for the four P.S.D. terms, yield:

$$P_o(f) = \sum_{n=1}^{4} \left[4\pi^2 V C \left| T_{on} \right|^2 \right] + \sum_{k=1}^{n-1} \Re \left[2\, T_{on}\, T_{ok}^{*}\, P_{nk} \right] \tag{D-16}$$

The first four terms in Equation D-16 are the square of the modulus of the transfer function between each of the inputs and the output in question, times the P.S.D. of equation D-15. The remaining 12 terms of Equation D-14 have been reduced to six terms in Equation D-16 by noting that this is a summation of complex conjugates which yields twice the real part of each pair. Since the surface roughness is represented by a profile which has a "white" velocity P.S.D. (Equation D-15), it can be shown[16] that the velocity cross-spectral density between any two parallel traces is zero. Thus, it can be assumed that the terms in Equation D-16, which contain cross-spectral densities between the left and right wheel inputs, are zero. The cross-spectral density between in-line following wheels is the Fourier transform of a Dirac delta function which is non-zero only for time t = wheel base/velocity.

With the wheels numbered 1, 2, 3 and 4 for left front, right front, left rear and right rear respectively and the distance between front and rear wheel given by $D = X_{s1} + X_{s3}$ (See Table C-2), the cross- spectral density terms in Equation D-16 can be written as:

$$P_{21} = P_{41} = P_{23} = P_{43} = 0 \tag{D-17}$$

and $$P_{31} = P_{42} = 4\pi^2 CV \left(\cos 2\pi f \frac{D}{V} + i \sin 2\pi f \frac{D}{V}\right) \quad \text{(D-18)}$$

Substituting Equations D-17 and D-18 into D-16 gives:

$$P_o(f) = 4\pi^2 CV \left[\sum_{n=1}^{4} |T_{on}|^2 + 2\mathcal{R}\left\{ (T_{o1} T_{o3}^* + T_{o2} T_{o4}^*) \left(\cos 2\pi f \frac{D}{V} + i \sin 2\pi f \frac{D}{V}\right) \right\} \right] \quad \text{(D-19)}$$

Equation D-19 gives the output P.S.D. for one motion of a vehicle with two sets of following in-line wheels. If the inputs are all separate parallel profiles (i.e., which are not in-line) then Equation D-19 can be further simplified to the form

$$P_o(f) = 4\pi^2 CV \sum_{n=1}^{4} |T_{on}|^2 \quad \text{(D-20)}$$

Equation D-20 was used to compute the output P.S.D. for the body bounce, pitch and roll for the vehicle model described in Section C.9 of Appendix C. The assumption of independent inputs to all four wheels of this vehicle model is subject to question, but the level of sophistication of the model and the limitations imposed by linearity did not seem to warrant the additional computation time required to include the coupling terms between the inputs for this demonstration of frequency domain analysis.

D.4 Results of Model Analysis

The numerical values of Tables C-2 and C-3 in Appendix C were substituted into Equation D-9 for analysis. The imaginary components of the diagonal terms in the impedance matrix were equated to zero to estimate the natural frequencies. These uncoupled, undamped resonant frequencies are listed in Table D-1.

Table D-1 APPROXIMATE RESONANT FREQUENCIES

Degree of Freedom	Frequency
Body vertical	1.04 cps
Body roll	1.74 cps
Body pitch	.92 cps
Wheels vertical	10 cps
Fuel cell vertical	10 cps

The resonant frequency of the fuel cell was chosen equal to the wheel frequency to allow the fuel cell to damp the body vertical bounce motion at the wheel hop frequency.

A digital computer was used to tabluate the transfer functions from Equation D-9 by computing the outputs for each degree of freedom in discrete frequencies between 0.4 and 40 cps for each input separately. Figures D-1 through D-4 show the transfer functions between the body vertical motion and each of the four wheels and are direct reproductions of digital "print out plots." The differences between left and right wheel inputs are due to the asymmetrical location of the fuel cell. The small difference between front and rear wheel inputs is due to the asymmetry of the body center of gravity.

Since the body is nearly symmetrical, the transfer functions for each of the wheel inputs are approximately the same. Therefore, only a representative sample of the results will be presented. The transfer functions between the body bounce, roll, and pitch and the left front wheel are shown in Figure D-5 in the frequency range of 0.4 to 14 cps, which covers the resonant frequencies of the three body motions. The resonant frequencies noted in the transfer functions show good agreement

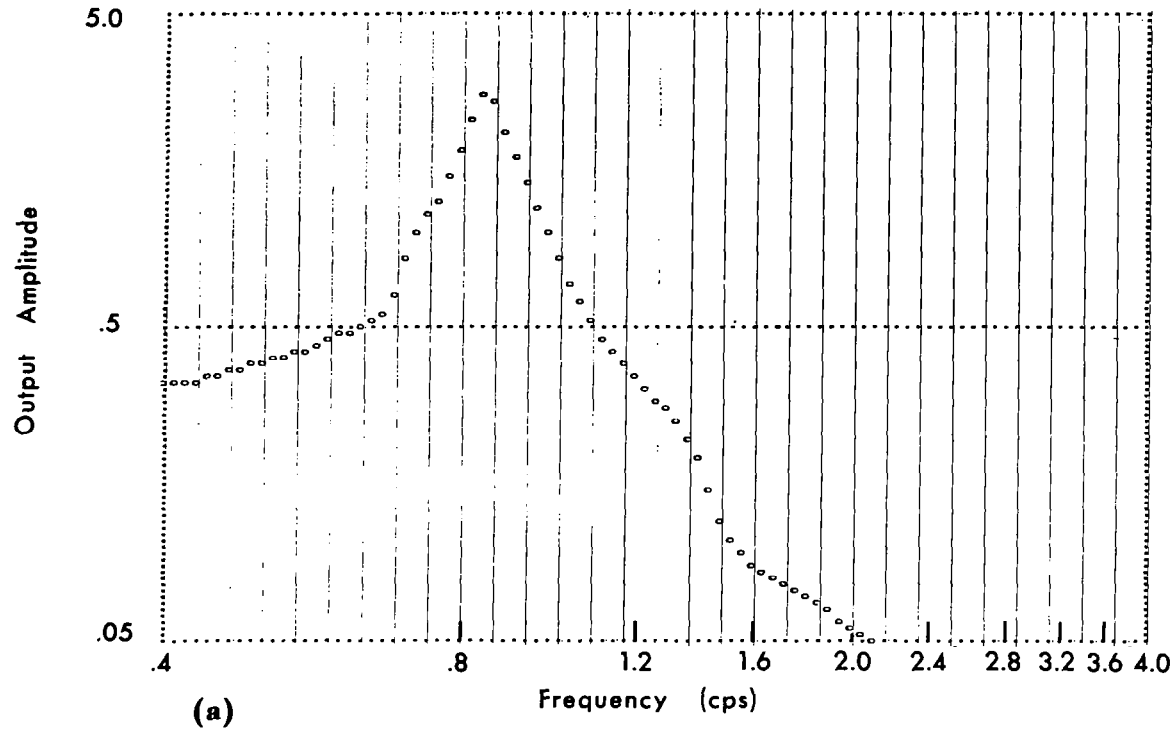

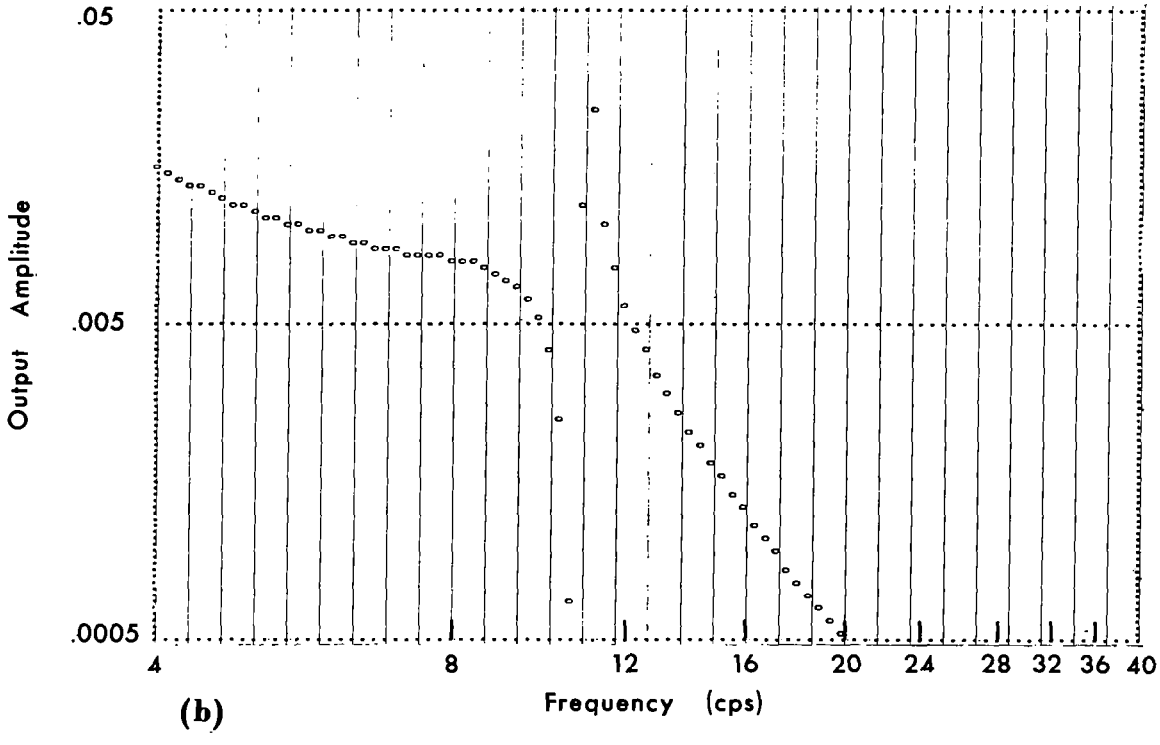

Figure D-1 BODY VERTICAL DISPLACEMENT FOR UNITY INPUT TO LEFT FRONT WHEEL

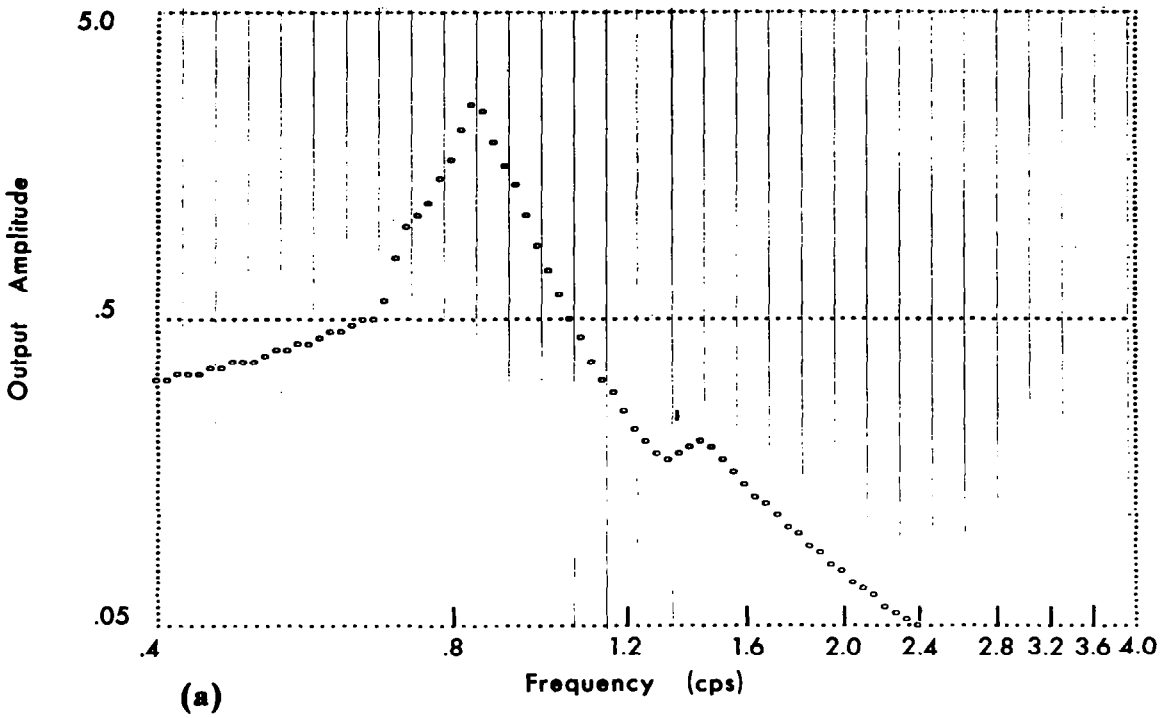

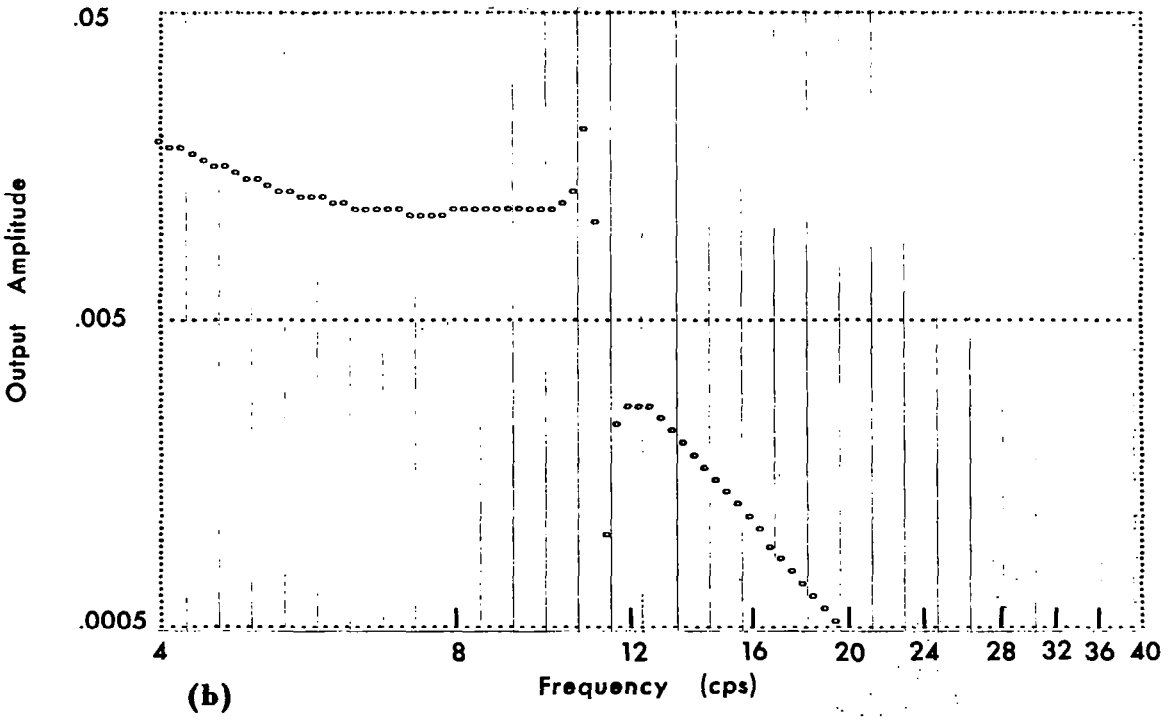

Figure D-2 BODY VERTICAL DISPLACEMENT FOR UNITY INPUT TO RIGHT FRONT WHEEL

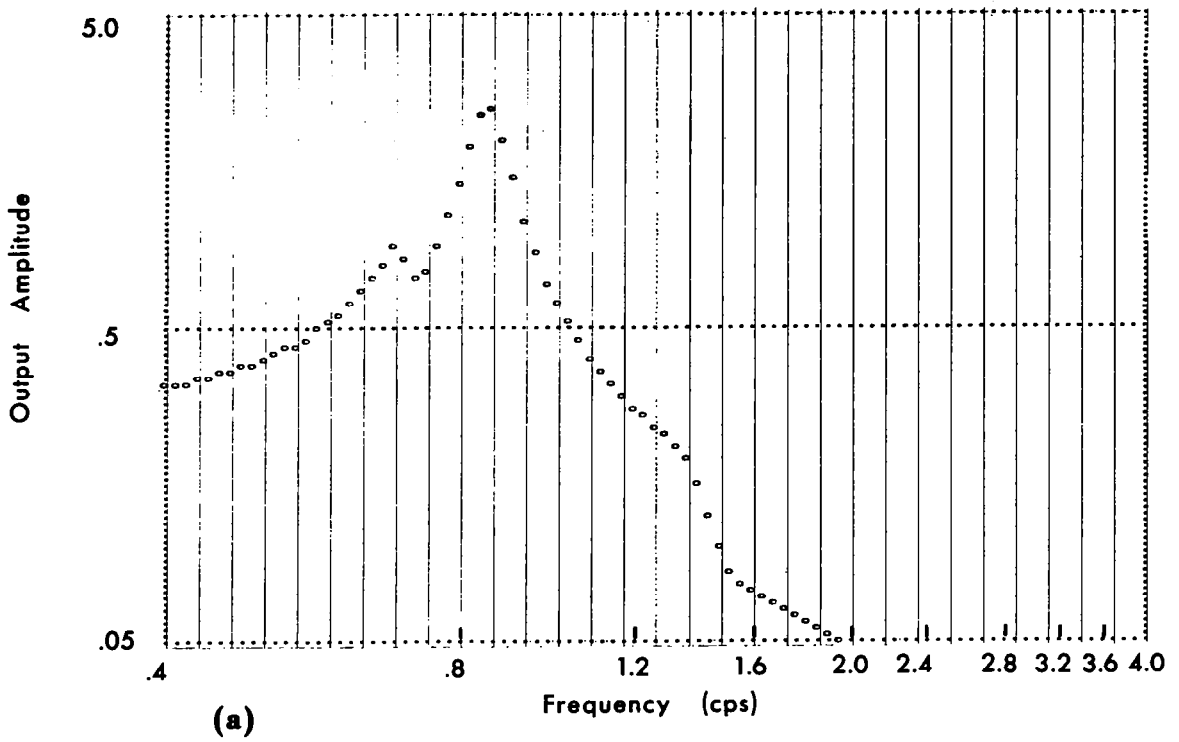

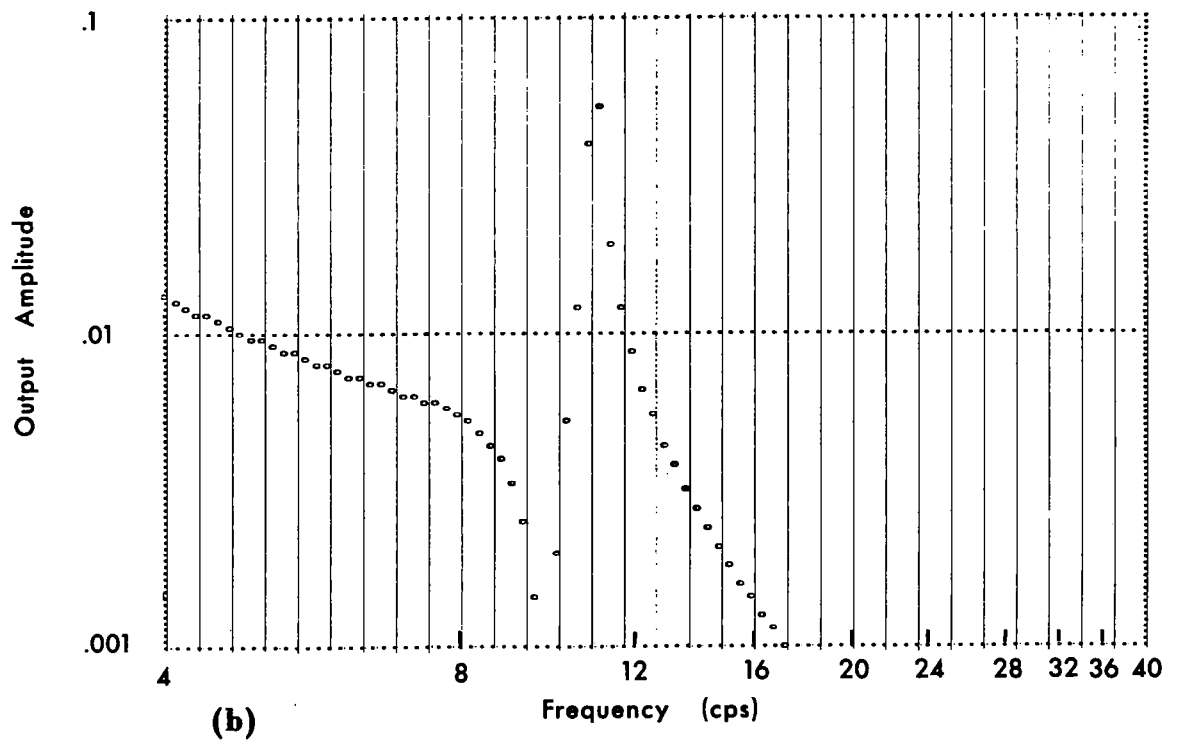

Figure D-3 BODY VERTICAL DISPLACEMENT FOR UNITY INPUT TO LEFT REAR WHEEL

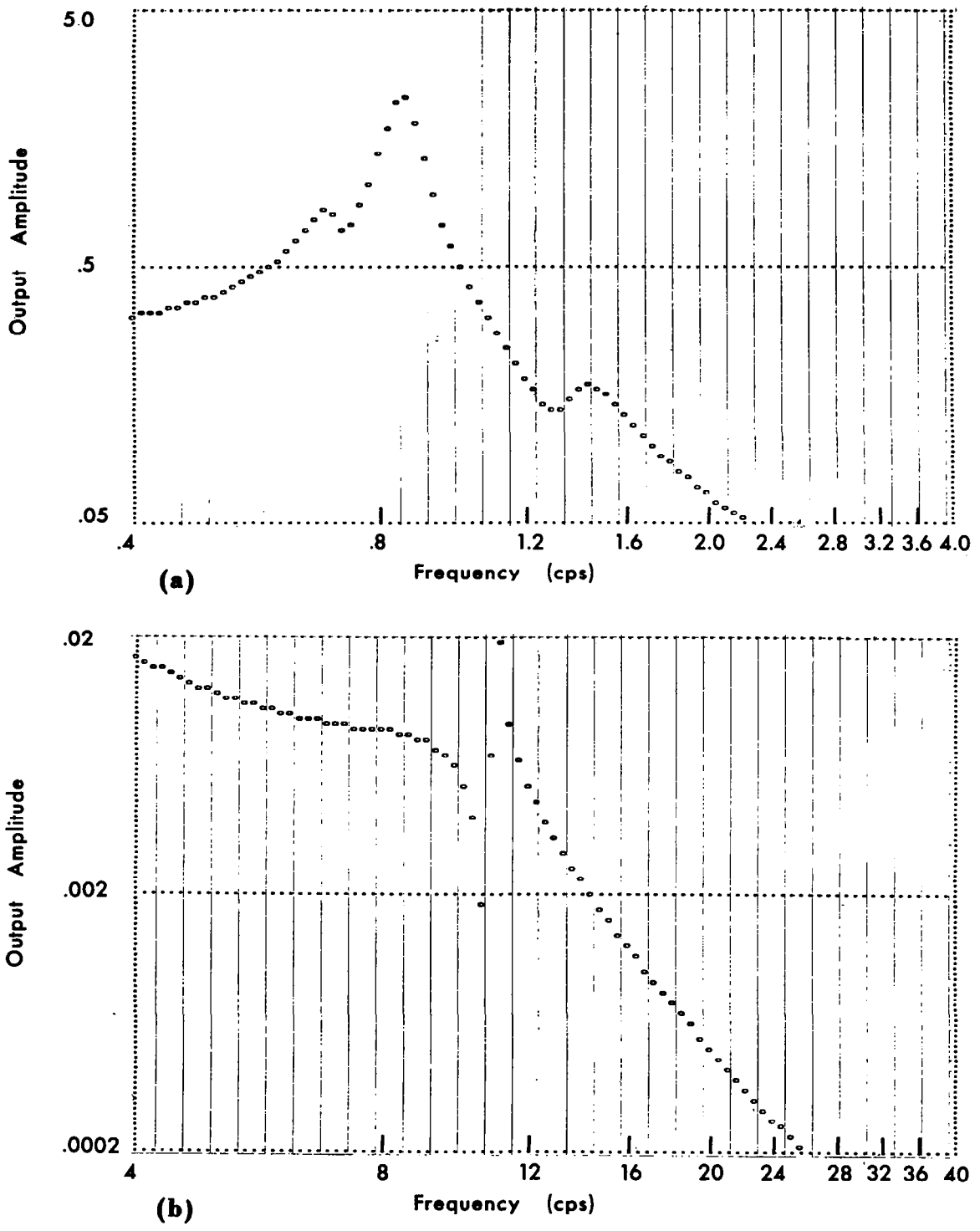

Figure D-4 BODY VERTICAL DISPLACEMENT FOR UNITY INPUT TO RIGHT REAR WHEEL

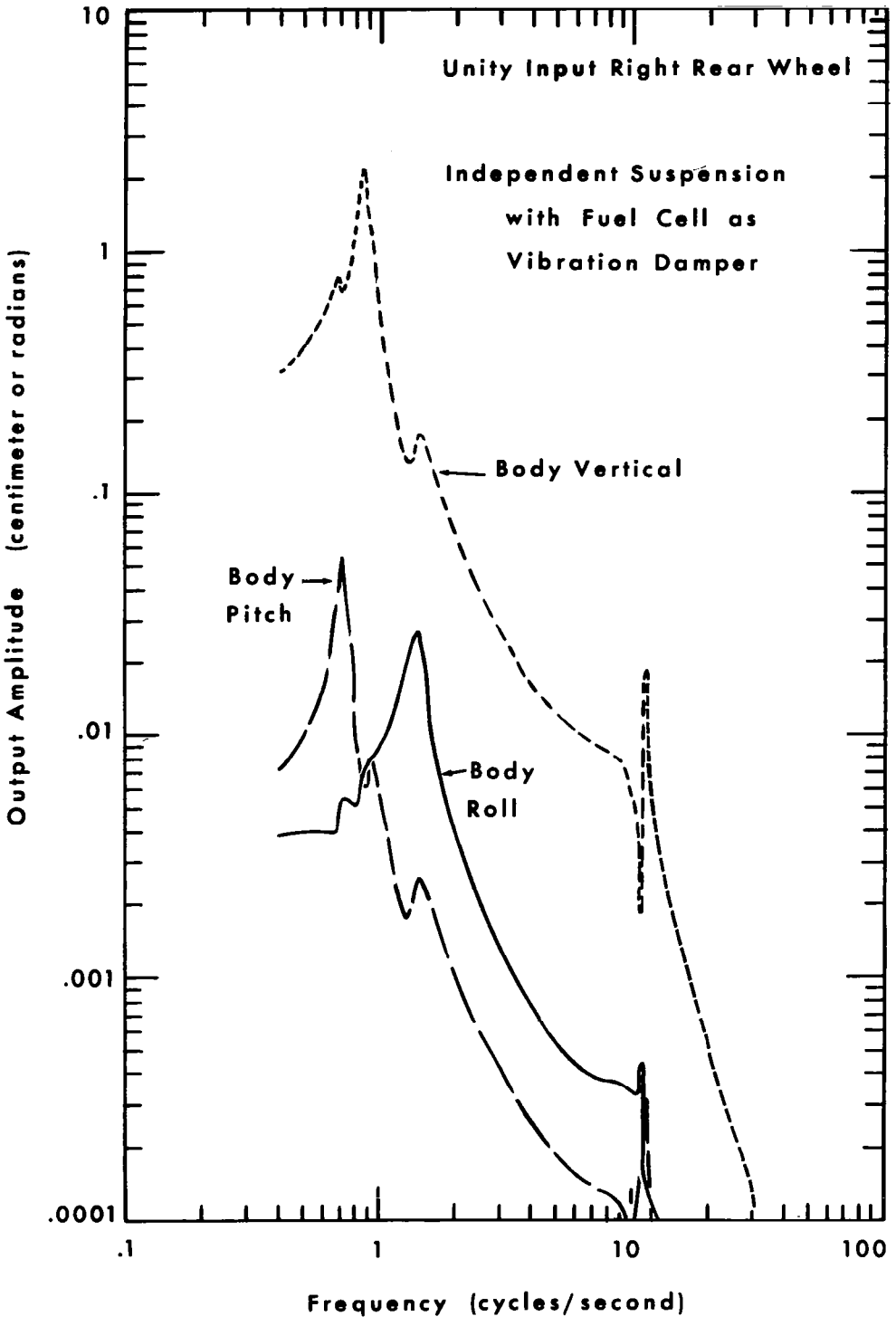

Figure D-5 FREQUENCY RESPONSE
OF BODY BOUNCE, PITCH & ROLL

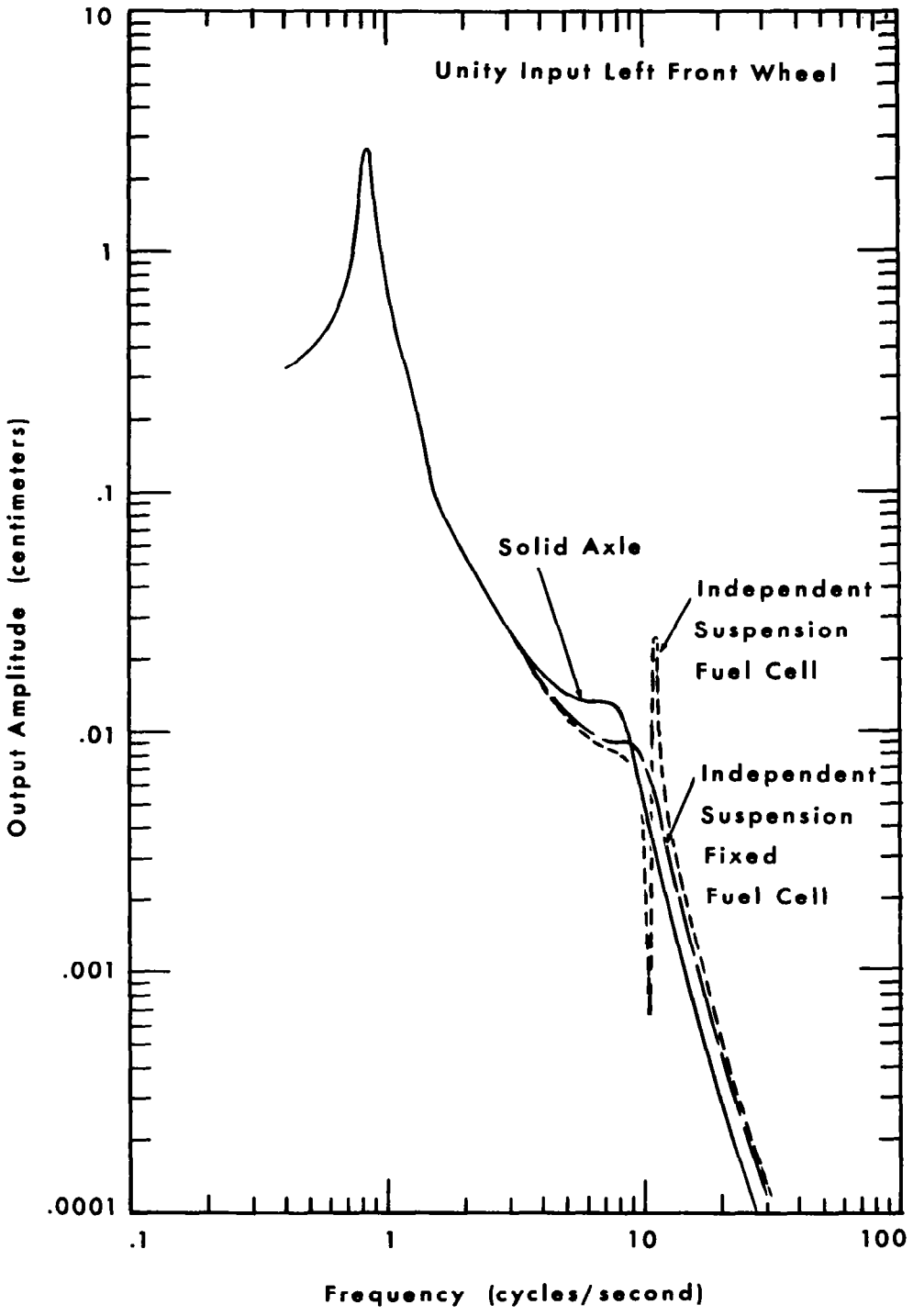

Figure D-6 FREQUENCY RESPONSE OF BODY VERTICAL FOR 3 MODELS

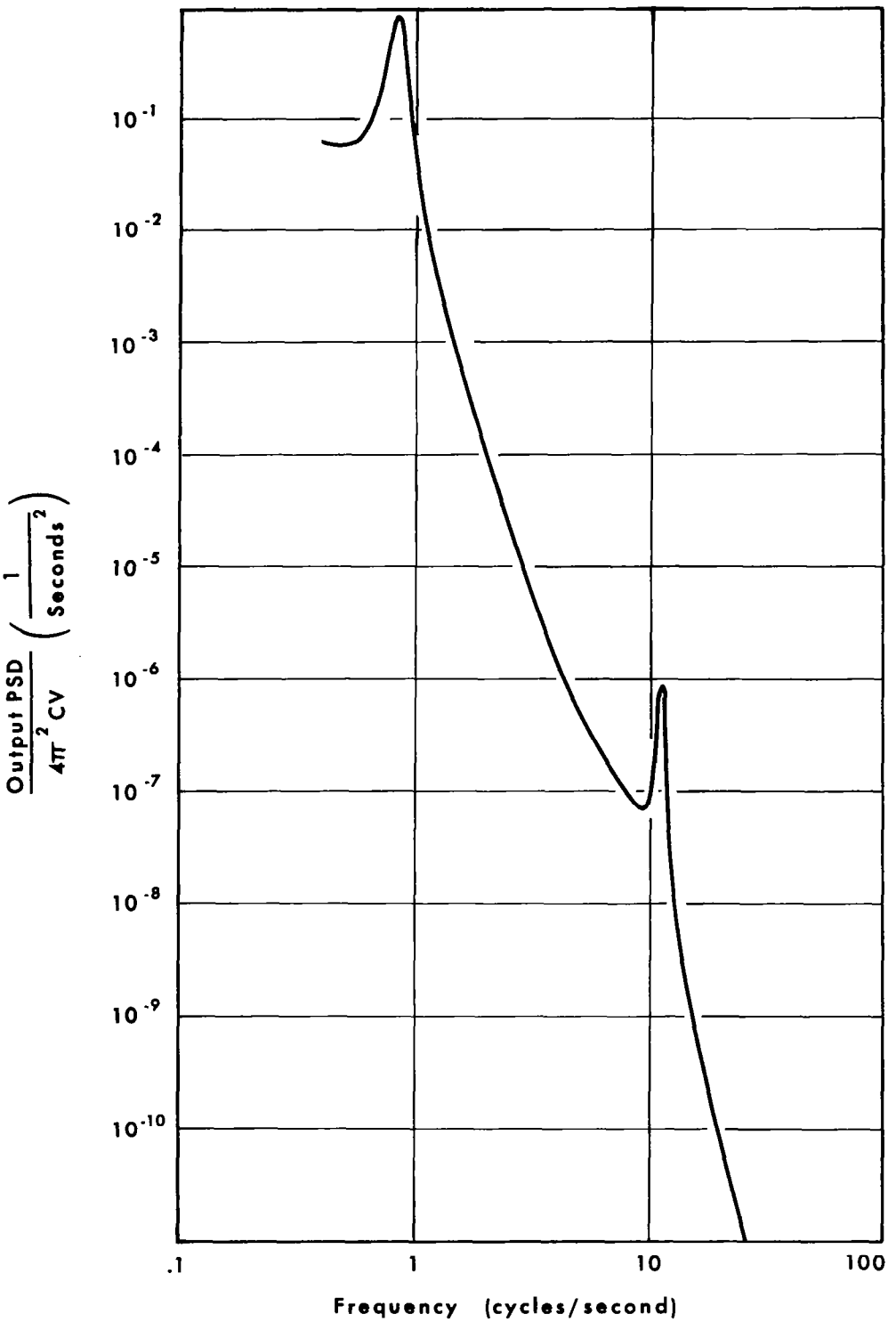

Figure D-7 POWER SPECTRAL DENSITY OF BODY VERTICAL DISPLACEMENT

with those listed in Table D-1. Figure D-6 shows the transfer function between body vertical and the left front wheel with and without the fuel cell. Also shown in Figure D-6 is the transfer function for a solid axle version of the vehicle. The similarity of the three transfer functions shows that vehicle suspension geometry does not significantly alter the gross dynamic behavior of the vehicle.

Figure D-7 is a plot of the power spectral density of the body bounce displacement calculated from Equation D-20 with a white velocity input to all four wheels. This P.S.D. is normalized by making the vertical scale $P_d(\Omega) / 4\pi^2 CV$. It is apparent that most of the vibrational activity is concentrated in the frequency range near the body resonances.

In Appendix A it was shown that a Gaussian assumption for the distribution of profile height is valid. If a Gaussian random process is applied as an input to a linear system, the output is also Gaussian. Since the mean value has been assumed to be zero in this analysis, the variance (or its square root; the standard deviation) is sufficient to predict the probability of exceeding any given level. The variance is the integral of the P.S.D. on frequency and can be computed from Equations D-21, D-22 and D-23 for the displacement, velocity and acceleration respectively.

$$\sigma_d^2 = \int_0^\infty P_d(f)\, df = 4\pi^2 CV \int_0^\infty \left(\frac{1}{2\pi f}\right)^2 \sum_{n=1}^{4} |T_{on}|^2\, df \qquad (D\text{-}21)$$

$$\sigma_V^2 = \int_0^\infty P_v(f)\, df = 4\pi^2 CV \int_0^\infty \sum_{n=1}^{4} |T_{on}|^2\, df \qquad (D\text{-}22)$$

$$\sigma_a^2 = \int_0^\infty P_a(f) = 4\pi^2 CV \int_0^\infty (2\pi f)^2 \sum_{n=1}^{4} |T_{on}|^2\, df \qquad (D\text{-}23)$$

Equations D-21, D-22 and D-23 predict that the variance of the vehicle motion is directly proportional to the surface roughness coefficient, C, and to the vehicle velocity, V, for this linear model with independent input to each wheel. The integrals on the right hand side of these equations can be evaluated numerically over the frequency range of interest from the digital tabulation of the transfer function. These values specify the essential dynamic characteristics of the vehicle model. The effects of vehicle velocity and surface roughness can then be easily evaluated in terms of the probability of exceeding design limitations.

Figure D-8 is a plot of the probability of vehicle lift-off (percent of the time of surface-vehicle separation) versus vehicle speed for two different values of surface roughness. The surface roughness coefficients were chosen from Table A-3 as extremes for the lunar surface segments analyzed in Appendix A. The variance of the vertical c.g. acceleration for the independent suspension model with suspended fuel cell was calculated via Equation D-23. Lift-off was defined as the percent of the time that the Gaussian distribution of body vertical acceleration exceeded one lunar g.

Figure D-9 shows a similar plot for the probability of vehicle pitchover. In this case the pitch displacement was calculated from Equation D-21 and the limit was established at that point where pitch displacement exceeded the static equilibrium position. The pitch motion was chosen since the unusual vehicle geometry gives a higher probability of pitchover than rollover. While in the realistic case, the vehicle operator will undoubtedly take the appropriate evasive action to avoid pitchover of the vehicle, the estimate of this probability for a straight line path at a constant velocity is a meaningful parameter for vehicle configuration comparison.

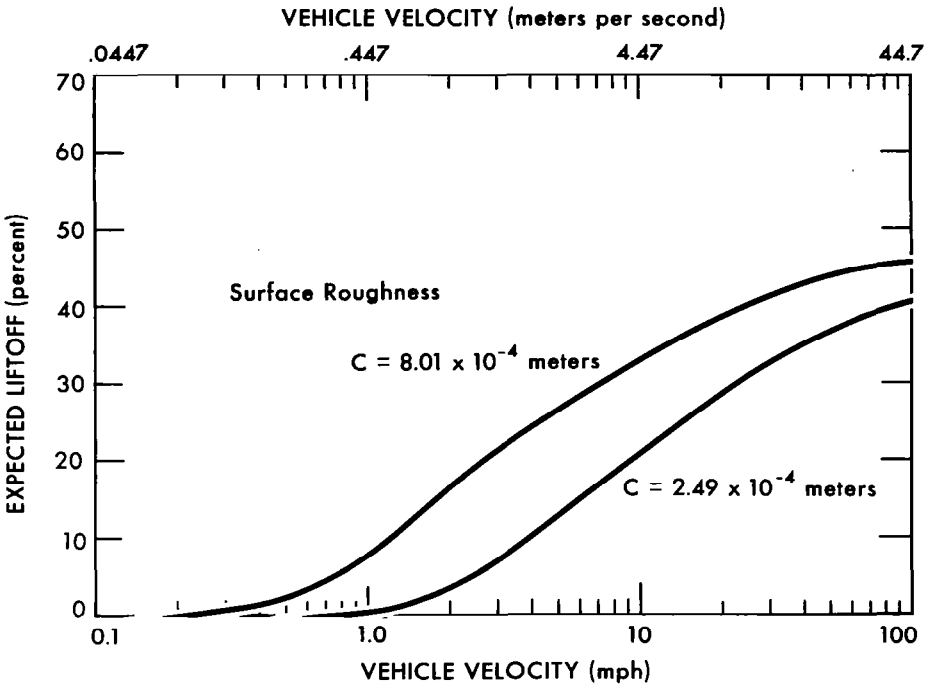

Figure D-8 PROBABILITY OF LIFTOFF

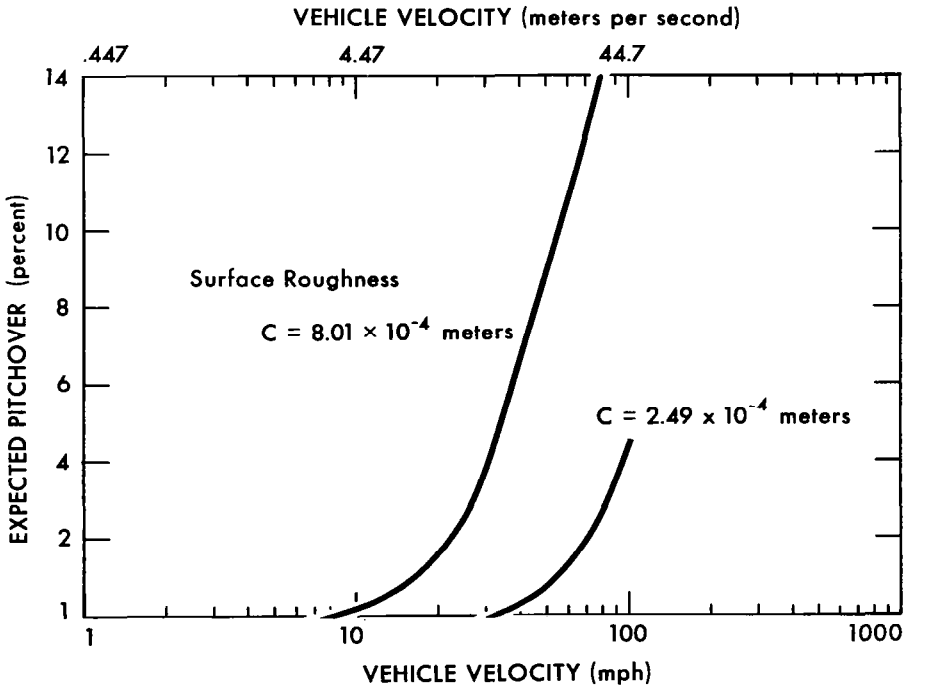

Figure D-9 PROBABILITY OF PITCHOVER

APPENDIX E

TIME DOMAIN ANALYSIS

TIME DOMAIN ANALYSIS

By: C. H. Hoppe

The model described in Section C.9 of Appendix C was analyzed in two different forms using analog computer techniques in order to demonstrate time domain analysis.

1. By making the assumptions of left to right symmetry for the vehicle and by assuming identical inputs to both sides (i.e., correlated inputs to the right and left sides of the vehicle), it is possible to collapse the vehicle into a two dimensional model having six degrees of freedom. The remaining six degrees are the vehicle body vertical translation and pitch rotation modes as well as the vertical translation of the wheel and rim masses. This model was analyzed on a yielding surface using an adaptation of the computer network shown in Figure C-5.

2. The second form was a seven degree of freedom model which included the bounce, pitch and roll motions of the vehicle body and the vertical translation of each of the four unsprung masses. This model is described together with an analog computer network for simulation in Reference 14. This model was analyzed on a non-yielding surface with uncorrelated inputs to the left and right front wheels which were time delayed to the rear wheels. Separate uncorrelated random inputs were also used to all four wheels of this vehicle model in order to allow a comparison with the results of the frequency domain analysis in Appendix D.

E.1 Input Considerations

A Scott random noise generator was used to generate the random velocity white noise function necessary for vehicle analysis. The output of this generator is a white noise with

Gaussian distribution between the frequencies of 10 cps and 10^6 cps. Since the analog computer simulation of the vehicle model was programmed for real time, it was necessary to lower the frequency range of the white noise to accomodate the vehicle body resonances near one cps. For this reason, and also to allow multiple inputs for vehicle analysis, the output of the noise generator was recorded on a Precision Instruments eight channel f.m. tape recorder. The recording speed was 37.5 inches per second and by playing back at a speed of .375 inches per second a random noise signal was obtained which was white between the frequencies of .1 and 100 cps. The high frequency cut-off was determined by the limitation of the tape recorder at this playback speed. Four different channels were recorded at different times from the white noise generator to allow uncorrelated random noise signals.

Figure E-1 is a strip chart recording of the random noise signal and its integral. The integral was obtained by direct analog integration with a low frequency cut-off at .5 cps to eliminate drift. Figure E-2 shows a power spectral density plot of the white noise input calculated directly on the analog computer using techniques discussed in Reference 12. While this integration does not adequately account for long wave length surface slope characteristics these can be taken into account in the analysis of the output.

Scaling of the input was achieved by equating the variance of the white noise input evaluated on an analog computer with the variance of the vertical velocity of a typical lunar profile. The variance of a lunar profile, in temporal frequency, has been shown to be equal to $(f_1 - f_2)\, 4\pi^2 VC = K_o$, where C is a measure of surface roughness, V is the vehicle horizontal velocity and f_1 and f_2 are limits of integration in the frequency domain. For a selected surface roughness ($C = 3.6 \times 10^{-4}$ meters) and a vehicle velocity of unity, the variance could be evaluated numerically. The gain of the output of the analog determination of the variance (volts) could be adjusted to be consistent with the scaling (meters/volt) previously

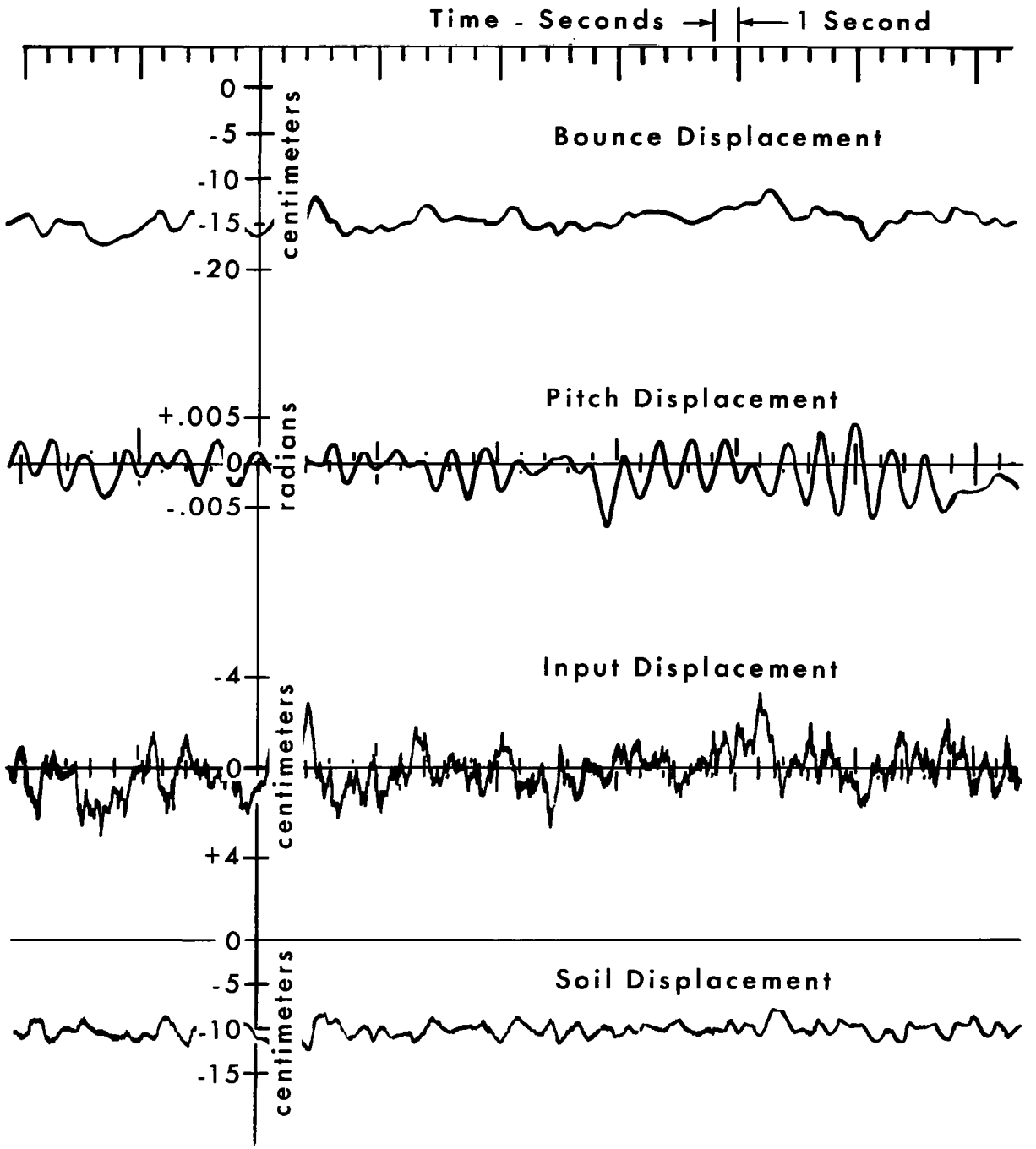

Figure E-3 TIME TRACES OF SOIL AND VEHICLE RESPONSE

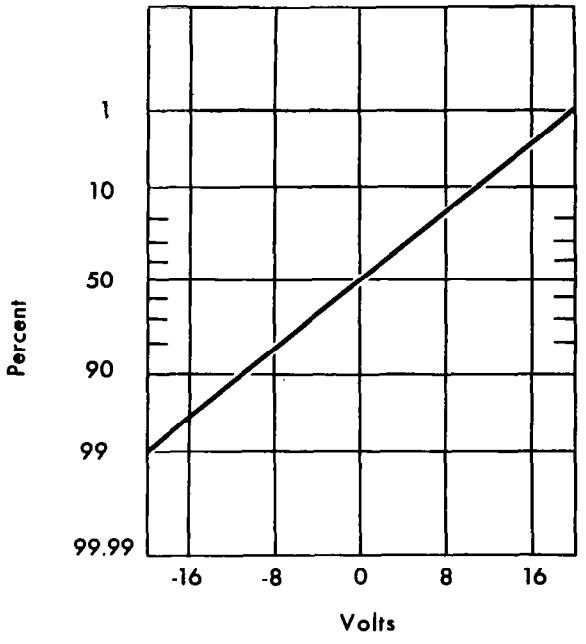

Figure E-4 A.P.D. OF INTEGRATED WHITE NOISE (Displacement Input)

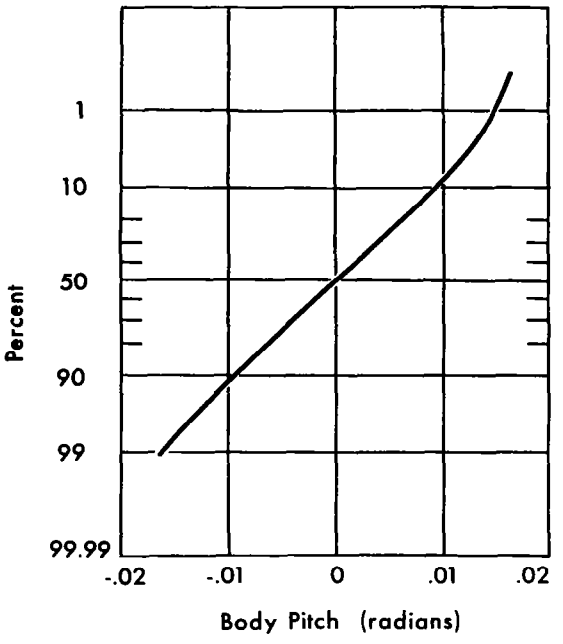

Figure E-5 A.P.D. OF VEHICLE BODY PITCH ON YIELDING SURFACE AT 1 MPH

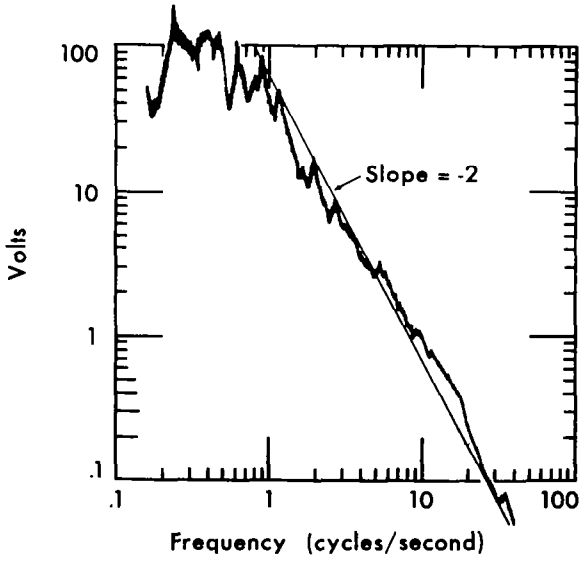

Figure E-6 P.S.D. OF INTEGRATED WHITE NOISE (Displacement Input)

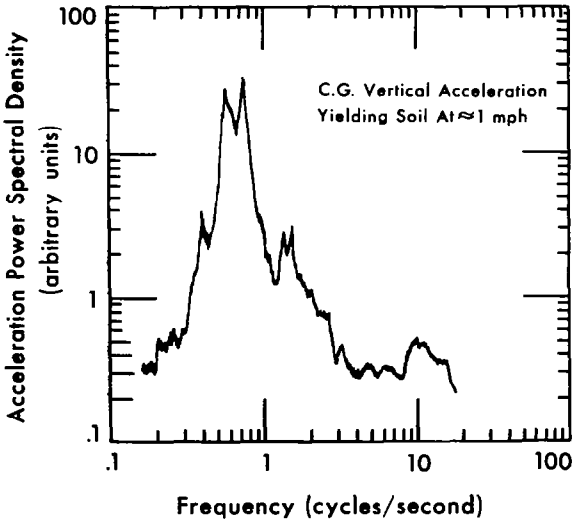

Figure E-7 OUTPUT P.S.D. ON YIELDING SOIL

is noted that the integrated displacement input to the vehicle has a P.S.D. with a slope of -2. Figure E-7 shows the output P.S.D. of the vehicle c.g. vertical acceleration. The two peaks below one cps are the vehicle body pitch and bounce resonances. A second harmonic of these resonances can be seen which is due to the non-linearities of the vehicle system. The resonance of the vertical wheel motions can be seen at approximately 10 cps in Figure E-7.

The P.S.D. and A.P.D. plots in Figures E-2, E-4, E-5, E-6, and E-7 were calculated directly on the analog computer. In order to accomplish this calculation the appropriate signals were recorded on a magnetic tape loop. The analog circuit for A.P.D. calculation is discussed by the author in Reference 12 and the P.S.D. circuit is given in page 102 of Reference 38.

Figure E-8 shows a comparison of the time traces of vehicle body motions for yielding and non-yielding soils. A difference in the equilibrium position of the vehicle bounce motions is noted between the yielding and non-yielding surfaces. The yielding surface shows lower frequency components for both body pitch and bounce motions as compared with the non-yielding surface. This is due to the additional compliance of the surface. The effects of the hysteresis damping of the soil can also be noted by comparing decay rates of vehicle body motions in Figure E-8.

A preliminary parametric analysis of the suspension spring rates and damping was performed for this vehicle. The rear suspension spring rate was changed first to a value of one-half and then to a value of two times the original rate. The mean squared accelerations for the vertical translation and pitch rotation modes of the vehicle body were measured in each case. When the rear spring rate was one-half the original value the front spring rate was also lowered by the same ratio. Similar variations in suspension damping were made. In this case the front damping was doubled at the same time the rear damping was increased. Figures E-9 and E-10 show graphically the effects of changing spring rates and damping coefficients for both soft soils

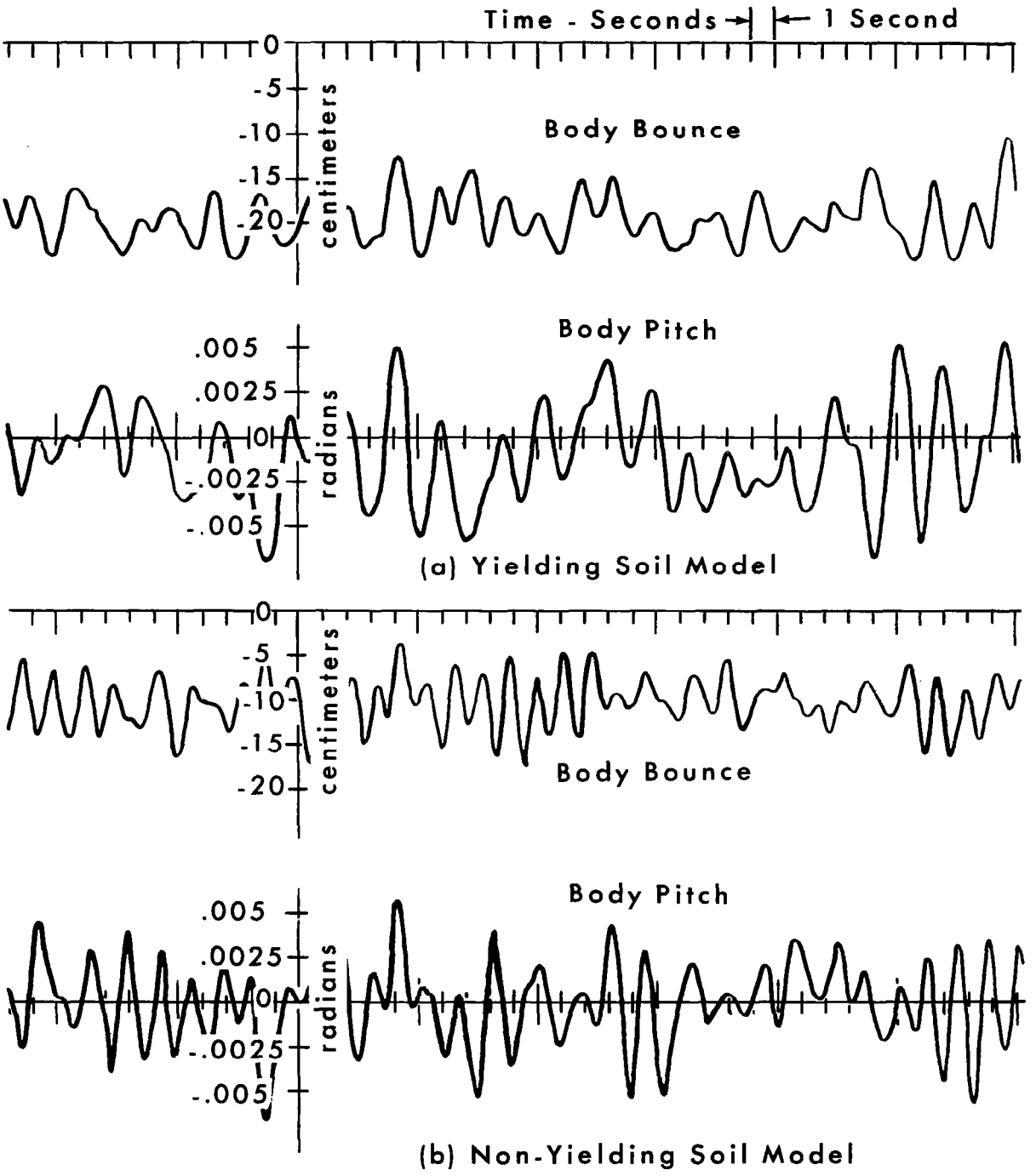

Figure E-8 TIME TRACES OF VEHICLE RESPONSE

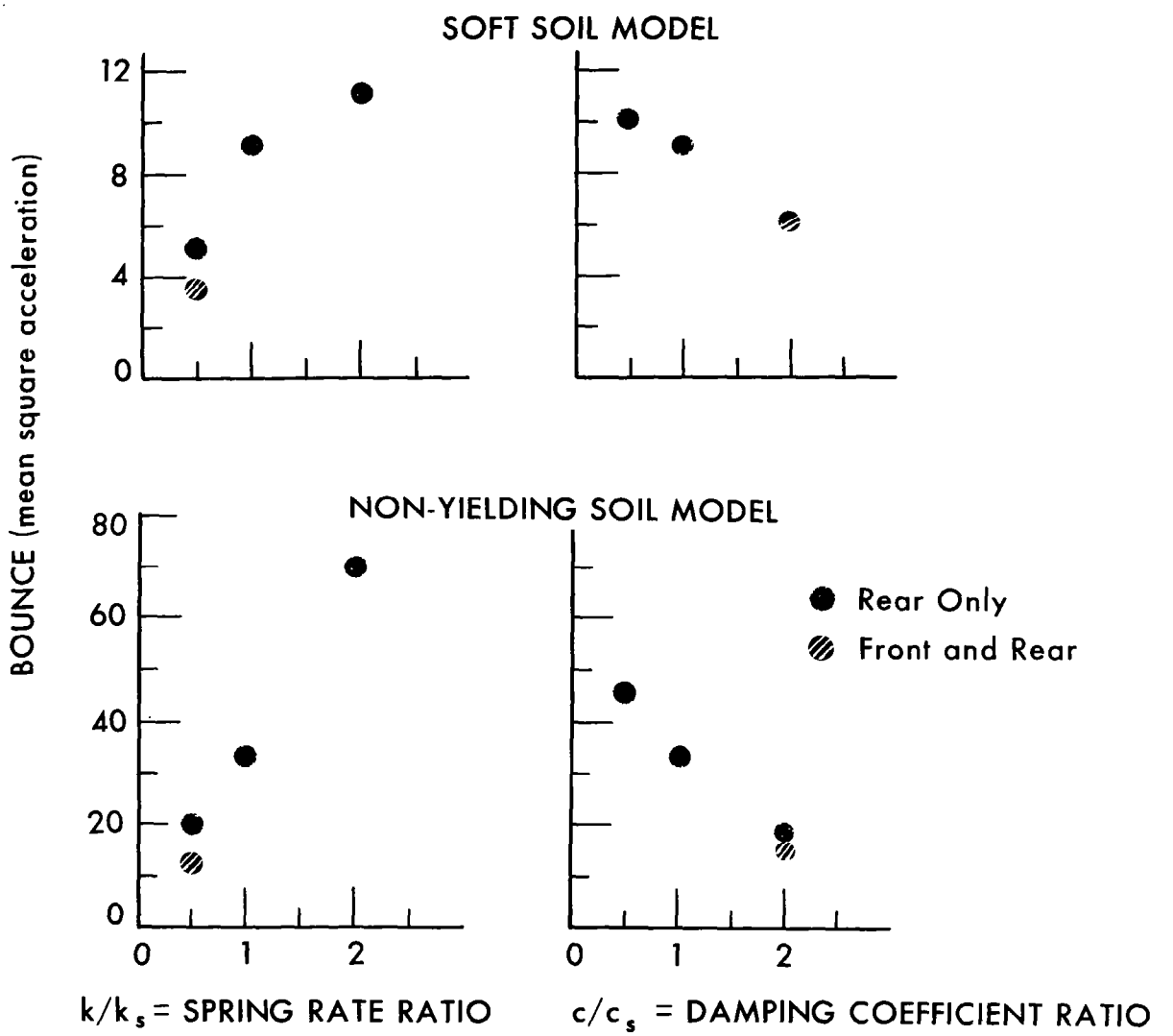

Figure E-9 EFFECT OF SUSPENSION SPRING RATE & DAMPING ON VERTICAL BODY ACCELERATION

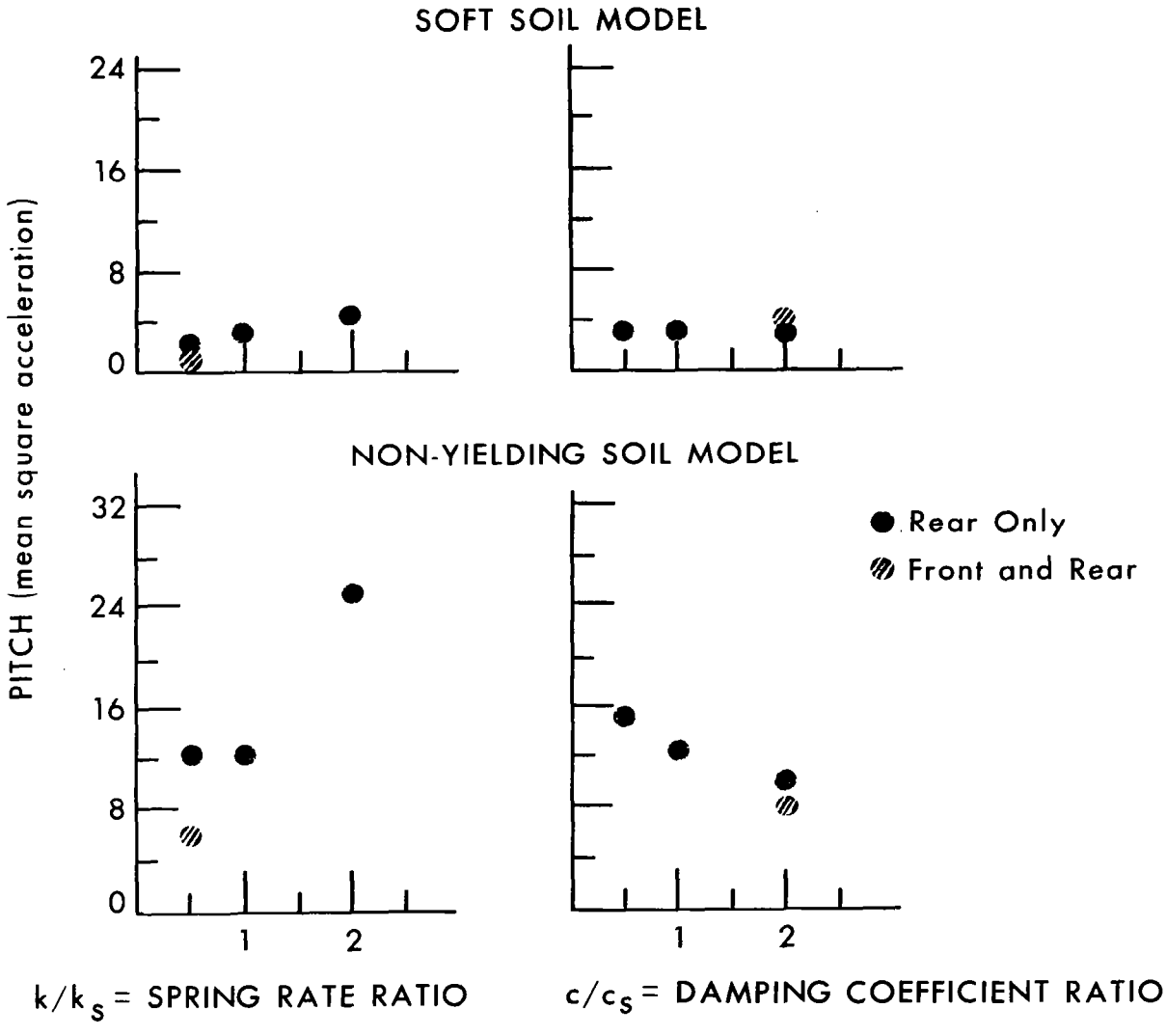

Figure E-10 EFFECT OF SUSPENSION SPRING RATE & DAMPING ON BODY PITCH ACCELERATION

and non-yielding soils. From these figures it can be seen that the effects are more pronounced when the vehicle is operating on non-yielding soils. In general, the mean squared acceleration was less with decreased spring rates and increased damping. The lower limit on spring rate is not a function of acceleration of the vehicle but is a function of the static deflection and limiting motions of the vehicle wheels due to jounce and rebound constraints. As damping is increased the mean squared acceleration is lowered to an optimum value of damping and then increases with increased damping above this optimum value.

E.3 Three Dimensional Model Analysis

A three dimensional seven degree of freedom vehicle model was analyzed using random inputs on a non-yielding surface. In this case independent random inputs were used for the left and right hand sides of the vehicle and were properly time delayed to the rear wheels. The feedback diode on the amplifier used for input in Figure C-5b gives an indication of surface vehicle separation. This amplifier has approximately a one-half volt output at the time separation has occurred due to the diode characteristics. This output can be amplified and shaped to allow indication of wheel separation with the surface. It is possible to use hard limiters set at the proper voltage to measure the time when one or any combination of wheels has separated from the surface. Figure E-11 shows time traces of the vehicle body angular motions and the indication of front wheel and all four wheel lift-off for this vehicle model. The lift-off measurement is essentially a binary form where lift-off occurs at the lower level in the bottom two traces of Figure E-11 and surface contact is represented by the upper level. Figure E-12 shows the output P.S.D. calculated from the analog output for the vertical displacement of the body c.g. This is shown at two different vehicle speeds. The major peak in these plots is the

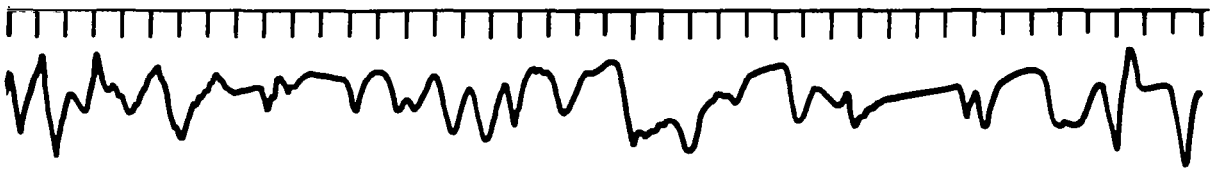

Roll Motion of Vehicle Body

Pitch Motion of Vehicle Body

Four Wheel Separation

Two Wheel Separation

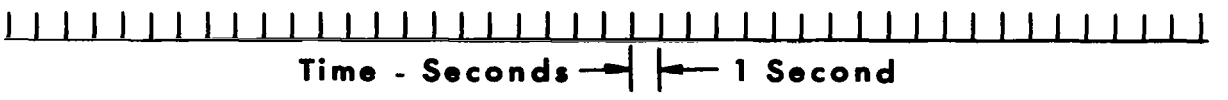

Figure E-11 TIME TRACES OF VEHICLE BODY MOTION SHOWING WHEEL LIFTOFF

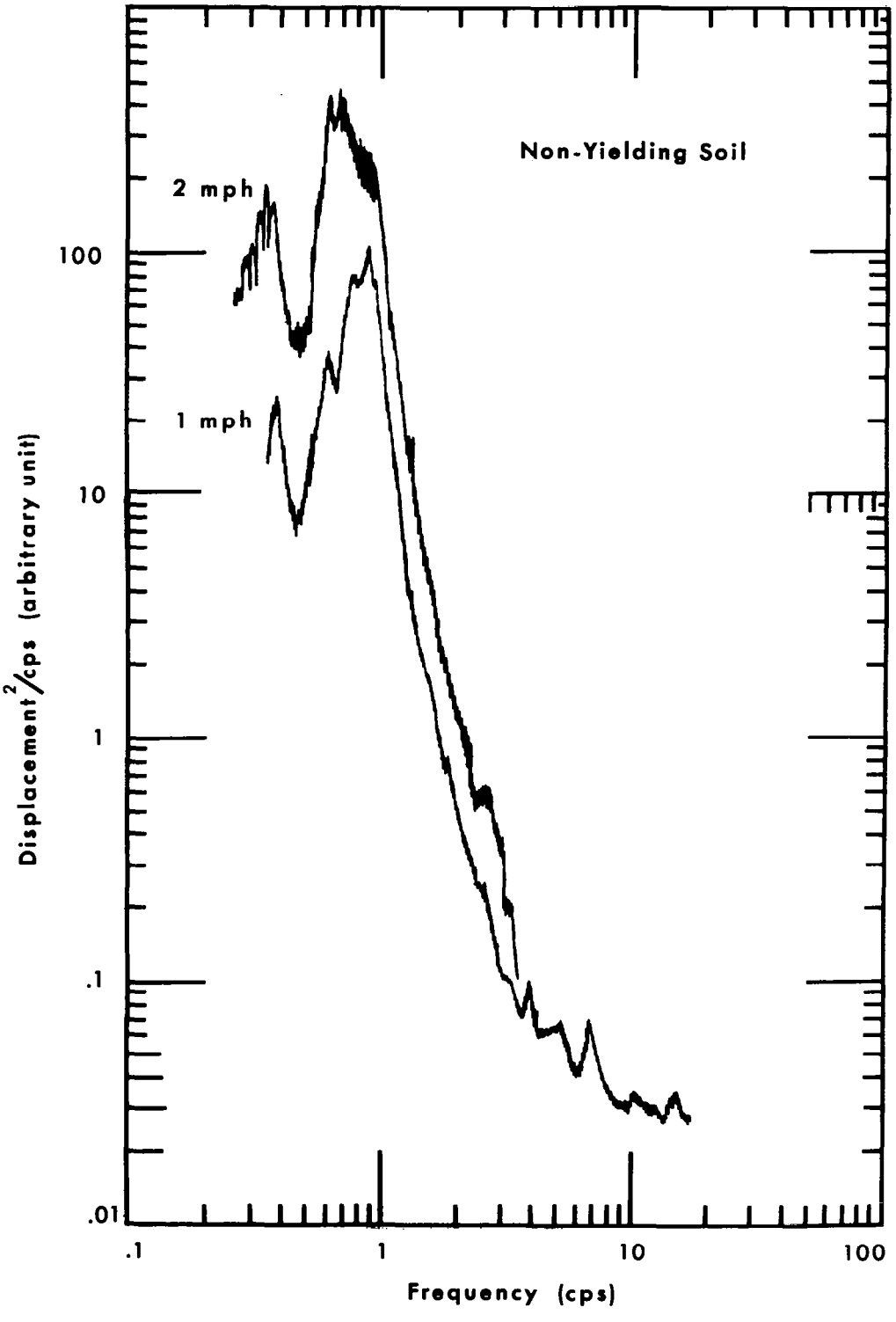

Figure E-12 P.S.D. OF VEHICLE C.G. VERTICAL DISPLACEMENT AT 1 & 2 MPH

vehicle bounce resonance. At two mph this resonance appears at a slightly lower frequency than at one mph. This is probably due to the fact that the vehicle suffers separation from the surface over a greater amount of the time at this speed. The surface separation will tend to broaden the bounce resonance and lower it in frequency due to the non-linear spring effects of gravity which acts as the restoring force after separation has occurred.

The second harmonic of basic body motions noted in Figure E-6 is not apparent in Figure E-12 and it would seem that this harmonic is due to the non-linearities of the non-yielding surface model.

In addition to the time delayed inputs a separate independent input was used to excite each of the four wheels of this model to allow comparison with the frequency domain results of Appendix D. Figure E-13 gives a summary of the results of the four wheeled vehicle with indpendent inputs to each of the wheels. The first time that the pitch, angular motion exceeded the static equilibrium limit occurred at approximately 2.8 meters per second (six mph). The same vehicle model was employed in this instance as in the linear frequency domain approach of Appendix D with the major difference that vehicle-surface separation (a non-linearity) was allowed in the analog simulation. The restoring force on the vehicle for the analog simulation is gravity. For the linear model analysis of Appendix D this restoring force was the vehicle wheel and suspension springs in tension. With this non-linearity a surface separation greater than 50 percent of the time can be obtained. At the speed where surface separation of all four wheels occurred 50 percent of the time, the vehicle suffered the first pitch-over. Table E-1 is a tabulation of the vertical body acceleration and percent lift-off of all four wheels. The percent lift-off is calculated as a probability of exceeding one lunar g from a Gaussian distribution determined by the measured standard deviation of vertical body acceleration and is also directly measured from the analog simulation.

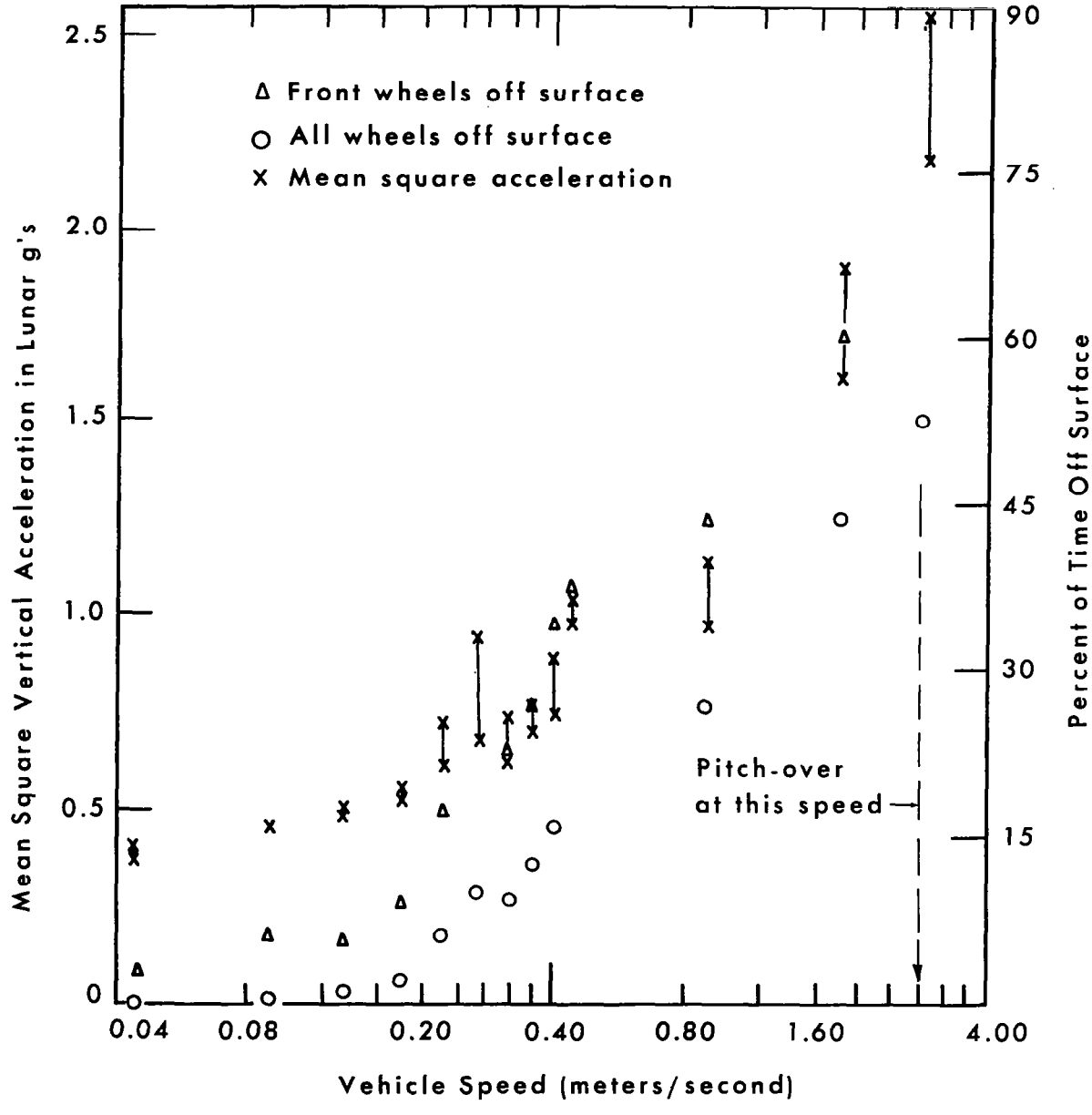

Figure E-13 SUMMARY OF RESULTS FROM
4-WHEEL SUSPENSION VEHICLE ON NON-YIELDING SURFACE

Table E-1 shows good agreement between the two measurements at about σ = 1 lunar g. For values below this level the analog simulation gives less lift-off than the theoretical prediction and above this value the analog simulation gives a greater percent of vehicle-surface separation.

Table E-1 VERTICAL BODY ACCELERATION AND % LIFT-OFF

Speed (mph)	"Measured" Standard Deviation of Vertical Body Acceleration (Lunar g's)	% of time Lift-off Theoretical Prediction from Lunar g. (See Appendix D)	% of time Lift-off "Measured" Analog Simulation
.1	.63	5.6	0
.2	.66	6.4	0.2
.3	.69	7.1	1.0
.4	.73	8.5	1.6
.5	.82	11.2	6.0
.6	.90	13.4	9.6
.7	.80	10.4	9.0
.8	.85	12.1	12.5
.9	.90	13.4	15.5
1.0	1.00	15.9	21.1
2.0	1.03	16.6	26.5
4.0	1.32	22.4	43.5
6.0	1.52	25.5	52.4

E.4 Summary of Results of Non-Linear Analysis

In this appendix a vehicle model which included a non-linear yielding surface was investigated in contrast to the linear model discussed in Appendix D. In both cases linearization of rotational motion (small angle assumptions) has been used; the non-linearities in this analysis included the freedom of the wheels to lift-off the surface, and a non-linear spring rate representing the surface deformation. Comparing the results from these two studies show the following: both models adequately predict resonances of the various motions, predictions of lift-off agree fairly well at those speeds for which the body vertical acceleration (standard deviation) is near one lunar g, predictions of limiting speed at which pitch-over is likely to occur show some agreement. For the non-linear model the first pitch-over was detected at a speed of approximately six miles per hour, while the linear analysis showed the probability of pitch-over occurring was about 0.01 percent at this speed. These comparisons are based on a non-yielding surface. It has been shown that the motion of the body is reduced when traversing a yielding surface, so the limiting conditions predicted above are conservative estimates for yielding surfaces. It should also be kept in mind that linearity of angular motion has been assumed, so that although the estimates of exceeding limiting conditions are not precise they do represent "ball park" values.